AD-A053 745 PENNSYLVANIA STATE UNIV UNIVERSITY PARK APPLIED RESE--ETC F/G 11/6
HOT CORROSION AND OXIDATION STUDIES ON COBALT-BASED ALLOYS.(U)
JUL 77 V F HOCK N00017-73-C-1418
UNCLASSIFIED ARL/PSU/TM-77-274 NL

1 OF 2
AD A053745

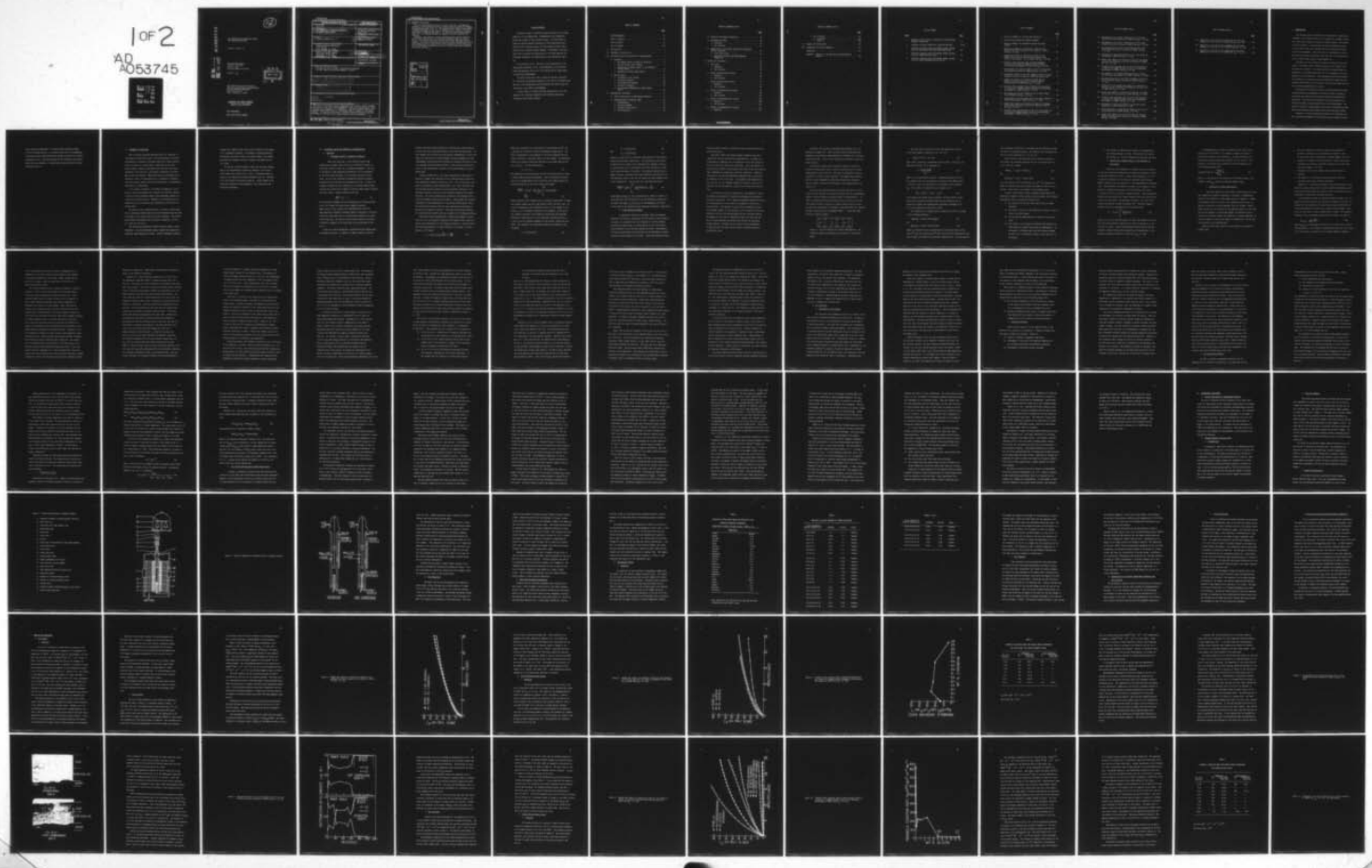

(12)

HOT CORROSION AND OXIDATION STUDIES ON COBALT-BASED ALLOYS

Vincent F. Hock, Jr.

Technical Memorandum
File No. TM 77-274
July 13, 1977
Contract N00017-73-C-1418

Copy No. 5

The Pennsylvania State University
Institute for Science and Engineering
APPLIED RESEARCH LABORATORY
Post Office Box 30
State College, PA 16801

NAVY DEPARTMENT

NAVAL SEA SYSTEMS COMMAND

UNCLASSIFIED

SECURITY CLASSIFICATION OF THIS PAGE (When Data Entered)

REPORT DOCUMENTATION PAGE

READ INSTRUCTIONS BEFORE COMPLETING FORM

1. REPORT NUMBER: TM-77-274
2. GOVT ACCESSION NO.:
3. RECIPIENT'S CATALOG NUMBER:

4. TITLE (and Subtitle): (6) HOT CORROSION AND OXIDATION STUDIES ON COBALT-BASED ALLOYS.
5. TYPE OF REPORT & PERIOD COVERED: MS Thesis, Metallurgy March 1978
6. PERFORMING ORG. REPORT NUMBER: TM 77-274

7. AUTHOR(s): (10) Vincent F. Hock, Jr.
8. CONTRACT OR GRANT NUMBER(s): (15) N00017-73-C-1418

9. PERFORMING ORGANIZATION NAME AND ADDRESS:
Applied Research Laboratory
P. O. Box 30
State College, PA 16801

10. PROGRAM ELEMENT, PROJECT, TASK AREA & WORK UNIT NUMBERS:

11. CONTROLLING OFFICE NAME AND ADDRESS:
Naval Sea Systems Command
Department of the Navy
Washington, D. C. 20362

12. REPORT DATE: (11) 13 Jul [illegible] 1977
13. NUMBER OF PAGES: 159 pages & figures (12) 161 p.

14. MONITORING AGENCY NAME & ADDRESS (if different from Controlling Office):

15. SECURITY CLASS. (of this report): Unclassified, Unlimited
15a. DECLASSIFICATION/DOWNGRADING SCHEDULE:

16. DISTRIBUTION STATEMENT (of this Report)

Approved for public release, distribution unlimited, per NSSC (Naval Sea Systems Command), 11/25/77.

17. DISTRIBUTION STATEMENT (of the abstract entered in Block 20, if different from Report)

(14) ARL/PSU/TM-77-274

18. SUPPLEMENTARY NOTES

(9) Master's thesis,

19. KEY WORDS (Continue on reverse side if necessary and identify by block number)

corrosion
oxidation
cobalt alloys
sulfidation

20. ABSTRACT (Continue on reverse side if necessary and identify by block number)

The rates of oxidation and hot corrosion of pure cobalt, cobalt-chromium, cobalt-silicon and cobalt-chromium-silicon alloys were determined at 1000°C in oxygen at a pressure of 0.1 atmosphere. The hot corrosion studies were conducted under conditions of a continuous supply of Na_2SO_4 to the sample surface. In addition, the effect of thermal cycling on the hot corrosion resistance of the Co-15 Cr-Si alloy group was also investigated.

DD FORM 1 JAN 73 1473 EDITION OF 1 NOV 65 IS OBSOLETE

391 007

UNCLASSIFIED

SECURITY CLASSIFICATION OF THIS PAGE (When Data Entered)

20. ABSTRACT (Continued)

For the cobalt-chromium alloys, it was found that a considerable decrease in the oxidation and hot corrosion rates occurred at chromium concentrations about 15 wt. %. The cobalt-silicon binary alloys showed a dramatic increase in the rate of oxidation up to 0.05 wt. % silicon according to normal doping theory. At silicon concentrations greater than 5 wt. %, a marked decrease in oxidation and hot corrosion was observed.

Generally, the series of cobalt-chromium-silicon alloys exhibited much better oxidation and hot corrosion resistance than the binary alloys. The lowest rates were obtained for alloys with high silicon contents. One alloy in particular, Co-10 Cr-10 Si, exhibited the lowest total weight gain per unit area for both oxidation and hot corrosion. The hot corrosion resistances of the Co-15 Cr-Si alloys were decreased by thermal cycling.

ACKNOWLEDGEMENTS

The author wishes to express his deep gratitude to Dr. George Simkovich for his suggestions, recommendations and inspiration during the conduct of this research project. He also wishes to thank the Applied Research Laboratory at The Pennsylvania State University for financial support of this research project under contract with the Naval Systems Command. Furthermore, the author would like to express his appreciation to Dr. Earle Ryba for his invaluable assistance in completing the x-ray diffraction analysis.

The assistance of Mr. John Daly in the construction of the experimental apparatus, of Mr. Leland Eminhizer in the electron probe microanalysis, and of Mr. Bruce Warnes and Mr. Mark Prugar is gratefully acknowledged.

The author would also like to thank the faculty, especially Dr. John Hoke, the graduate students and the staff of the Metallurgy Section at The Pennsylvania State University for their varied contributions to the author's development.

He also wishes to express his deep appreciation to his wife Wanda for her continual inspiration and technical assistance throughout this research project.

TABLE OF CONTENTS

TABLE OF CONTENTS (Cont.)

TABLE OF CONTENTS (Cont.)

LIST OF TABLES

LIST OF FIGURES

LIST OF FIGURES (Cont.)

LIST OF FIGURES (Cont.)

I. INTRODUCTION

Hot corrosion may be defined as the accelerated or catastrophic oxidation of the substrate metal due to fluxing of a normally protective oxide such as Al_2O_3 or Cr_2O_3 by an alkali surface. The problem of "hot corrosion" or "sulfidation" has grown considerably within the last twenty years upon introduction of the gas turbine engine to marine environments. Rejection rates for sulfidation of blades and vanes on overhaul from ships, naval aircraft and hovercraft has risen to 50% for some stages of some engines (1).

Sulfidation or hot corrosion is usually initiated by the deposition of an alkali sulfate (usually Na_2SO_4) on the turbine blade and guide vane surfaces. The sodium sulfate is formed during the combustion of a sulfur-bearing fuel oil in the presence of sea salt ingested with the intake air. Two developments which have enhanced the problem of hot corrosion are the utilization of higher gas temperatures (850°-1250°C) at the turbine inlet and first stage and the use of low-grade high-sulfur fuel oils.

The potential solutions to the hot corrosion problem have been centered around the development of protective surface coatings or new alloys with improved hot-corrosion resistance and mechanical properties. The current trend appears to be the utilization of protective surface coatings rather than in alloy development. The need for additional investigation into the area of alloying the base metal with components which promote protective scales was evident.

Therefore, a study concerning the effects of an oxidizing and hot corrosion environment on the protective scales formed on cobalt-

based alloys was undertaken. The cobalt-based system was chosen for the following reasons: 1) a previous study (43) on corresponding nickel-based alloys indicated Ni-Cr-Si alloys have good hot corrosion resistance, and 2) it has been reported in the literature that cobalt-based alloys are superior to nickel-based alloys under hot corrosion conditions (60,61).

II. STATEMENT OF OBJECTIVES

One of the main problems associated with "hot corrosion" or "sulfidation" attack upon alloys is the acceleration of corrosion due primarily to fluxing of the solid oxide by an alkali sulfate, which is present as a liquid phase. Since most of the solid oxides normally formed on superalloys are electronic conductors, the growth of the scale as a solid phase is governed by the movement of the ionic species. When these scales are liquefied due to fluxing by a salt, an accelerated rate of oxidation is observed, since ionic motion, which controls the growth rate, is considerably increased in a liquid phase.

It is logical, therefore, to consider the growth of a scale which is controlled primarily by the motion of electronic species in the solid state and whose growth, upon liquefying, remains controlled by electronic motion. Therefore, the accelerated rate of oxidation will not be observed upon liquefaction of an ionic conducting scale.

To obtain an ionic conducting scale, a series of cobalt-based alloys containing chromium and silicon were formulated with the hope of forming an SiO_2 scale, which is an ionic conductor. The cobalt-based alloys were divided into three basic categories: I, Co-Cr; II, Co-Si; III, Co-Cr-Si.

The alloys were prepared by induction melting under an inert atmosphere. From the solidified ingots, samples were prepared for subsequent high-temperature testing. Initial isothermal oxidation

studies were conducted upon these alloys at 1000°C in dry oxygen at 0.1 atmospheric pressure. An automatic recording Ainsworth microbalance was used to detect the weight change of the sample, which was the parameter utilized to measure the growth rate of the scales.

For the hot corrosion studies, there were two major changes made in the experimental procedure as compared to the earlier nickel-based alloy studies (43). First, a continuous supply of Na_2SO_4 to the sample was utilized throughout each run. Additionally, some thermal cycling was introduced. Scales formed on the alloys were examined by metallographic, x-ray diffraction and microprobe techniques.

III. LITERATURE REVIEW AND THEORETICAL CONSIDERATIONS

A. Oxidation

1. The Wagner Theory of Parabolic Oxidation

Some fifty years ago, it was observed that, at high temperatures, a compact scale will act as an effective barrier to the further attack of metal by an oxidizing atmosphere. The rate of oxidation at high temperatures, therefore, will be determined by the solid state diffusion of the reactants across the oxide layer. As the oxide thickness increases, the diffusion distance increases and the reaction rate decreases with time. If $\Delta m/A$, the increase in weight per unit surface area, is plotted versus time, a parabola will result, and if $(\Delta m/A)^2$ is plotted versus time, a straight line will result. Thus, the parabolic rate law

$$\left(\frac{\Delta m}{A}\right)^2 = K_p \cdot t \,, \qquad (1)$$

first derived by Tammann (12) and independently by Pilling and Bedworth (13) becomes the time law most commonly observed. Wagner (14), in 1933, advanced the phenomenological theory of high temperature parabolic oxidation based on diffusion of reactants across the oxide layer due to a concentration gradient as the rate controlling step. The theory of point defects which is the basis of material transport in an oxide layer will be discussed in Section 2.

There are certain preliminary considerations which Wagner made concerning his theory. It applies to compact scales of reaction

products and where volume diffusion of reacting ions, (point defects), or electrons across the growing oxide is the rate-controlling step. He also assumed that electrons and ions migrate independently of each other under the influence of an electrochemical potential gradient and that thermodynamic equilibrium exists between the reactants and oxide at both the oxide/gas and metal/oxide interface. Since diffusion through the scale is rate determining, reactions at the phase boundary are considered rapid.

Using the models for p- and n-type semiconductors (described in Section 2), Wagner (15) expressed the two limiting cases by which the high temperature oxidation process can occur. For an oxide scale with metal ion vacancies (p-type semiconductor, e.g., CoO), the metal ions and electrons diffuse outward from the metal/oxide interface to the oxide/gas interface, with the cation vacancies moving in the opposite direction. The cation vacancies are produced at the oxide/gas interface and consumed at metal/oxide interface. Where oxygen ion vacancies predominate (n-type semiconductor), the anions diffuse inward toward the metal/oxide interface with the anion vacancies and electrons migrating in the opposite direction. The anion vacancies are produced at the metal/oxide interface and are consumed at the oxide/gas boundary.

Based upon these considerations or limitations, Wagner's derivation (9, 15) of the parabolic oxidation rate equation first takes into account the diffusion due to the chemical potential, μ, and that due to the electrical potential, ψ, where the flux J of species i in equivalents per cm^2 equals

$$J_i = Z_i C_i V_i = Z_i C_i B_i \left(\frac{d\mu_i}{dx} + Z_i \frac{F d\psi}{dx}\right) \quad , \qquad (2)$$

where Z_iC_i represents the concentration in equivalents per cm^3, and V_i and B_i are the particle velocity and mobility, respectively. The term in parentheses is the gradient of the electrochemical and electrical potentials μ_1 and $Z_iF\psi$, where F is the faraday. The equivalent currents of cations, anions and electrons in the oxide layer will be J_1, J_2 and J_3. For electroneutrality,

$$J_1 = J_2 + J_3 \ . \tag{3}$$

Flux equations can now be derived for the ions and electrons in terms of their chemical-potential gradients. Upon calculating the mobilities of the charged species from electrical data, Wagner derived the following equation for the flux of metal and oxygen

$$\frac{d(n/q)}{dt} = J_1+|J_2| = \frac{1}{\Delta x}\left\{\frac{1}{|Z_2|F^2}\int_{\mu_o'}^{\mu_o''}(t_1+t_2)t_3K d\mu_o\right\}$$

$$= \frac{K_r}{\Delta x} \ , \tag{4}$$

where $d(n/q)/dt$ is the oxidation rate in terms of equivalents of oxidation product formed per unit cross section (cm^2) q per unit time. Δx is the instantaneous scale thickness in cm, Z_2 is the valence of the anions, μ_o is the chemical potential of the nonmetal, μ_o' and μ_o'' are the chemical potentials of the anions at metal/oxide and oxide/gas interfaces, respectively, K is the electrical conductivity, and t_1, t_2 and t_3 are the transport numbers for the cations, anions and electrons. The transport (or transference numbers) are defined by the following:

$$t_1 = \ell_1/(\ell_1+\ell_2+\ell_3) \ , \tag{5}$$

$$t_2 = \ell_2/(\ell_1+\ell_2+\ell_3) \tag{6}$$

and

$$t_3 = \ell_3/(\ell_1+\ell_2+\ell_3) \ , \tag{7}$$

where ℓ_1, ℓ_2 and ℓ_3 are the specific conductivities of the cations, anions and electrons, respectively. The expression in the braces in Equation (4) is equal to the "rational rate constant", where K_r is the reaction rate in equivalents per cm^2 per second for a layer of the reaction product 1 cm thick. An alternative method used by Wagner (15) was to determine the ionic mobilities from data for the self-diffusion rates of the ions as long as the oxide exhibits electronic conductivity. The reaction rate then takes the form of

$$\frac{d(n/q)}{dt} = \frac{1}{\Delta x}\{Ceq \int_{a_o'}^{a_o''} (\frac{Z_1}{|Z_2|}D_1^* + D_2^*)d\ln a_o = \frac{K_r}{\Delta x}\} \ , \tag{8}$$

where $Ceq = Z_1C_1 = |Z_2|C_2$ is the concentration of cations or anions in equivalents per cm^3, D_1^* and D_2^* are the self-diffusion coefficients for metal and oxygen, a_o' and a_o'' are the thermodynamic activities of the anion at the metal/oxide and oxide/gas interfaces, respectively.

2. Point Defects in Oxides

A significant feature of the Wagner theory of parabolic oxidation is the direct correlation with the theory of point defects in solids. As stated earlier, the formation of a thick, compact, and pore-free oxide layer on a metal surface is due to the solid state diffusion of the reactants through the oxide. The mechanism of solid state diffusion occurs because of the formulation of imperfections or point defects in the oxide. These point defects include

cation and anion vacancies, interstitial ions, quasi-free electrons and electron holes.

Most metal oxides and sulfides exhibit primarily electronic conductivity and are classified as semiconductors. In these non-stoichiometric compounds, the concentrations of the ionic point defects and electronic defects are equivalent. Since the mobility of the electronic species is much greater than that of the ionic defects, these compounds are essentially electronic conductors. Therefore, the growth of the electron-conducting compounds will be controlled by diffusion of one of the ions. In accordance with Equations (4), (5), (6) and (7), the transport number for electron t_3 will be essentially one and the quantity (t_1+t_2), will be much less than one (75).

In the case of pure ionic conductivity, the numbers of cations and anions are equivalent to maintain stoichiometry and therefore electrical neutrality. Ionic conducting compounds exhibit much greater concentrations of ionic defects as compared to electrons or electron holes. The quantity (t_1+t_2) will be essentially one and the transport number for the electron t_3 will be much less than one. Therefore, the rate controlling species is the electronic species. An example of this class of compounds is AgCl (2), where the number of cation vacancies and interstitial cations are equivalent (Frenkel defect). Movement of the cations is then accomplished by shifting into the vacant lattice sites or drifting along the interstitial sites.

The models for electronic semiconducting compounds was first expressed by Wagner (3). There are three types of semiconducting compounds as described by Kubaschewski (75) and Hauffe (2): intrinsic, n-type and p-type. Only n- and p-types are of interest in most oxidation studies.

Excess metal cations and an equivalent number of electrons located on interstitial lattice sites are characteristic of n-type semiconductors such as ZnO (2). This type of compound can also be considered in terms of anion vacancies. The Wagner theory predicts that for n-type compounds the electrical conductivity decreases (lattice defect concentration decreases) as the oxygen pressure increases (1).

For the p-type semiconductors such as CoO (75),(4),(5), a deficiency in metal cations or an excess of anions with the corresponding number of electron defects (electron holes) is characteristic. In order to maintain electrical neutrality when the structure contains some cation vacancies, cations of a higher valence state are created which are equivalent to the number of electron holes, ⊕. Electron movement takes place via an exchange between the lower and higher cations as shown in Figure 1.

$O^{=}$	Co^{++}	$O^{=}$	Co^{3+}	$O^{=}$	Co^{++}
Co^{++}	$O^{=}$		$O^{=}$	Co^{++}	$O^{=}$
$O^{=}$	Co^{++}	$O^{=}$	Co^{3+}	$O^{=}$	Co^{++}

Figure 1. CoO as an example of a p-type semiconductor. The trivalent cobalt ions represent the location of the electron holes.

The point defect equations for the high temperature reaction of CoO with oxygen are written as (6), (7), (9):

$$\frac{1}{2}O_2(g) \rightleftarrows V(Co)^{'} + \oplus + CoO \quad , \tag{9}$$

where $V(Co)^{'}$ represents a monovalent cation vacancy. From this, the mass action balance can be expressed as:

$$K = \frac{[V(Co)^{'}]\cdot[\oplus]}{P_{O_2}^{1/2}} \quad , \tag{10}$$

where K is the equilibrium constant. Combining Equation (10) with the condition that the concentration of electron holes $[\oplus]$ is equal to $[V(Co)^{'}]$, then the relationship of the oxygen partial pressure P_{O_2}, to the defect concentration can be shown to be:

$$[\oplus] = [V(Co)^{'}] = \text{Const} \cdot P_{O_2}^{1/4} \quad . \tag{11}$$

By increasing the oxygen partial pressure, the point defect concentration will therefore increase along with the oxidation rate as predicted by Wagner and experimentally confirmed by Bridges et al. (8) in the temperature range 950 to 1150°C.

The introduction of higher valent cations such as Cr^{3+}, according to the following equations:

$$2\oplus + Cr_2O_3 = 2Cr(Co)^{\cdot} + 2CoO + \frac{1}{2}O_2(g) \tag{12}$$

and

$$\frac{1}{2}O_2 + Cr_2O_3 = 2Cr(Co)^{\cdot} + 2V(Co)^{'} + 4CoO \tag{13}$$

leads to a decrease in the concentration of the electron holes, since some Co^{3+} ions are replaced by Cr^{3+} ions, but this also increases the number of cobalt ion vacancies, according to Equation (13). The end result is

that electrical conductivity is decreased and the diffusion through the scale is increased and, hence, the oxidation rate increases with up to 9 wt.% Cr additions (75, 2, 9, 10, 11).

Since silicon is the other major alloy addition utilized in this study, the following equations will be of interest when silicon is used as a dopant:

$$2\oplus + SiO_2 \rightleftarrows S_i(Co)^{\cdot\cdot} + CoO + \frac{1}{2} O_2 \qquad (14)$$

and

$$\frac{1}{2} O_2 + S_iO_2 \rightleftarrows Si(Co)^{\cdot\cdot} + 2V(Co)' + 3CoO \quad . \qquad (15)$$

As is the case for Cr^{+3} ion additions, the Si^{+4} ions decrease the number of electron holes and increase the number of cobalt ion vacancies. This leads to an increase in the oxidation rate.

In order to successfully apply the Wagner doping theory when additions of higher or lower valence cations are made, the following requirements exist as outlined by Kofstad (10):

(1) The oxidation of the pure metal must follow the Wagner mechanism.

(2) The defect structure of the oxide must be known in order to select the proper dopant.

(3) The foreign ion additions must be soluble in the parent oxide.

(4) The valence of the foreign ion addition when dissolved in small amounts in another oxide must be predetermined. As an example, if niobium, which can have valences ranging from +2 to +5, is dissolved in TiO_2, it will have a +4 or +5 valence.

(5) The foreign ion additions are assumed to be homogeneously distributed through the oxide. This implies that parent and foreign ion rates of oxidation and diffusion are equal.

3. Application of Wagner Theory to the Oxidation of Pure Cobalt

Sufficient electrochemical or diffusion data are available to test the theoretical assumptions for parabolic oxidation of cobalt as outlined in Sections 1 and 2. Carter and Richardson (6, 7) calculated the oxidation rate of cobalt to cobaltous oxide by using Wagner's Equation (8) and compared it to the experimentally determined rate. They measured the oxidation of cobalt in the presence of inert markers of radioactive platinum, and self-diffusion coefficient of cobalt in CoO as a function of oxygen pressure. These measurements showed that the oxidation of cobalt occurred only by cation diffusion across the oxide film to the gas/oxide interface. The point defect equation postulated is shown by Equation (9). Therefore, Wagner's Equation (10) can be expressed in the following terms:

$$K_r = |Z_2| Ceq \int_{a_o'}^{a_o''} \frac{Z_1}{|Z_2|} D_1^* d\ln a_o \quad , \tag{16}$$

where Z_1, Z_2 are the average valency of cobalt and oxygen in the CoO, D_1^* is the self diffusion coefficient of cobalt in CoO, and a_o is the activity of oxygen. Carter and Richardson obtained better than 90% agreement between measured and calculated rate constants (K_r) at temperatures ranging from 1000° to 1350°C and a P_{O_2} of 1 atm.

In thermogravimetric studies of oxidation rates such as were carried out in this study, it is common to express the results in terms of the parabolic rate constant K_p, as shown in Equation (1). The units are usually expressed as $(\text{gm } O_2)^2$ per cm^4 per sec. The parabolic rate constant K_p is related to the rate constant K_r by the following Equation (10):

$$K_p(\text{gm } O_2)^2/\text{cm}^4\text{-sec} = \frac{2db(M_x)^2}{rM_{M_a x_b}} K_r \quad , \tag{17}$$

where d is the density of the oxide, M_x is the atomic weight of the nonmetal, and $M_{M_a x_b}$ equals the molecular weight of $M_a x_b$.

4. Oxidation of Cobalt-Based Alloys

Since pure metals are rarely used in applications where good high temperature oxidation resistance is required, a comprehensive review of the oxidation of cobalt-based alloys is required. A number of additional factors will have to be considered, since alloys, in general, contain two or more components that will oxidize. Some of these factors are: the affinity of the component metals for each other and for the nonmetal, in particular oxygen; the diffusion rates of atoms in the oxidation layers; the formation of ternary compounds; the relative volumes of the various phases; the temperature; and the partial pressure of the oxidizing gas.

There are three basic types of alloy oxidation as outlined by Kofstad (10):

1. Selective oxidation in which the least noble component of an alloy is selectively or preferentially oxidized to form an outer oxide layer consisting of one phase [Wagner, (11, 17)].
2. Formation of composite scales consisting of oxides which may be considered to be mutually insoluble and which do not react with each other [Wagner, (11, 16)].
3. Formation of scales with complex oxides (double oxides or spinels).
4. The formation of discontinuous oxide particles within the continuous alloy phase (internal oxidation).

Wagner (11), in constructing models to explain the types of alloy oxidation listed, assumed that virtually complete thermodynamic equilibrium exists between adjacent phases and that the oxidation rates are determined by steady-state diffusion processes.

In developing the model for selective oxidation, Wagner (11, 17) neglected internal oxidation and the mutual solubility of oxides, and assumed that the oxide AO is a p-type oxide in which A diffuses by a vacancy mechanism and electrons by a positive hole mechanism. Also, A and B do not react to form a double oxide or spinel. For exclusive formation of AO, the minimum concentration of element A is given by

$$N_{A(min)} = \frac{1}{16 Z_A C}\left(\frac{\pi K_p}{D}\right)^{\frac{1}{2}} , \qquad (18)$$

where $N_{A(min)}$ is the minimum concentration of A (also called critical concentration), C is the number of gram-atoms of metal per unit volume, Z_A is the valence of A atoms, 16 is the atomic weight of oxygen, D

is the interdiffusion coefficient, which is independent of the composition of the alloy, and K_p is the parabolic rate constant for exclusive formation of the A oxide. Wagner assumed the formation of a compact, pore-free oxide scale in order for the above relationship to hold.

The cobalt-chromium alloys are important examples of selective oxidation. One of the earliest studies of the scaling behavior of Co-Cr alloys was completed by Preece and Lucas (18). They reported single values of weight increase for 50 hr exposure in air or burnt paraffin simulating a gas turbine atmosphere at 800-1200°C for alloys up to 40% chromium. Their data indicate a sharp rise in weight increase for 10% Cr additions with a subsequent drop for 25% additions. The scales formed on alloys with less than 25% Cr consisted of CoO with some cobalt chromite ($CoCr_2O_4$). For higher additions of Cr, the scales consisted of Cr_2O_3 only. Preece and Lucas concluded from their work that the diffusion of oxygen ions through the scale was possible and the formation of the spinel greatly accelerated the oxidation process. Phalnikar, et al. (19) studied the oxidation of Co-Cr alloys in the temperature range 900-1200°C in air. They confirmed that optimum oxidation resistance was obtained for alloys containing 25% Cr additions. The composition of the oxides proved to be mixtures of CoO and $CoCr_2O_4$ for Cr additions below 25% and essentially Cr_2O_3 above 25% Cr. As in the case for pure Co, Phalnikar et al. (19) concluded that cobalt rich alloys form outer scales which are metal deficient and grow by outward diffusion of cobalt ions and that the spinel may be formed by inward

diffusion of oxygen ions. Again, spinel formation had no beneficial effect on the oxidation resistance.

Kofstad et al. (20) studied the oxidation of Co-10 wt.% Cr in the temperature range 800°-1300°C at oxygen pressures from 0.05 to 760 torr. They found the overall oxidation to be parabolic and dependent on O_2 pressure. The Co-10 Cr alloy also oxidized faster than pure cobalt. Extensive metallographic studies were performed on the oxidized specimens along with some electron-probe microanalysis. The oxide scale was found to be double-layered with the outer layer consisting of CoO, and an inner layer of $CoCr_2O_4$ and Cr_2O_3 particles embedded in a CoO matrix. The inner layer also contained 30-35 vol.% porosity. It was concluded from this study that the oxidation was controlled by Co-vacancy diffusion in the CoO phase. This reinforced what previous investigators (19) have found. Kofstad (20) postulated that the spinel inclusions inhibit the oxidation by decreasing the effective diffusion area in the scale, and that the pores serve to increase the oxidation. The pores partially short circuit the solid state diffusion through the scale due to oxygen transport across the pores. A study (21) was also conducted on Co-25 wt.% Cr under identical experimental conditions. The oxidation mechanism for this alloy was more complex since, at P_{O_2} >100 torr, a duplex scale was formed consisting of an outer layer of CoO and an inner layer of $CoCr_2O_4$ with small amounts of CoO and Cr_2O_3 (the Cr_2O_3 was concentrated near the alloy/scale interface). At low oxygen pressures, the Cr_2O_3 is the dominant oxide. The transition from high to low pressure oxidation involved preferential or

selective oxidation of chromium, and was accompanied by a large, almost abrupt decrease in the oxidation rate. The oxidation of alloys with higher concentrations of Cr (Co-35 Cr) were independent of oxygen pressure and were comparable to the low pressure oxidation of Co-25 Cr (21). Other investigators (22), (23) confirmed that as the chromium is increased up to 25 to 30 wt.%, the oxidation rate decreases with increased spinel formation due to a blocking in the inner layer.

The effect of silicon on the oxidation rate of cobalt-based alloys is not generally known, since data for these systems are rather sparse. Generally speaking, the addition of silicon should improve the oxidation resistance of the cobalt-based alloys by preferential oxidation to form a layer of SiO_2 adjacent to the alloy surface. The initial formation of this inner layer of SiO_2 will result in a lower diffusion rate, since SiO_2 is a low-conductivity scale, according to Wagner's defect theory. Bausch et al. (40) in a study on the effect of alloying on the properties of wrought cobalt established that silicon, aluminum, and chromium all impart oxidation resistance to cobalt. This study, however, was not concerned with the oxidation products, but only with the effect of the alloying elements on strength at high temperature.

Douglass and Armijo (24) studied the effects of up to 3% silicon on the oxidation of Co-20% Cr alloys at 1100 and 1200°C in air. On the pure Co-20 Cr alloy, the initial oxide was CoO which formed very rapidly [about 100 times faster than the NiO formed on Ni-20 Cr (41)] by outward cation diffusion. A chromium-enriched substrate layer subsequently reacted via internal oxidation to form a continuous

film of Cr_2O_3 as in the case of nickel alloys (41). The formation of $CoCr_2O_4$ occurred rapidly [nearly 10 times faster than the growth rate of $NiCr_2O_4$ (41)], by the reaction of CoO and Cr_2O_3. Silicon additions reduced the oxidation rate, but the layers were highly susceptible to spalling upon cooling as well as during isothermal oxidation. The scales contained Cr_2O_3, $CoCr_2O_4$, and Co_2SiO_4. The ortho-silicate was present as isolated particles and did not form a continuous protective film. The reduced oxidation rate was associated with a thin inner film of Cr_2O_3. The results obtained by Douglass and Armijo (24) for the oxidation of Co-20 Cr and Co-20 Cr-1 to 3 Si are analogous to those obtained by other investigators (42, 43) for Ni-Cr alloys.

In a study on the effect of small amounts of silicon on the high temperature oxidation of a high-purity Co-25 Cr alloy, an interesting anomaly was revealed. Phalniker et al. (19) reported that Co-25 Cr oxidizes slowly at temperatures in the range of 1000 to 1200°C in air forming a protective Cr_2O_3 scale; whereas, Kofstad and Hed (21) reported very rapid oxidation in the temperature range 900-1300°C in oxygen at pressures greater than 100 torr. In contrast, an outer layer of CoO and an inner mixture of Cr_2O_3 and $CoCr_2O_4$ particles in a CoO matrix was observed. Both of these studies (19, 21) have been discussed earlier. Jones and Stringer (44) surmised that the anomaly could be caused by one of four factors: (a) method of initiating the oxidation; (b) minor constituents of the alloys; (c) surface preparation; or (d) grain size. After some preliminary experiments, they found

that a minor amount of silicon was responsible for the slow oxidation of Co-20 Cr alloy. Kofstad (21) used high purity cobalt on the order of 99.99% Co. Accordingly, they produced two alloys, Co-20 Cr-0.1% Si and Co-20 Cr-0.05% Si from Kofstad's Co-20 Cr master alloy. Both of these alloys exhibited slow oxidation rates with the development of a continuous Cr_2O_3 layer. Utilizing a high purity Co-20 Cr master alloy, a Co-20 Cr-0.05% Si alloy was produced which oxidized rapidly. This suggested that silicon alone was insufficient to cause the slow oxidation rate. Further investigation revealed that for silicon additions (as low as 0.05 wt.%) to promote oxidation resistance in Co-Cr alloys, they must be present as an internal distribution of SiO_2 in much the same way that dispersions of Y_2O_3, ThO_2 and Al_2O_3 promote the formation of Cr_2O_3 layers in Ni-Cr and Co-Cr alloys as reported by Stringer et al. (45).

The effect of other ternary additions to Co-32% Cr alloy relative to scale adherence and oxidation resistance was carried out by Preece and Lucas (18) in an atmosphere of burnt paraffin at a temperature of 800-1200°C. They observed that for a nominal 0.5 wt.% addition of

(1) B, Be, Nb and V, a serious loss of oxidation resistance was encountered due to the formation of low-melting point oxides.

(2) Ti, Zn and Ca, only a small beneficial effect was noticed, probably due to the formation of spinels of the type AB_2O_4 (where B positions are generally Cr^{3+} ions).

(3) Ta, Al, Ce, Si and Th, the oxidation resistance was markedly improved, especially by the Si and Th additions. It was thought that the formation of an SiO_2 layer adjacent

to the alloy/oxide interface would lower the rate of diffusion of ions and electrons through the outer layer of Cr_2O_3,

Davin et al. (23) demonstrated the effects of ternary additions on both Co-10 Cr and Co-30 Cr alloys oxidized in still air between 800 and 1200°C. They found an outer oxide layer, which was rich in cobalt, a middle layer rich in chromium, and a third layer, adjacent to the metal, rich in the ternary addition with a high affinity for oxygen (W, Al, etc.). The oxidation resistance of Co-10 Cr was greatly improved by a 6 wt% Ta addition. Additions of Fe, Ni, B or Y had no effect on the oxidation kinetics of Co-30 Cr; with additions of Ta, W, Al, Ti, Zr, Ce and Nb, the oxidation obeyed the parabolic rate law. The oxidation of Co-30 Cr was improved by additions of Zr, Ce, Al or B. Molybdenum and niobium led to catastrophic oxidation at high temperature.

Additions of 1% or less of elements such as yttrium and hafnium should improve the adhesion of scales on superalloys and, in some cases, reduce the oxidation rate (25). The explanation given was the formation of a partial or complete layer of a compound such as $YCrO_3$ developed at the alloy/oxide interface. Another study by Giggons et al. (26) indicated that the improved oxide scale adhesion was due to the selective internal oxidation of yttrium and hafnium to Y_2O_3 and HfO_2, which pegged the oxide scale to the metal. Beltran (27) showed that yttrium, when added to a Co-30% Cr alloy, improved the scale adherence and reduced the oxidation rate of this alloy between 900 and 1200°C. Very little $CoCr_2O_4$ and CoO were formed on

the ternary alloy as compared to the binary Co-30 Cr. The reduction in reaction kinetics was due to the presence of a Co/Y matrix precipitate which blocked Cr^{3+} diffusion at the metal/oxide interface, as well as improving scale adherence by acting as a site for vacancy "precipitation" to eliminate interfacial porosity.

The oxidation kinetics and scale behavior of cobalt-based industrial superalloys such as L-605, MAR-M302, and WI-52 are quite complex, since these alloys may contain up to a dozen elements without counting the usual impurities. Wlodec (28) characterized the oxidation of L-605 (Co-20 CR-10 Ni-15 W-1.5 Mn-0.15 C-0.5 Si) and X-40 (Co-25 Cr-10 Ni-8 W-1.5 Fe-0.5 C, Mn and Si) in air from 980 to 1200°C. During parabolic oxidation at lower temperatures, small amounts of Cr_2O_3 and CoO were found; the $CoCr_2O_4$ spinel formed in all other instances. At 1200°C, catastrophic oxidation occurred with the formation of a low melting scale of $CoWO_4$, Co_3O_4, CoO, and $CoCr_2O_4$. The X-40 alloy with its lower W content exhibited a less severe catastrophic oxidation.

Lowell (29) studied the oxidation of WI-52 (Co-19.5 Cr-11 Ni-1.5 Nb-1 Ni-0.4 C-0.3 Mn and Si) at 870, 980, and 1095°C in air for periods up to 100 hours. The alloy exhibited poor oxidation and spalling resistance, which seemed related to a very rapid initial Cr_2O_3 formation which depleted the substrate. The Cr_2O_3 was not a continuous protective layer. The CoO scales which formed later, spalled upon cooling to room temperature. Some $CoCr_2O_4$ also formed and the severe spalling was thought to be attributed to the carbide-induced formation of $CoNb_2O_4$, which is incompatible with the $CoCr_2O_4$ spinel.

The oxidation kinetics of MAR-M-302 (Co-21.5 Cr-10 W-0.85 C-9 Ta-0.2 Zr) have been extensively studied by Felten et al. (30) and Kosak et al. (31) in the temperature range 850 to 1200°C. Felten (30) found that between 850 and 1200°C, the oxidation is diffusion controlled with the formation of Cr_2O_3 (very protective to about 1200°C), $CrTaO_4$ and $CoTa_2O_6$, and that above 1200°C the amount of chromium and tantalum oxides decrease, and CoO, $CoWO_4$ and $CoCr_2O_4$ increase. The oxidation rate of the alloy also increases above 1200°C. Kosack et al. (31) determined two techniques which control the oxidation of the alloy above 980°C: (1) formation of Cr_2O_3 and $CrTaO_4$ according to a parabolic rate law; and (2) the evaporation of WO_3 and Cr_2O_3 according to a linear rate law. The formation of $CrTaO_4$ was due to the preferential oxidation of the tantalum carbides in the matrix (internal oxidation).

It should be noted that in industrial alloys such as MAR-M-302, (31) the attack on inter-metallic phases present in the matrix or grain boundaries may be more detrimental to the life of the material than the formation of an external scale. Internal oxidation is usually enhanced by the presence of carbides or other constituents, such as precipitates at grain boundaries (32). Thermal shock, as well as application of static stress and dynamic stresses (such as encountered in gas turbine operation) during oxidation, also enhances internal oxidation. Thermal shock, in particular, can cause cracking and spalling of protective oxide layers.

Two alloys, FSX-414 (Co-30 Cr-10 Ni-7 W-0.25 C) and FSX-418 (Co-30 Cr-10 Ni-7 W-0.25 C-0.10 Y) exhibited the best oxidation resistance

when compared to the previously mentioned superalloys. This was attributed to the 30% Cr level, which led to formation of greater amounts of Cr_2O_3 and greater scale adherence. The significant improvements due to yttrium in FSX-418 were associated with the (a) almost total suppression of CoO formation, (b) formation of pore-free $MnCr_2O_4$, and (c) vastly improved scale adherence due to a keying or mechanically locking of the external oxide scale to the alloy substrate. Thermogravimetric analysis techniques were employed in order to compare the oxidation rates of these alloys in air at a temperature of 1100°C (33).

B. Hot Corrosion

1. The Nature of the Problem

Hot corrosion was recognized as early as the 1940's as the major cause of fireside deterioration in boilers (34). Attention to "sulfidation" arose on the introduction of the gas turbine engine to marine application. The terms "hot corrosion" and "sulfidation" have in actuality slightly different meanings. The accelerated rate of oxidation which occurs when metals and alloys are coated with (a) salts, (b) liquid metal oxides, and (c) mixtures of the two is commonly called "hot corrosion" (35). "Sulfidation" attack is a form of hot corrosion which occurs when metals and alloys are coated with a salt composed primarily of sodium sulfate (35). Sulfidation or catastrophic oxidation is usually initiated by combustion of a high sulfur-bearing fuel oil (as high as 3.5%) in the presence of sea salt ingested in the intake air (36) to form Na_2SO_4. DeCrescente and

Bornstein (37) have proven that sulfidation occurred only if Na_2SO_4 was present in the condensed state.

There are a number of theories which attempt to explain how the condensation of sodium sulfate on the alloy surface causes fluxing of a normally protective oxide layer such as Al_2O_3 or Cr_2O_3. Simons et al. (46) postulated that the accelerated rates of oxidation associated with sulfidation attack were related to the rapid preferential oxidation of sulfide phases, which were formed when a reducing agent in the alloy reacted with Na_2SO_4. Another group (47,48) postulated that the loss of oxidation resistance was due to chromium-depletion of the alloy at the alloy/oxide interface through the formation of chromium-rich sulfide precipitates. Quets and Dresher (49) indicated that the formation of alkali compounds, i.e., $NaAlO_2$ or Na_2CrO_4, was the necessary driving force to release sulfur for sulfide formation. Bornstein and DeCrescente (50,51), as well as Goebel and Pettit (36,52,53), proposed that the accelerated oxidation observed with nickel-base alloys was related to the inability of the alloy to form a protective oxide scale due to the presence of oxide ions in the Na_2SO_4 layer.

Along with Na_2SO_4, there are other impurities present both in the fuel gas initially and as combustion residues which enter into the corrosion process. The gas turbine environment, therefore, contains O_2, H_2, N_2, CO_2, SO_2, and SO_3 gases as well as gaseous, liquid or solid Na_2SO_4, NaCl, Na_2O, V_2O_5, PbO, and $PbSO_4$ at high temperature, pressure and velocity. It is evident that the hot corrosion or sulfidation mechanism can become quite complex. This was shown by Pantony et al. (38) who studied the corrosion of cobalt in molten

V_2O_5 slags, and the investigation by Bornstein et al. (35) on the effect of vanadium and sodium compounds on the accelerated oxidation of nickel-based alloys. A study (39) was also made on the effect of the presence of lead compounds (PbO and $PbSO_4$) in the environment on the corrosion resistance of alloys, such as MAR-M-302.

Thus, there is a substantial amount of data available concerning the hot corrosion or sulfidation process. Unfortunately, a detailed understanding of the nature of the hot corrosion mechanism cannot be formulated from these data for the following reasons (36):

(1) Hot corrosion degradation can be initiated by a variety of ash deposits and therefore there are probably a number of mechanisms by which this degradation occurs.

(2) Materials ranging from pure metals to complex alloys have been examined but the results of these tests cannot be compared due to the variation in testing procedures.

2. Potential Solutions

There does not appear to be any simple solution to the problem of hot corrosion or sulfidation. A number of methods have been used to combat hot corrosion. These are:

(1) Control or removal of aggressive impurities.

(2) Development of new alloys with improved combination of hot-corrosion resistance and mechanical properties.

(3) Development of protective surface coatings.

The most obvious solution would be to prevent the active constituents in the hot corrosion process from entering the turbine. Sodium can be reduced by using air filtration systems (58), and crank water washing. The sulfur cannot be removed by simple techniques. The trend is to use low-grade fuel oils, which may contain several parts per million of sodium and up to 3% sulfur. It is quite difficult, therefore, to eliminate the aggressive impurities in the hot corrosion process.

At a significant reduction in thermal efficiency, the surface temperature of components in the reaction zone could be reduced to a point where the hot corrosion process could not occur. This, however, is not economically feasible, since the advantages of a higher firing temperature far outweigh the advantages of cooling.

The two most promising solutions to the problem of hot corrosion are development of protective coatings and/or new alloys. There are three major classes of protective coating systems for superalloys: aluminide coatings, metallic claddings or overlay coatings, and glass ceramic coatings. The first practical coating for nickel and cobalt-based superalloys was based on the intermetallic compounds NiAl and CoAl (aluminide coatings) produced by elevated temperature diffusional interaction of aluminum with the substrate alloys (56). Goward (54, 55) recognized these coatings can be lost by periodic spalling of the protective layer, diffusion of aluminum into the substrate, and abrasion of the coating. The addition of yttrium to coatings to improve the spalling resistance of the oxide layer has led to the development of Co-Cr-Al-Y, Ni-Cr-Al-Y, and Fe-Cr-Al-Y coatings, which

which are applied as overlays rather than by diffusion (56,57). Electron beam vapor deposition, sputtering and plasma spraying are the processes currently being used to apply these types of coatings (57).

Within the last ten years, the development of new alloys with an improved combination of hot corrosion resistance and mechanical properties has been accomplished through modification of nickel-chromium and cobalt-chromium based alloys. These modifications have been centered around the use of strengthening mechanisms such as control of grain orientation, dispersion of oxide particles (dispersoids), and dislocation networks (59). Wright (60) has recently shown that the addition of Y_2O_3 dispersoids to Co-Cr-Al alloys improved not only the hot corrosion resistance but the oxidation resistance of this alloy. The addition of the dispersed oxide particles to Co-20 Cr-Al alloys allowed the formation of complete Cr_2O_3 scales at chromium concentrations of 20% or less, instead of the 30% or more required in dispersion-free alloys. As reported previously (61), the cobalt-based alloys exhibited better hot corrosion resistance than comparable nickel-based alloys (60). Both the cobalt and nickel-based alloys contained similar chromium levels and both formed adherent Cr_2O_3 scales. Alumina-forming Co-Cr-Al alloys appeared superior to equivalent Ni-Cr-Al alloys; however, the alloys forming Al_2O_3 scales were more susceptible to hot corrosion than alloys forming Cr_2O_3 scales (60).

3. Gas Turbine Environments

In order to develop a meaningful laboratory test for examining the hot corrosion of materials, it is essential that the

environmental factors within the gas turbine be known. Some of these environmental factors are (62):

(1) Metal temperatures and fluctuations.

(2) Gas temperature and composition and fluctuations.

(3) Gas pressure and velocity.

(4) Presence of certain impurities in the fuel or intake air, e.g., Na, V, K, Pb, etc.

The temperatures to which the alloys are subjected in the engine depend very much on the particular application. A high performance aircraft turbine may have a turbine inlet temperature above 1250°C, but due to blade cooling, the overall metal temperature may be 850-900°C. Dils (63) has shown surface temperature fluctuations greater than 15°C per second for turbines operating at constant power settings. Blades are also highly stressed, e.g., average stresses for an aircraft turbine are 20,000 psi. Thermal cycling of the turbine occurs during normal operation and blade lifetimes vary from 5,000 to 10,000 hours. A typical turbine engine is cooled to room temperature and heated up again for 2 or 3 hours running time (62).

The atmosphere in a turbine is nearly always highly oxidizing, with the exception of take-off and landing where it is fuel rich. Fuel/air ratios have been quoted by Tschinkel (64) as about 0.36 at take-off, dropping to 0.2 during cruising, and as low as 0.05 during idle. The composition of the ingested sea air will be 0.15-0.20 mole fraction oxygen, 0.73 mole fraction nitrogen, and 0.05 mole fraction of both CO_2 and H_2O. The gas pressure, depending on the compression ratio, will be in the 10-20 atm traveling at a velocity of Mach 0.9.

During combustion of a fuel containing 0.5 wt% sulfur, the SO_2 concentration could be of the order of $1x10^{-4}$ mole fraction and the SO_3 concentration will be $0.4x10^{-4}$ to $0.1x10^{-4}$ mole fraction. In actuality, the SO_3/SO_2 mole ratio is around 1/100 due to the fact that only a small portion of the air burns in the primary combustion zone and the residence time in the turbine for this portion will be on the order of 5 to 10 milliseconds (64).

The presence of certain impurities in the fuel or intake air is the cause of hot corrosion. The most important of these are sodium salts, which react with the sulfur in the fuel to form Na_2SO_4. Estimates of the amount of sea salt ingested with the intake air vary from 1.5ppm at 20 feet above sea level to 0.01 ppm at several thousand feet altitude (64). Both Tschinkel (64) and DeCrescente and Bornstein (37) have reported that condensation of Na_2SO_4 should not occur with NaCl concentrations of less than 5 ppm at blade temperatures of 900°C. At temperatures slightly below 800°C, less than 0.1 ppm of NaCl was required for Na_2SO_4 condensation.

Vanadium is present in lower grade fuels and concentrations could be as high as 500 ppm. The vanadium forms a liquid slag layer, which fluxes the protective oxide and allows direct oxidation of the metal to occur. The liquid slag could contain both V_2O_5 and Na_2SO_4.

4. Formation of Na_2SO_4

DeCrescente and Bornstein (37) compared the equilibrium vapor pressure of NaCl to the partial pressure of NaCl as a function of

temperature and pressure. They concluded that NaCl was present in the turbine section as a vapor above 725°C for salt concentrations as high as 1 ppm and at pressures from 1 to 20 atm (engine compression ratio 20 to 1). The NaCl vapor then reacted with the SO_2 or SO_3 gases produced from the combustion of sulfur present in the fuel according to the following equations:

$$2NaCl_{(g)}+SO_{2(g)}+\frac{1}{2}O_{2(g)}+H_2O_{(g)}\rightleftarrows Na_2SO_{4(g)}+2HCl_{(g)} \qquad (19)$$

and

$$2NaCl_{(g)}+SO_{3(g)}+H_2O_{(g)}\rightleftarrows Na_2SO_{4(g)}+2HCl_{(g)} \quad . \qquad (20)$$

They also calculated the equilibrium constants K_p for the temperature range of 430-1230° K at constant temperature. The large values of K_p, 10^{15} at 430 °K to 10^7 at 1030 °K for reaction (20), indicated that formation of Na_2SO_4 and HCl was thermodynamically favored over this temperature range. Therefore, the conversion of NaCl to Na_2SO_4 was expected to be high.

The value of the equilibrium constant K_p at 1000 C and atmospheric pressure was used to calculate the amount of HCl formed (equal to 2 times the amount of Na_2SO_4 formed) from NaCl present in the intake air at a concentration of 1 ppm. The equilibrium constant K_x in terms of of mole fraction (x) of reactant and product varied with pressure according to the relationship:

$$K_x = K_p P_t^{-\Delta n} \quad , \qquad (21)$$

where Δn was the sum of the number of moles of gaseous product minus the sum of the number of moles of gaseous reactants. According to Equation (19), $\Delta n = 2.5$; therefore,

$$K_x = K_p P_t^{2.5} = \frac{X^2_{HCl}}{X_{SO_2} \cdot X_{H_2O} \cdot X_{O_2} \cdot X^2_{NaCl}} \cdot (22)$$

The mole fractions (x) of the reactants and products were calculated and, substituting into Equation (22), it was found that 75% of the NaCl was converted to Na_2SO_4 and HCl. At higher pressures and lower temperatures, almost complete conversion of NaCl to Na_2SO_4 would have to be assumed.

Tschinkel (64) pointed out that above 1100°C, the conversion of NaCl to NaOH would become important according to the following equation:

$$NaCl_{(g)}+H_2O_{(g)} \rightleftarrows NaOH_{(g)}+HCl_{(g)} \qquad (23)$$

and, subsequently, the conversion of NaOH to Na_2SO_4:

$$2NaOH_{(g)}+SO_{3(g)} \rightleftarrows Na_2SO_4(g)+H_2O \ . \qquad (24)$$

Based on equilibrium calculations, Tschinkel (64) also pointed out that: (a) $SO_{3(g)}$ would be dominant at low gas temperatures as during idling, whereas $SO_{2(g)}$ would prevail at high temperatures during take-off; (b) the formation of Na_2SO_4 vapor could occur only at the lower temperatures prevailing in the secondary combustion zone; and (c) Na_2SO_4 vapor dissociated strongly above 1100°C. As a consequence of a, b, c, Na_2SO_4 would condense and deposit on airfoils at low power levels (e.g., during idling) (65).

5. Hot Corrosion Mechanisms of Cobalt-Based Alloys

A number of mechanistic studies on the sulfidation and hot corrosion of pure cobalt and cobalt-based alloys have been undertaken. However, a clear description of the hot corrosion process has still not been provided, due to the inability to compare results from the

various types of hot corrosion tests. Before a survey of these mechanisms can be undertaken, a description of the various testing methods is in order. The ideal test would be to study materials obtained from gas turbines used in actual service. From the discussions on gas turbine environments and formation of Na_2SO_4, it is obvious that conditions could not be adequately controlled in a gas turbine in order to compare one test with another. For this reason, researchers have attempted to evolve suitable laboratory tests, while alloy developers have utilized simulator rig tests. The burner-rigs or dynamic combustors attempt to reproduce, as far as possible, the conditions existing in a gas turbine.

The isothermal crucible test was one of the earliest methods used in the laboratory to evaluate hot corrosion resistance of superalloys. A specimen was completely or partially submerged in a container of fused salt such as Na_2SO_4 or Na_2SO_4-NaCl mixtures at an elevated temperature. Gases could be bubbled through the melt or passed over it to provide oxidizing or reducing environments. Additional variations included alternately dipping and removing the specimens from the melt. The crucible test has been useful in ranking alloys of similar base composition as to their relative hot corrosion resistance.

An alternative laboratory technique was introduced by Simons et al. (46) in which the specimen was first coated with a thin layer of salt (usually 1 mg/cm^2 of Na_2SO_4) and then oxidized in a thermobalance. The major drawback to this test was that the specimen surface was not continually supplied with a coating of

Na_2SO_4. The test therefore proceeded with changing chemical potentials of the Na_2SO_4, since some of the salt was consumed in the corrosion reaction. Modifications of this technique have been introduced such as periodically dipping the sample into molten salt to renew the coating and thermal cycling of the sample.

A recent technique originally suggested by Dean (66) has been used in an attempt to overcome the lack of a continual supply of Na_2SO_4 to the sample surface. In this test, the salt was introduced into the gas stream as a vapor by passing the gases over heated Na_2SO_4 before reacting with the specimen. The Na_2SO_4 is at a higher temperature than that of the specimen so that continual condensation of the Na_2SO_4 was expected.

The burner rig or dynamic combustor tests used by alloy developers such as General Electric and Pratt and Whitney were designed to simulate conditions in a gas turbine. Sulfur-bearing fuel oils (as high as 3.5%) were burnt with air from an auxiliary compressor, and specimens were exposed to the combustion gases downstream. Salt could be introduced either in the fuel or in the air as an aqueous solution of synthetic sea-salt. The majority of these rigs ran at atmospheric pressure and low gas velocities of the order of 50-100 meters/second. There were a few high speed and pressure rigs which ran at a velocity in excess of 300 meters/second and operated at pressures up to 20 atm. The salt content ranged from 1 to 200 ppm, but more recently, salt levels of 1 to 5 ppm have been used (67).

The salt-coated oxidation test (46) was used by Goebel et al. (36) to construct a model for the hot corrosion of pure cobalt.

This model was an extension of suggestions originally proposed by Bornstein and DeCrescente (37,50,51). In this study, specimens of pure cobalt were coated with Na_2SO_4 and then oxidized in air at 1000°C. Initially, a thin oxide layer of CoO was formed beneath the Na_2SO_4; diffusion of oxygen through the molten salt was slow so that the activity of sulfur became sufficient to diffuse through the oxide and react with the metal to form cobalt sulfides. The removal of sulfur from the salt produced a consequent increase in oxide ion activity (that is, the salt became more basic) at the salt-oxide interface. This oxide was reacted with the CoO to form CoO_2^{2-} ions which diffused to the Na_2SO_4/gas interface (region of lower oxide ion activity) where CoO was reprecipitated. The formation of CoO_2^{2-} ions allowed the layer of CoO to be penetrated by the Na_2SO_4 in localized regions, and portions of the oxide then became detached from the metal. Successive layers of oxide were detached by a similar mechanism and the oxidation rate was increased because the oxidation product was formed as a series of discontinuous layers rather than as one dense, continuous and adherent layer. This is "basic fluxing." Metallographic examination of the hot corroded specimens revealed that initially a porous non-protective oxide developed, but in the steady state region, a compact oxide developed beneath this first formed porous oxide.

A recent study by Johnson et al. (68) examined the effect of Na_2SO_4 coatings on the oxidation of pure cobalt in oxygen (P_{O_2}=1 atm) at 900°C. They found the Na_2SO_4 coating produced no initial accelerated attack and, in fact, the rate was consistently reduced by the salt layer. The scale formed on cobalt was compact but the metal/

oxide interface showed marked irregularity with considerable amounts of sulfides present. The fact that sulfur penetrated the protective CoO layer and formed cobalt sulfides indicated that the oxide ion activity (the Na_2O content) of the salt was increased. Also, since there was no increase in the oxidation rate and no change in the scale morphology of the coated specimens, Johnson et al. (68) concluded that either: (a) the oxide ion activity increased, but not sufficiently enough to form cobaltate ions CoO_2^{2-}; or (b) such a cobalt containing species as CoO_2^{2-} does not exist. Coupons of CoO were subsequently reacted with Na_2SO_4 made artificially basic by additions of Na_2O to determine if the formation of CoO_2^{2-} was possible. The coupon showed considerable weight loss and it appeared that CoO_2^{2-} could be formed. Therefore, the basicity achieved during the coating test was insufficient to flux the CoO and it was concluded that the "basic fluxing" mechanism was of minor importance in the hot corrosion of cobalt. A further study by Johnson et al. (69), utilizing a technique originally developed by Dean (66) for continual deposition of Na_2SO_4 at the sample surface, confirmed that, at 950°C, basic fluxing did not occur.

When hot corrosion first became a problem, it was found that chromium was the key element in preventing severe high temperature corrosion. Davin et al. (23) studied the hot corrosion of Co-10 Cr and Co-30 Cr alloys in an atmosphere of burnt fuel oil (sulfur content 1%) and air from 800 to 1000°C. Brine was also injected into the combustion furnace to ensure formation of Na_2SO_4. At 1000°C, the Co-10 Cr was heavily corroded, while the Co-30 Cr alloys showed good resistance. Microprobe examination of the Co-10 Cr alloy

revealed that the scale consisted of several layers. A Cr_2O_3 layer was found adjacent to the metal. The next layer was composed of a mixture of Cr_2O_3 and CrS, followed by a cobalt sulfide layer, and finally by an outer layer of CoO. It was concluded that the Na_2SO_4 acted as a reducing agent, causing elemental sulfur to form and attack the subjacent metal. Additions of aluminum, tantalum, and yttrium to the Co-30 Cr alloy led to some improvement in the corrosion resistance of the base alloy. It was also noted that cobalt-based alloys exhibited better hot corrosion resistance than corresponding nickel-based alloys. Kaufman (70) examined a number of experimental alloys based on Co-25 Cr and found the corrosion resistance was better than the Ni-25 Cr-based alloys. From further studies, Wagenheim (71) concluded that chromium was beneficial up to 30% and yttrium was also beneficial in improving the corrosion resistance of cobalt-based alloys.

Goebel et al. (36) studied the catastrophic oxidation of cobalt-chromium and cobalt-aluminum alloys which contained tungsten or molybdenum. The specimens were coated with 0.5 mg/cm^2 of Na_2SO_4 and oxidized under cyclic conditions in pure oxygen (P_{O_2} = 1.0 atm) at 1000°C. Fresh Na_2SO_4 was applied to the sample surface prior to each two-hour oxidation cycle. An alloy such as Co-25 Al-12 W, which forms a protective scale of Al_2O_3 during normal oxidation, was used as an example to explain the Na_2SO_4-induced catastrophic oxidation. During the initial stages of oxidation, an Al_2O_3 scale was formed. The Al_2O_3 was not penetrated via the basic fluxing process as was the case for pure cobalt. This was because the tungsten (or molybdenum) oxides, which were formed initially along with the Al_2O_3 scale, reacted with the Na_2SO_4 and decreased the

concentration of oxide ions in the Na_2SO_4 by forming WO_4^{2-} ions. Under cyclic conditions or long isothermal exposure, the Al_2O_3 scale cracked and allowed the Na_2SO_4 to penetrate to the metal surface where it reacted with tungsten (or molybdenum). The modified Na_2SO_4 (WO_3^- rich) reacted with the CoO via an acidic fluxing reaction to form a porous outer scale of CoO and Al_2O_3. Alloys such as Co-25 Cr-12 W, Co-25 Cr-6 Mo, and Co-25 Al-6 Mo were observed to undergo catastrophic oxidation according to the acidic fluxing mechanism.

Goebel et al. (36) noted that high chromium contents in cobalt-based alloys were beneficial in providing hot corrosion resistance regardless of the type of degradation mechanism. The Cr_2O_3 scales formed on Co-35 Cr alloys were not penetrated by the Na_2SO_4.

Johnson, Whittle and Stringer (68,72) designed a program to study the applicability of the salt-fluxing models described by Goebel et al. (36) to cobalt-based systems. They also wanted to verify that cobalt-based alloys were superior in hot corrosion to nickel-based alloys. In the preliminary study (68), Co-Cr, Co-W, and Co-Cr-W alloys were coated with Na_2SO_4 (0.5 to 1.85 mg/cm^2) prior to suspension in a helical pyrex spring thermobalance in oxygen (P_{O_2}=1 atm) at 900°C. The oxidation rate of Co-7.5 W increased compared to pure cobalt when coated with Na_2SO_4. A loose, porous CoO scale was formed as the salt became acid. This implied that the "acid fluxing" mechanism was operative, with the cobalt being removed into the salt presumably as Co^{2+} and oxidized at the outer surface of the Na_2SO_4 to form a porous CoO layer. The function of

chromium was found to be more complicated. For alloys which contained 20% Cr or less, the degree of accelerated oxidation produced by Na_2SO_4 was independent of the chromium content. There was evidence that the salt became more acid for these alloys, but the lower stability of sodium chromate meant that the salt would not become as acid as in the case of the Co-W alloys. Therefore, the acid fluxing process was not initiated. Alloys with greater than 25% Cr exhibited low-accelerated oxidation rates. This was attributed to the formation of a continuous Cr_2O_3 scale which was unaffected by the salt and blocked the outward diffusion of cobalt.

In a further study (72), Johnson et al. described the Na_2SO_4 induced accelerated oxidation of commercial nickel and cobalt-based superalloys. The superalloys which formed protective Al_2O_3 scales such as B1900, IN.713LC and MAR-M-246 were found to be more susceptible to Na_2SO_4 induced oxidation than Cr_2O_3-forming alloys such as X-40 and MAR-M-509. The following sequence of reactions was suggested for alloys forming Al_2O_3 scales:

(a) Acidic fluxing occurs, producing an outer, porous oxide layer and sulfides within the alloy.

(b) The outer porous layer falls away from the surface.

(c) The sulfides penetrate further into the alloy followed by internal oxidation; a protective oxide layer cannot be re-established due to severe depletion of the required reactive element.

A similar sequence of events was applicable for Cr_2O_3-forming alloys, with the exception of the first step. Cr_2O_3 layers have to be rendered ineffective either by thermal cycling or spalling due to

the presence of NaCl in the gas stream. Additions of refractory elements, tungsten, molybdenum or niobium which are present in most superalloys as solid solution strengtheners caused acidic fluxing by reacting with the oxide ions in the condensed Na_2SO_4.

Johnson et al. (72) concluded that acidic fluxing is more important than basic fluxing as evidenced from the above discussion. Acidic fluxing could be prevented by the rapid establishment of a protective Cr_2O_3 layer. The stability of Cr_2O_3 layer under acidic conditions accounted for the superiority of cobalt-based alloys over nickel-based alloys, since most cobalt-based alloys contain higher levels of chromium.

The behavior of cobalt and nickel-based superalloys was also studied by Johnson et al. (69) under conditions of a continual supply of Na_2SO_4 to the sample surface. The normally corrosion-resistant Co-25 Cr alloy was found to undergo acidic fluxing. It was found that the protective Cr_2O_3 layer was removed due to the formation of Na_2CrO_4. Considerable penetration of sulfur into the alloy and precipitation of chromium-rich sulfide particles in the grain boundaries then occurred. Additions of aluminum and manganese were found to reduce the formation of Na_2CrO_4 slightly, since both of these elements have a higher affinity for sulfur than chromium.

The effect of carbon on the hot corrosion of cobalt-based alloys was studied by El-Dahshan et al. (72). Carbon is present in most cobalt-based superalloys since it is required for the formation of carbides for strengthening. It was thought to react with the chromium to form stable chrome carbides; thus reducing

the chromium content of the matrix. Both crucible and coated specimen tests were used. The samples were immersed in Na_2SO_4 at 900°C up to 100 hours. These results indicated that pure Na_2SO_4 was relatively inactive towards Co-Cr alloys containing up to 2% C.

Finally, Sims et al. (73) summarized the behavior of cobalt and nickel-based superalloys when tested in a burner rig or dynamic combustor which simulates a gas turbine environment. They found that cobalt-based alloys such as X-40 and FSX-414 had excellent overall hot corrosion resistance up to 1900°F when compared to nickel-based alloys.

IV. EXPERIMENTAL PROCEDURES

A. General Description of Experimental Methods

The rate of oxidation and hot corrosion of pure cobalt and a series of cobalt-based alloys containing varying amounts of chromium and silicon were determined by continuous thermogravimetric measurements for both isothermal and thermal cycling tests. The isothermal oxidation studies were performed in an atmosphere of dry oxygen at 0.1 atmospheric pressure. Both the isothermal and cyclic hot corrosion studies were conducted utilizing a continuous supply of Na_2SO_4 to the sample surface. A constant reaction temperature of 1000°C was maintained for all experiments. The oxide layers which formed were then examined by metallographic, x-ray diffraction and microprobe techniques.

B. Thermogravimetric Analysis (TGA)

1. Thermobalance

An Ainsworth Type FV-AU-1 automatic recording microbalance with a capacity of 5 grams and a full scale range of 1.0 mg was used in this investigation. The balance sensitivity was 0.01 mg with a readability of 0.001 mg and reproducibility of $\pm$ 0.003 mg. Beam deflections caused by weight changes were transmitted to a strip-chart recorder which recorded the weight change as a function of time. A flow of helium was maintained in the bell jar and pyrex tube connecting the balance with the reaction chamber to prevent any of the corrosive gases in the reaction chamber from reaching the balance assembly.

2. Reaction Chambers

The balance was mounted above the furnace and the specimens were suspended by a quartz fiber into the hot zone of the reaction chamber for oxidation tests,while a platinum chain was used for the hot corrosion tests. The balance-furnace-reaction chamber assembly is shown schematically in Figure 2. The same type of reaction chamber was used for both the oxidation and hot corrosion experiments as shown in Figure 3. The reaction chamber, which was a Mullite (MV-30) tube (1.0"O.D.),was positioned inside an outer chamber of Vycor. The inner Mullite tube was necessary to preclude interaction between the Na_2SO_4 used in the hot corrosion studies and the Vycor chamber. For the hot corrosion experiments,an alumina crucible containing approximately two grams of Na_2SO_4 was positioned on top of the lower thermocouple well.

The design of the reaction chamber enabled the gases to be preheated prior to entering the reaction zone. Gas preheating was utilized in order to aid in maintaining a uniform temperature of 1000°C at the sample surface. The gas flow is shown in Figure 2. Reference thermocouple wells were also placed as close as possible to the sample and alumina crucible in order to provide an accurate temperature measurement of the two hot zones inside the reaction chamber.

3. Furnace and Controller

A two-zone furnace was constructed by dual winding a Mullite (MV-30) furnace tube. Each zone, approximately the same length, was non-inductively wound with Kanthal A-1 wire at nine

Figure 2. Balance-Furnace-Reaction Chamber Assembly.

A. Ainsworth automatic recording balance (FV-AU-1)

B. Pyrex bell jar

C. Brass disc with 2-mm diameter hole

D. Pyrex-brass seal

E. Pyrex tube

F. Vycor fiber

G. O-ring

H. Pyrex tube 275 mm long with 6 mm inside diameter

I. Ground glass joint

J. Vycor fiber

K. Steel guide rods

L. Furnace guide tubes

M. Sample suspended in hot zone-1

N. Inner Mullite reaction chamber

O. Outer Vycor tube

P. High temperature Mullite furnace tube

Q. Refractory cement

R. Kanthal A-1 furnace winding; zone-2

S. Kanthal A-1 furnace winding; zone-1

T. Furnace shell

U. Alumina crucible containing Na_2SO_4 in hot zone-2

V. Lower thermocouple well

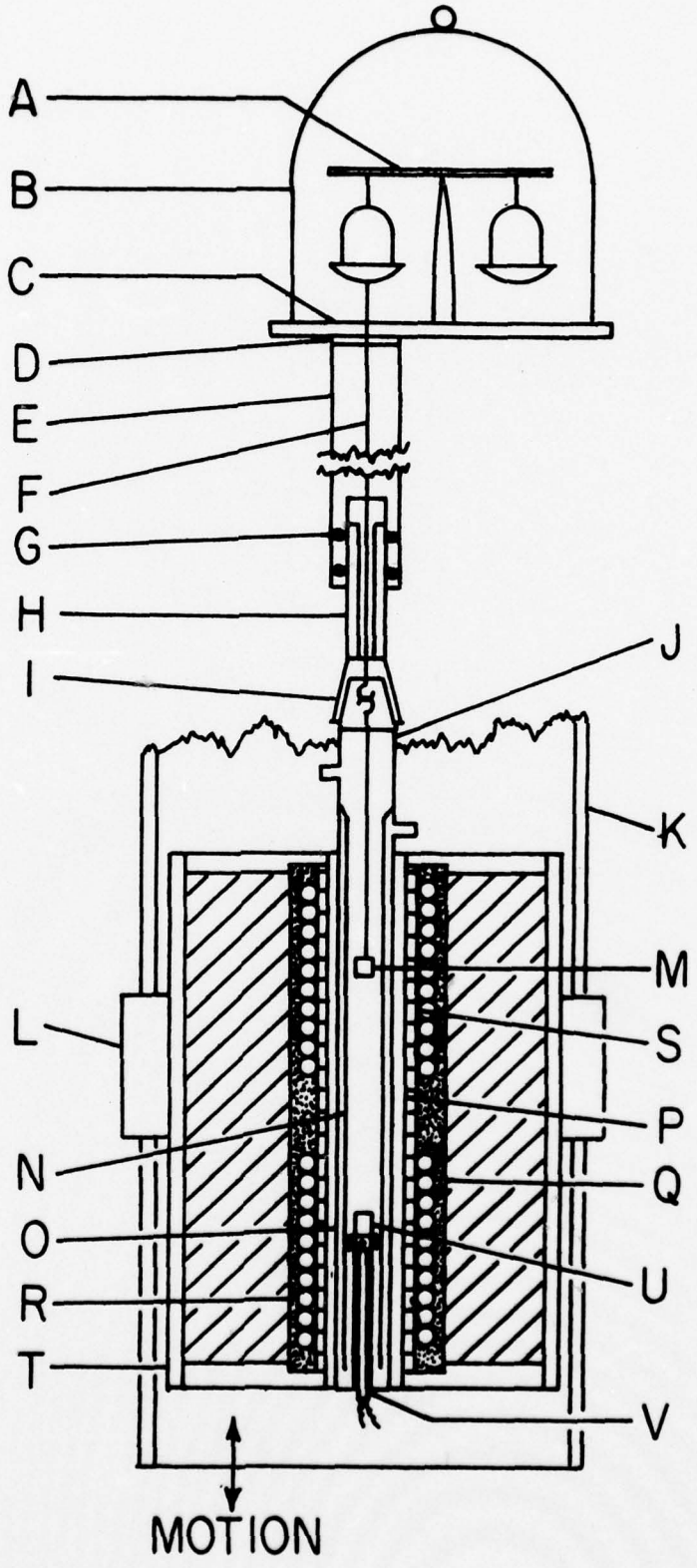
A
B
C
D
E
F
G
H
I
J
K
L
M
S
P
N
Q
O
U
R
T
V
MOTION

Figure 3. Reaction chambers for oxidation and hot corrosion studies.

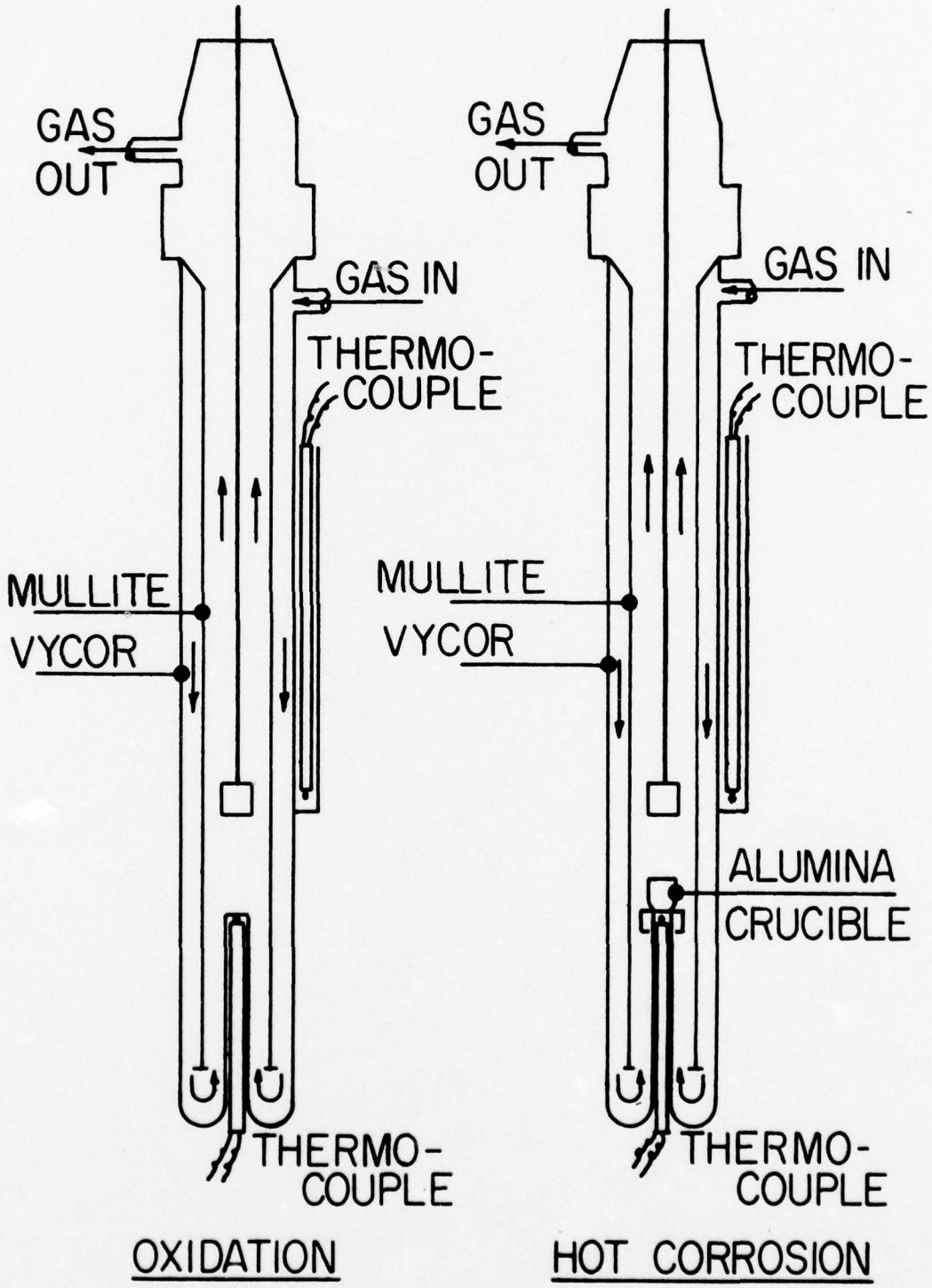
GAS
OUT
GAS IN
THERMO-
COUPLE
MULLITE
VYCOR
THERMO-
COUPLE
OXIDATION
GAS
OUT
GAS IN
THERMO-
COUPLE
MULLITE
VYCOR
ALUMINA
CRUCIBLE
THERMO-
COUPLE
HOT CORROSION

turns per inch. Alumina beads were used to insulate the Mullite furnace tube from the steel furnace shell.

The temperature of each hot zone was maintained by a Leeds and Northrup controller to within $\pm$ 2°C. The controlling thermocouples(platinum-platinum-10% rhodium) were encased in Mullite tubes, which were cemented adjacent to the furnace windings. Reference thermocouples of platinum-platinum-10% rhodium were used to measure the temperature of each hot zone inside the reaction chamber. This temperature was correlated to the temperature measured by the controlling thermocouples. The controllers were then adjusted to maintain a temperature of 1000°C in the upper hot zone (specimen-containing zone) and 1050°C in the lower hot zone (zone containing the Na_2SO_4 in an alumina crucible during the hot corrosion experiments).

Provision was also made to permit thermal cycling of the specimen by periodically raising and lowering the furnace. This was accomplished by connecting a motor-gear drive assembly, which was operated by a timer, to the furnace shell.

4. Gas Preparation

The gases used in this investigation were commercial-grade oxygen, helium, hydrogen and a special mixture of oxygen + 0.15 vol.% SO_2 obtained from Airco, Inc., which was utilized in the hot corrosion experiments. The hydrogen was passed through a commercial catalytic purifier in order to react the oxygen present as an impurity with hydrogen to form water vapor. The water

vapor was then removed by passing the gas through a Drierite ($CaSO_4$) column. Helium was purified by first passing it through a copper oxide catalyst at 175°C to react any hydrogen, present as an impurity, with the copper oxide to form water vapor. The helium was then dried by passing it successively through a magnesium perchlorate column, two Ascarite columns, and a Drierite column. The dry helium was then passed through a sintered copper pellet catalyst at 175°C to remove any oxygen, present as an impurity, followed by a magnesium perchlorate column and a liquid nitrogen trap to remove any residual water vapor. The pure oxygen and (oxygen + SO_2) gases were passed through a Drierite column to remove water vapor.

Manometric flowmeters were used to regulate the gas flow, so that the desired ratio of these gases could be obtained for the oxidation or hot corrosion reactions. Di-butyl phthalate was used in the manometers and in the blow-off columns of all flowmeters. The flowmeters were calibrated by measuring the rate at which the gas from a flowmeter displaced a soap bubble up a column of known volume. After the gases were metered, they were passed through a mixing chamber to insure uniform composition.

C. Materials and Sample Preparation

Oxidation and hot corrosion experiments were carried out on pure cobalt, cobalt-chromium, cobalt-silicon, and cobalt-chromium-silicon alloys. The alloys were produced by melting the constituent metals in an induction furnace under an inert atmosphere of helium. Base materials for the alloys were cobalt metal grade V.P. (99.9% Co) from Materials Research Corp., silicon metal (99.09% Si, 0.01% Ca,

0.01% Al, 0.49% Fe), and electrolytic chromium (99.8% Cr, 0.2% Fe). Analyses of the materials used in this study are given in Tables 1 and 2.

The ingots obtained were homogenized at 1020°C for 24 hours in an evacuated Vycor tube. Samples approximately 11 mm x 9 mm x 1.3 mm were then cut from the ingots and a 1.59 mm (1/16 inch) hole was drilled through the sample to facilitate suspending the coupon by quartz fibers from the balance pan. The coupons were then polished through 120, 240, 320, 400, and 600 grit silicon carbide paper. Just prior to suspending the sample in the reaction chamber, the coupon was again polished with 600 grit to ensure all oxide films had been removed, and then rinsed with acetone to degrease them. This sample preparation procedure was maintained throughout to ensure a valid comparison and analysis of the experimental data.

D. Experimental Method

1. Oxidation

An oxidation run was initiated by suspending a sample from the balance into the reaction chamber by quartz fibers. The balance was then tared, and the gas lines and reaction chamber were flushed with purified helium for thirty minutes. Helium was also introduced into the bell jar and pyrex tube connecting the balance with the reaction chamber to prevent any of the corrosive gases from reaching the balance assembly. The helium flow to the chamber was terminated and purified hydrogen was introduced at a flow rate of 38 cm^3/min. Five minutes after initiation of the hydrogen flow, the furnace was raised and the sample brought to reaction temperature (1000°C).

TABLE 1

ANALYSIS OF PURE COBALT METAL AS SUPPLIED BY THE MATERIALS RESEARCH CORPORATION

Impurities are given in ppm (1 ppm = .0001 wt %)

Impurities	
Cobalt	balance
Oxygen	44.0
Nitrogen	0.9
Carbon	17.0
Boron	14.0
Lithium	0.003
Flourine	8.4
Sodium	3.6
Magnesium	26.0
Aluminum	2.2
Silicon	15.0
Sulfur	71.0
Chloride	2.9
Potassium	2.2
Calcium	0.9
Chromium	10.0
Manganese	5.8
Iron	52.0
Nickel	150.0
Copper	9.5
Arsenic	4.6
Selenium	9.8
Tellurium	7.8

Other impurities not listed were not detected and have concentrations less than 0.5 ppm.

TABLE 2

ANALYSES OF ALLOYS PREPARED BY INDUCTION MELTING

Alloy Designation (Nominal Composition)	Chromium	Silicon	Cobalt
Pure Cobalt	----	----	balance
Co-0.1 Cr	0.064	----	balance
Co-0.5 Cr	0.50	----	balance
Co-2.5 Cr	2.44	----	balance
Co-5.0 Cr	4.87	----	balance
Co-10.0 Cr	9.74	----	balance
Co-15.0 Cr	14.65	----	balance
Co-0.01 Si	----	0.03	balance
Co-0.05 Si	----	0.06	balance
Co-0.1 Si	----	0.11	balance
Co-0.5 Si	----	0.47	balance
Co-1.0 Si	----	1.00	balance
Co-2.5 Si	----	2.47	balance
Co-5.0 Si	----	4.94	balance
Co-10.0 Si	----	9.98	balance
Co-5.0 Cr-1.0 Si	4.77	0.98	balance
Co-5.0 Cr-2.5 Si	4.89	2.46	balance
Co-5.0 Cr-5.0 Si	4.85	4.92	balance
Co-5.0 Cr-10.0 Si	4.97	9.95	balance
Co-10.0 Cr-1.0 Si	9.84	0.98	balance
Co-10.0 Cr-2.5 Si	9.80	2.44	balance

TABLE 2 (Cont.)

Alloy Designation (Nominal Composition)	Chromium	Silicon	Cobalt
Co-10.0 Cr-5.0 Si	9.81	4.97	balance
Co-10.0 Cr-10.0 Si	10.01	9.84	balance
Co-15.0 Cr-1.0 Si	14.82	0.99	balance
Co-15.0 Cr-2.5 Si	14.85	2.40	balance
Co-15.0 Cr-5.0 Si	14.85	4.88	balance
Co-15.0 Cr-10.0 Si	14.84	9.73	balance

The sample was annealed in hydrogen for thirty minutes to remove stresses and to reduce any oxide films that had remained on the surface. The weight losses were negligible during this time. The hydrogen gas flow was then stopped and helium was introduced at a flow rate of 180 cm^3/min. for 25 minutes to flush the chamber. After the 25-minute period, purified oxygen at a flow rate of 20 cm^3/min, was mixed with the helium to initiate the oxidation process. The partial pressure of oxygen was maintained at 0.1 atm. On termination of the run, the oxygen flow was stopped and the furnace lowered. The sample was cooled to ambient temperature in a helium atmosphere. Run duration was approximately 2800 minutes, with some runs being extended to 10,000 minutes.

2. Hot Corrosion

A hot corrosion run was initiated by first positioning an alumina crucible containing approximately two grams of Na_2SO_4 on top of the lower thermocouple well inside the reaction chamber. The sample was then suspended in the chamber with a platinum chain. The platinum chain was necessary, since quartz and Na_2SO_4 will react at 1000°C and form a molten phase. Helium gas was then introduced as previously described for the oxidation runs. However, hydrogen gas was not introduced into the reaction chamber as was the case for the oxidation experiments. After an initial 30-minute helium purge, the furnace was raised and the sample in the upper hot zone was brought to 1000°C, and the alumina crucible containing the Na_2SO_4 in the lower hot zone was brought to 1050°C. The purified helium continued to pass through

the reaction chamber at a flow rate of 180 cm^3/min. for 25 minutes. At the end of this period, a mixture of dry oxygen plus 0.15 vol.% SO_2 was introduced at a flow rate of 20 cm^3/min. with the helium to initiate the hot corrosion process.

The Na_2SO_4 was introduced into the gas stream as a vapor by passing the gases (P_{O_2} =0.1 atm) over the heated sodium sulfate (1050°C). The gas stream was then directed over the sample surface which was at a lower temperature (1000°C) than the salt. Condensation of the Na_2SO_4 on the sample surface was therefore expected. The temperature of the salt, 1050°C, which was maintained throughout the hot corrosion experiments, controlled the vapor pressure of the sulfate in the gas stream, and hence its concentration in the gas stream. According to the calculations of DeCrescente and Bornstein (37), the vapor pressure of Na_2SO_4 at 1050°C corresponded to a partial pressure of 0.1 torr. The run was terminated by stopping the oxygen gas flow and lowering the furnace. The sample was cooled to ambient temperature in a helium atmosphere. Run duration was 2800 minutes for all hot corrosion experiments.

E. Examination of the Oxides Formed After Oxidation and Hot Corrosion

The mechanism of oxidation and hot corrosion cannot be adequately defined by using only reaction rates obtained by thermogravimetric analyses. It is also necessary to examine the scale morphology to determine the nature of the oxide and the distribution of elements present in the scale. This was accomplished by x-ray diffraction, electron microprobe analysis, and metallographic examination.

1. X-ray Diffraction

Prior to polishing the oxidized specimens for microprobe and microscopic examination, some of the oxide was removed, ground and then placed in a glass capillary tube for x-ray analysis using a Debye-Scherrer powder diffraction camera. The capillary tube was mounted in the camera, film loaded, and a collimated beam of FeK_{α} radiation was directed at the sample through a manganese oxide filter. The sample was exposed for various times ranging from 10 to 14 hours with the angle of incidence varying as the sample was rotated through 360 degrees. This reduced any effects which might be produced by preferred orientation. The 2θ angle of diffraction line was measured and the interplanar spacing (d), corresponding to each line, was determined using tabulated values of d versus 2θ for FeK_{α} radiation. By using the x-ray powder diffraction file and the values of d, qualitative identification of the oxide compounds contained in the scale was made.

A technique for obtaining a diffraction pattern from a thin film oxide layer (less than 20 microns) using the Debye-Scherrer camera was also developed. The oxidized or hot corroded specimen was mounted in the camera, the film was loaded, and the specimen exposed to FeK_{α} radiation for a period of 3 to 4 hours. The angle of incidence varied from 6 to 12 degrees depending on the oxide film thickness. Qualitative identification of the oxide compounds was made by comparing the thin film diffraction pattern with a pattern obtained by the powder diffraction method, where the d values corresponding to each line were previously determined.

2. Microprobe Analysis and Metallographic Examination

Prior to microprobe analysis and metallographic examination, the samples were mounted in epoxy utilizing a coal petrographic technique in order to prevent the oxide layer from spalling during subsequent cross-sectioning and polishing. After placing the specimens in epoxy, the sample container was placed under vacuum, followed by centrifuging. This technique forces the epoxy into the pores and cracks of the oxide layer. The mounted coupon was then cross-sectioned and polished (final polish with magnesium oxide <0.5μ). An ETEC autoprobe with a spot size of 1 to 2μ, which produced a radiated sample area 5 to 10 times the impinging beam size, was used for the microprobe analysis. Before a quantitative distribution of the oxide compounds in the scale could be obtained, an elemental qualitative analysis had to be performed. The qualitative distribution of cobalt, chromium and silicon in the oxide layer was accomplished through the use of energy dispersive analysis (EDA), elemental x-ray mapping, and line profiles. The quantitative distribution of the oxide compounds present in the scale such as CoO, Cr_2O_3, SiO_2, and the spinels $CoCr_2O_4$ and Co_2SiO_4, previously identified by x-ray analysis, was accomplished through the use of well-characterized standards. A printout of the analysis in weight % was obtained using a slave computer.

In addition to microprobe analysis, the scale morphology was studied with the aid of a Vickers metallograph. Photomicrographs were taken of representative oxide samples at various magnifications up to 700 x.

V. RESULTS AND DISCUSSION

A. Pure Cobalt

1. Oxidation

The rate of oxidation of cobalt metal to cobaltous oxide (CoO) was determined in oxygen at a pressure of 0.1 atmosphere and temperature of 1000°C. The observed value of the parabolic rate constant (K_p) for pure cobalt of 138×10^{-10} $gm^2 \cdot cm^{-4} \cdot sec^{-1}$, given in Table 3, was determined by taking the slope of the straight line which resulted from plotting values of $(\Delta m/A)^2$ as a function of time. The experimental results were compared to those obtained by Bridges et al. (8) and Carter and Richardson (7). Bridges et al. (8), during an investigation of the oxidation behavior of cobalt from 800° to 1200°C over the oxygen pressure range 0.013 to 27.2 atm., determined a K_p of 104×10^{-10} $gm^2 \cdot cm^{-4} \cdot sec^{-1}$ for pure cobalt at 1000°C and a P_{O_2} of 0.125 atm. They also observed that the oxidation rate increased as the oxygen partial pressure increased, thus confirming that CoO is a p-type semiconductor, since increasing the P_{O_2} increases the point defect concentration along with the oxidation rate.

The slight difference in the oxidation rates of pure cobalt found in this investigation as compared to others can be attributed to the impurities present in the pure cobalt. Bridges et al. (8) used high-purity electrolytic cobalt with an average impurity content <5 ppm as compared to the cobalt metal used in this study where impurities as high as 150 ppm were found as shown in Table 1. Since CoO is a p-type semiconductor, an increased oxidation rate results as concentrations of higher valent cations increase in the compound.

Oxidation of pure cobalt results in a double-layered scale. The outer layer consists of a columnar structure with some porosity and cracks, while the inner layer contains irregularly-shaped pores. A slight separation can be seen between the two layers. Examination of the scale by x-ray diffraction and microprobe analysis showed a homogenous composition of 99 to 100 wt.% CoO for both layers.

The porosity of the inner layer may be due to vacancy condensation at the metal/oxide interface. As the cobalt ions diffuse outward through a vacancy mechanism, an equal number of cobalt vacancies move in the reverse direction. At the metal/oxide interface, the vacancies must be removed; this can occur either through plastic deformation or through formation of pores.

The experimental results have shown that cobalt metal oxides according to the parabolic rate law and that the reaction proceeds by cation diffusion across the oxide film to the oxide/gas interface.

2. Hot Corrosion

The hot corrosion behavior of pure cobalt was examined by exposing the sample surface to a continuous supply of Na_2SO_4. In this test, the salt is introduced into the gas stream (P_{O_2} = 0.1 atm P_{SO_2} = 0.00153 atm) as a vapour by passing the gases over heated Na_2SO_4 before they reach the sample surface. The temperature of the salt (1050°C) is higher than that of the specimen (1000°C) so that continued condensation of the sodium sulfate is expected. This technique overcomes one of the major disadvantages of the salt coating test utilized

in a previous study on the hot corrosion of nickel-based alloys (43) in which there was a limited amount of salt available.

Figure 4 shows the effect of Na_2SO_4 condensation on the oxidation of pure cobalt at 1000°C and P_{O_2} = 0.1 atm. with P_{SO_2} = 0.00153 atm. The condensation of Na_2SO_4 on the sample surface did not produce a significant increase in the oxidation rate. The total weight gain after 1800 minutes for the hot-corroded sample was 38.78 mg/cm^2 compared to 38.12 mg/cm^2 for the oxidized sample. The corresponding parabolic rate constants are 150×10^{-10} $gm^2 \cdot cm^{-4} \cdot sec^{-1}$ for the hot corrosion sample and 138×10^{-10} $gm^2 \cdot cm^{-4} \cdot sec^{-1}$ for the oxidized sample as given in Table 3.

The scale formed on the hot corrosion specimen is double-layered as was the case for the oxidized specimen. The inner layer is a fine-grained structure containing small irregular-shaped pores, while the outer layer is compact with some large longitudinal-shaped pores. The metal/oxide interface shows some irregularity with the oxide grains becoming elongated or columnar near the metal surface. No evidence of sulfide formation was found from metallographic examination.

Examination of the scale by x-ray diffraction and microprobe analysis indicated a uniform distribution of 98 to 99 wt. % CoO for both layers. The probe did not find any traces of sodium or sulfur within the scale.

The experimental results indicate pure cobalt does not undergo accelerated oxidation at 1000°C (P_{O_2} =0.1 atm.+P_{SO_2} =0.00153 atm.) when exposed to a continuous supply of Na_2SO_4 at the sample surface, as it was

Figure 4. Weight Gain ($\Delta m/A$) as a Function of Time for the Oxidation and Hot Corrosion of Pure Cobalt at 1000°C and P_{O_2} = 0.1 atm.

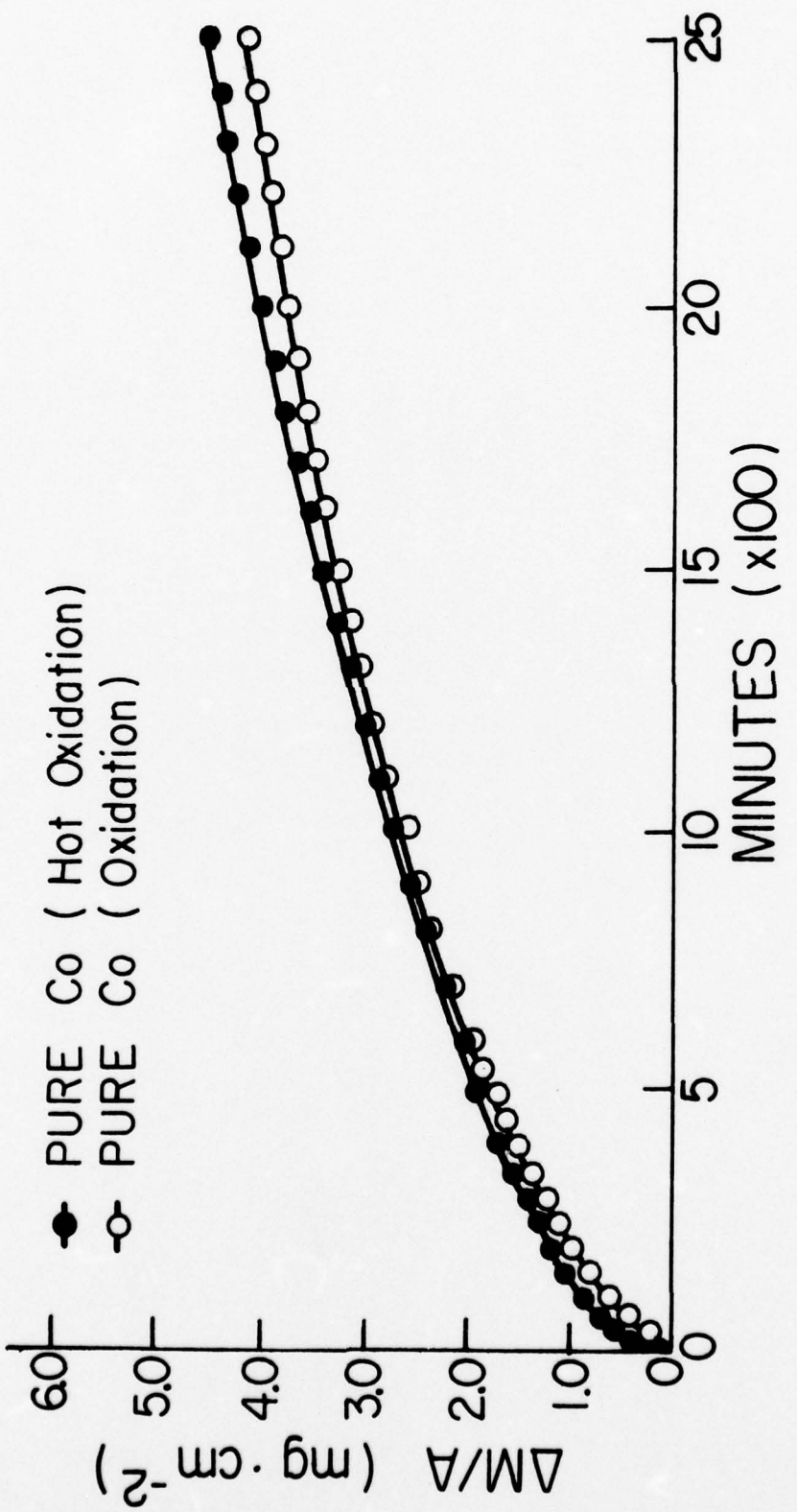
PURE Co (Hot Oxidation)
PURE Co (Oxidation)
ΔM/A (mg · cm⁻²)
6.0
5.0
4.0
3.0
2.0
1.0
0
0
5
10
15
20
25
MINUTES (x100)

for pure nickel coated with Na_2SO_4 (43). These results are in agreement with those obtained by Johnson et al., who studied the oxidation of pure cobalt and cobalt-based alloys utilizing both the salt-coating test (68) and a continuous supply of Na_2SO_4 to the sample surface (69). Johnson et al. (68,69) postulated that basic fluxing of CoO by Na_2SO_4 does not take place because the basicity of yhr Na_2SO_4 is not increased enough to flux the CoO and form CoO_2^{2-} ions. The basic fluxing model for pure cobalt described earlier was postulated by Goebel et al. (36). No explanation can be given for the absence of an inner layer of Co_3S_4 which was reported by both Johnson et al. (68,69) and Goebel (36). A more detailed microprobe examination of the metal/oxide interface is required.

B. Cobalt-Chromium Binary Alloys

1. Oxidation

The scaling behavior of a series of Co-Cr alloys, varying in composition from 0.10 to 15 weight percent chromium was studied at 1000°C and P_{O_2} of 0.1 atm. The results of the thermogravimetric studies are presented in Figures 5 and 6, and Table 3. Figure 5 shows the weight gain ($\Delta m/A$) as a function of time for some of the alloys oxidized, and the parabolic rate constants listed in Table 3 are shown in Figure 6 as a function of weight percent chromium.

In all cases, the oxidation is well-described by the parabolic rate law. An interesting anomaly, however, was observed for chromium additions of up to 2.5 wt.%; i.e., for Ni-Cr alloys, the oxidation rate did not increase significantly (43). The parabolic rate constants observed for Co-0.1 Cr and

Figure 5. Weight Gain ($\Delta m/A$) as a Function of Time for the Oxidation of Co-0.5 Cr and Co-15 Cr Alloys as Compared to Pure Cobalt. All at 1000°C and P_{O_2} = 0.1 atm.

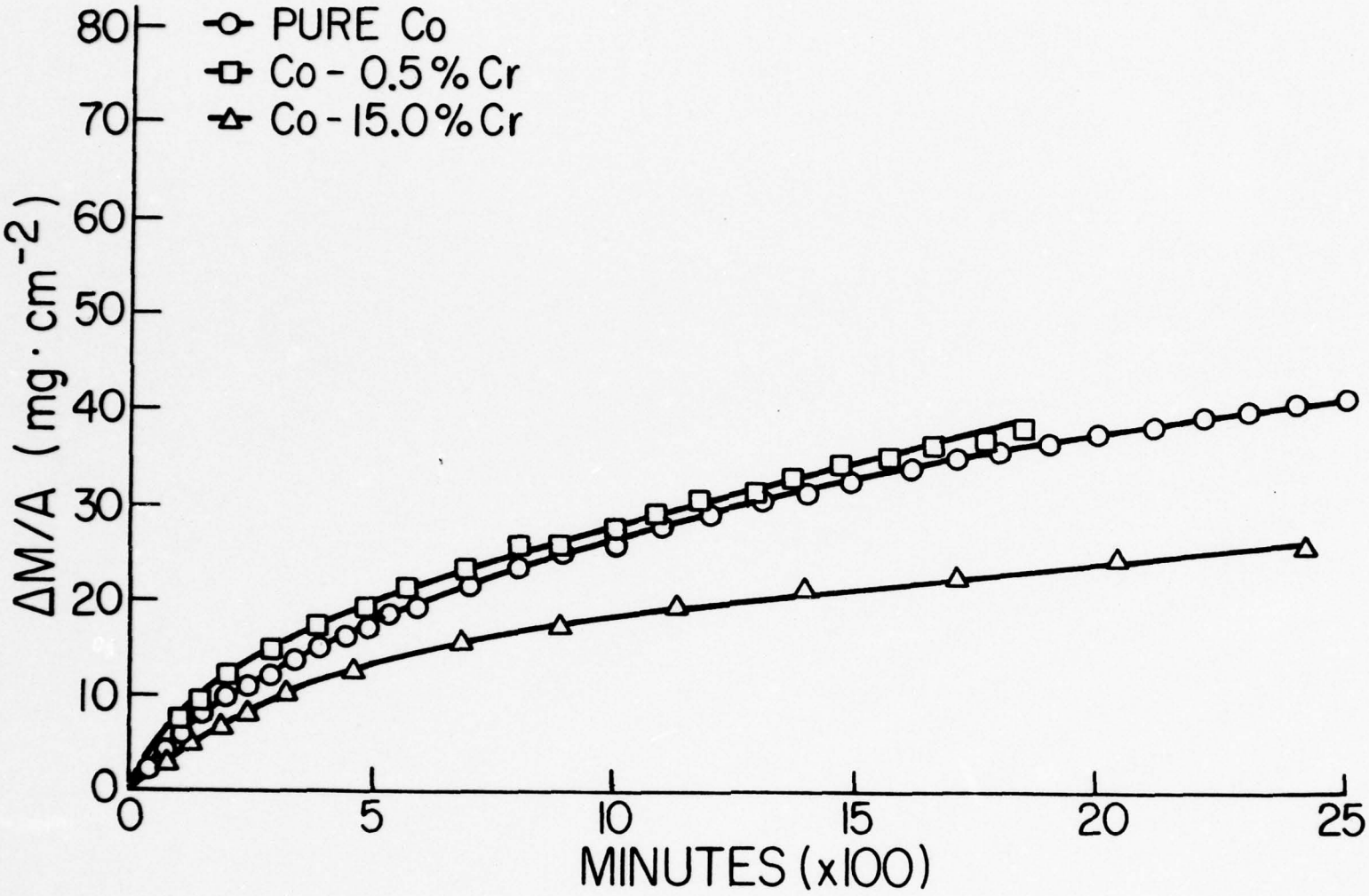
PURE Co
Co - 0.5% Cr
Co - 15.0% Cr
ΔM/A (mg · cm⁻²)
80
70
60
50
40
30
20
10
0
0
5
10
15
20
25
MINUTES (x100)

Figure 6. Parabolic Rate Constants (K_p) of Cobalt-Chromium Alloys as a Function of Weight Percent Chromium in an Oxidizing Environment at 1000°C and P_{O_2} = 0.1 atm.

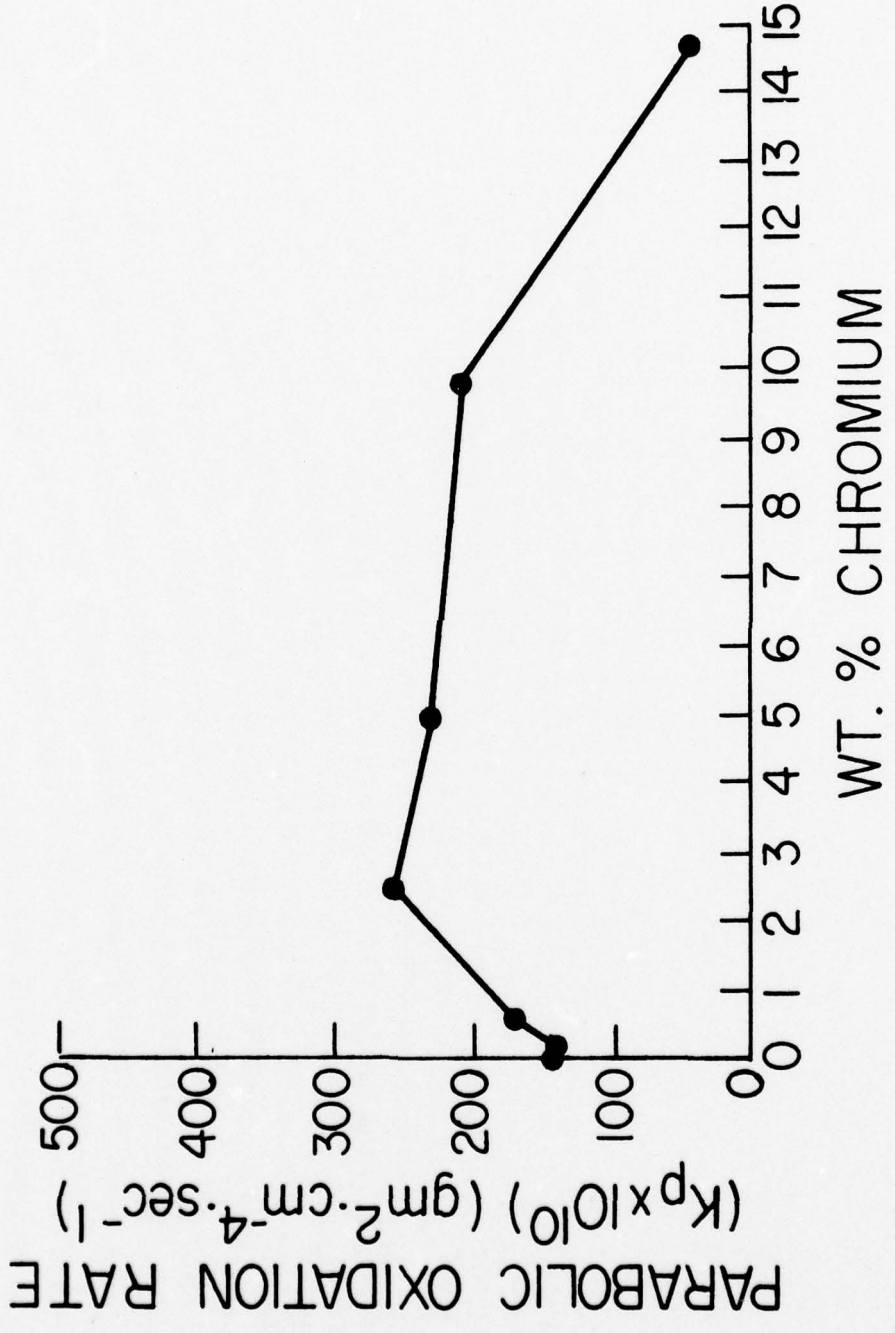
PARABOLIC OXIDATION RATE
($K_p \times 10^{10}$) ($gm^2 \cdot cm^{-4} \cdot sec^{-1}$)
500
400
300
200
100
0
0 1 2 3 4 5 6 7 8 9 10 11 12 13 14 15
WT. % CHROMIUM

TABLE 3

PARABOLIC OXIDATION RATES AND WEIGHT CHANGE INFORMATION

FOR PURE COBALT AND COBALT-CHROMIUM ALLOYS

Wt. %-Cr (Nominal)	Oxidation		Hot Corrosion	
	K_p	Total $\Delta M/A$ (1800 Min)	K_p	Total $\Delta M/A$ (1800 Min)
0.00	138	38.12	150	38.8
0.10	140	38.3	---	---
0.50	170	41.5	---	---
2.5	260	51.14	---	---
5.0	230	48.56	---	---
10.0	210	46.50	---	---
15.0	40	23.50	48	23.90

K_p units ($gm^2 \cdot cm^{-4} \cdot sec^{-1} \times 10^{10}$)

$\Delta M/A$ units ($mg \cdot cm^{-2}$)

Co-0.5 Cr alloys were 140 and 170×10^{-10} $gm^2 \cdot cm^{-4} \cdot sec^{-1}$, respectively, as compared to 138×10^{-10} $gm^2 \cdot cm^{-4} \cdot sec^{-1}$ for pure cobalt. These results are in contrast to those reported by various other investigators (18,19,20), where an increase in the oxidation rate for up to 10 wt. % chromium additions was reported. However, it should be noted that in virtually all of the previous investigations, no attempt was made to study the oxidation behavior of cobalt-chromium alloys with less than 8% chromium additions.

It is apparent from the above results that the semiconductor valence approach cannot be used to explain the oxidation of Co-Cr alloys with less than a few percent chromium.

Metallographic examination of the scale formed on the Co-0.1 Cr specimen did not reveal a double-layered structure. There was some porosity at the metal/oxide interface which also displayed a surface roughening effect. The composition of the oxide was CoO as determined by x-ray diffraction. Oxidation of the Co-0.5 Cr specimen resulted in a double layer with identical structures separated by a very small band of porosity. It was difficult to determine if the structure observed was in fact double-layered. The scale was composed entirely of CoO. Examination of the scale formed on the Co-2.5 Cr specimen did show a double-layered structure which is typical of Co-Cr alloys up to 25 wt. % Cr (24,20). The outer layer is compact with little porosity while the inner layer contained many large irregular-shaped pores. Surface roughening was also observed at the metal/oxide interface as well as a thin zone of internal oxidation. Both layers were composed of CoO.

It appears that the microstructures of the scales formed on these alloys were responsible for their anomalous oxidation behavior at high temperatures (78). It was also noted that increasing the chromium content enhanced scale adherence and reduced the tendency of the scale to crack when compared to the pure cobalt sample. This could enhance the cyclic behavior of the oxide layer.

The scales formed on Co-5 Cr and Co-10 Cr were similar in structure to that of Co-2.5 Cr with the exception of an increasing amount of porosity in both layers. However, the composition of the scale differed due to the formation of the spinel $CoCr_2O_4$, which was detected by x-ray diffraction. The formation of $CoCr_2O_4$ is a result of the reaction between CoO and Cr_2O_3 and is reported to be 10 times faster than the growth rate of $NiCr_2O_4$ (24). Unfortunately, no microprobe analyses were performed on these alloys, but it is assumed that the $CoCr_2O_4$ is contained within the inner layer and that the outer layer contains CoO.

The decrease in oxidation rate for the Co-15 Cr specimen is attributable to a direct "blocking" effect by either Cr_2O_3 or an increased amount of spinel (see discussion below). The microstructure of Co-15 Cr shown in Figure 7 is typical of a double layer. The inner layer contains irregularly-shaped pores, while the outer layer contains large triangular-shaped pores. It has been discussed (20) that an expanding inner layer places the outer layer under tension. This tension is relieved partially by the growth of the outer layer and partially by plastic deformation and creep. It was proposed that the pyramid-like pores in the outer layer result from mechanical shear and deformation. Microprobe analysis was performed on this alloy and a typical profile is

Figure 7. Micrographs of the Scales Formed on Co-15 Cr After Oxidation and Hot Corrosion at 1000°C and P_{O_2} = 0.1 atm.

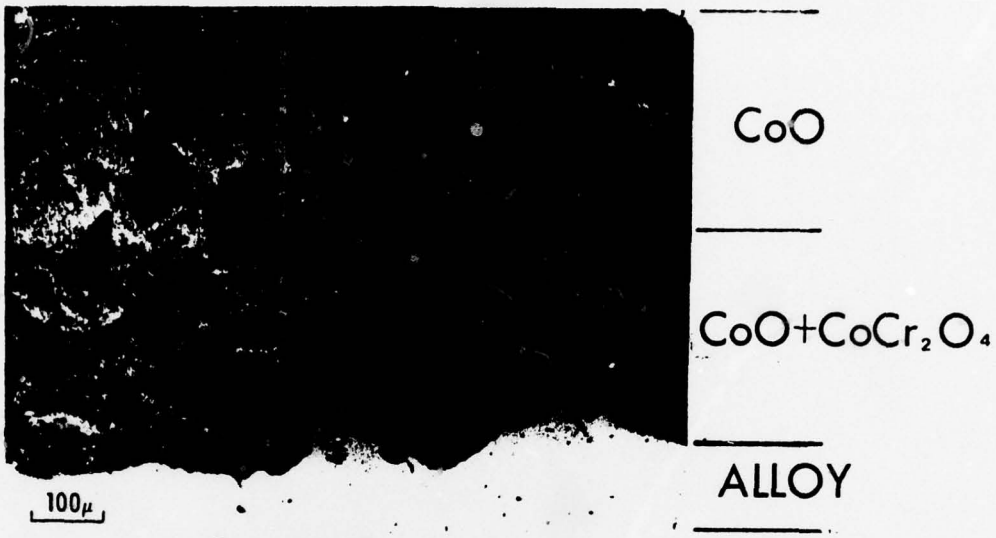

Co—15 Cr
(OXIDATION)
200 X

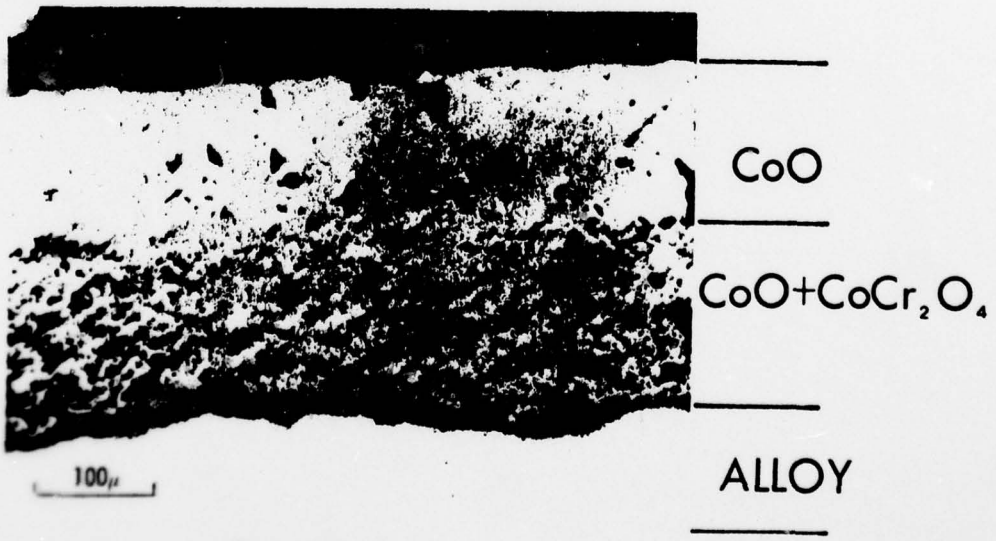

Co—15 Cr
(HOT CORROSION)
200 X

shown in Figure 8. This confirms that the inner layer has a high chromium content in the form of $CoCr_2O_4$, and that a sharp gradient exists at the interface of the two layers with the outer layer consisting of greater than 99 wt. % CoO.

The high-temperature oxidation of Co-10 Cr and Co-2 5 Cr was studied by Kofstad and Hed (20, 21) in the temperature range 800° to 1300°C at oxygen pressures from 0.2 to 760 torr. Since they observed an increase in oxidation rate for Co-10 Cr and a decrease for Co-2.5 Cr as compared to pure cobalt, their conclusions concerning the oxidation of Co-10 Cr are of interest to this study and will be discussed.

When considering the solid state diffusion processes in complex scales, such as was found on the Co-15 Cr specimen, the relative rates of diffusion of cobalt, chromium, and oxygen in CoO, Cr_2O_3, and $CoCr_2O_4$ are of primary importance. Carter and Richardson (5,6) and others (20) have shown that cobalt diffusion in CoO is three orders of magnitude faster than diffusion of Co or Cr in $CoCr_2O_4$ and two orders faster than that of Cr in Cr_2O_3. Oxygen diffusion in CoO, Cr_2O_3, and probably $CoCr_2O_4$ is slower than that of the cobalt or chromium ions. The diffusion of Co in the CoO phase is therefore the predominant process in the oxidation, and the presence of dispersed $CoCr_2O_4$ or Cr_2O_3 particles in the inner layer serves to effectively reduce the solid state diffusion area.

During the initial oxidation period, CoO and Cr_2O_3 form simultaneously. A continuous oxide film is built by diffusion of Co ions outward through the CoO phase. Internal oxidation of chromium to Cr_2O_3 probably occurs through solid state diffusion of oxygen at the same time. After the outer layer of CoO is formed, oxygen for the internal

Figure 8. Microprobe Profile of the Scale Formed on Co-15 Cr After Oxidation and Hot Corrosion at 1000°C and P_{O_2} = 0.1 atm.

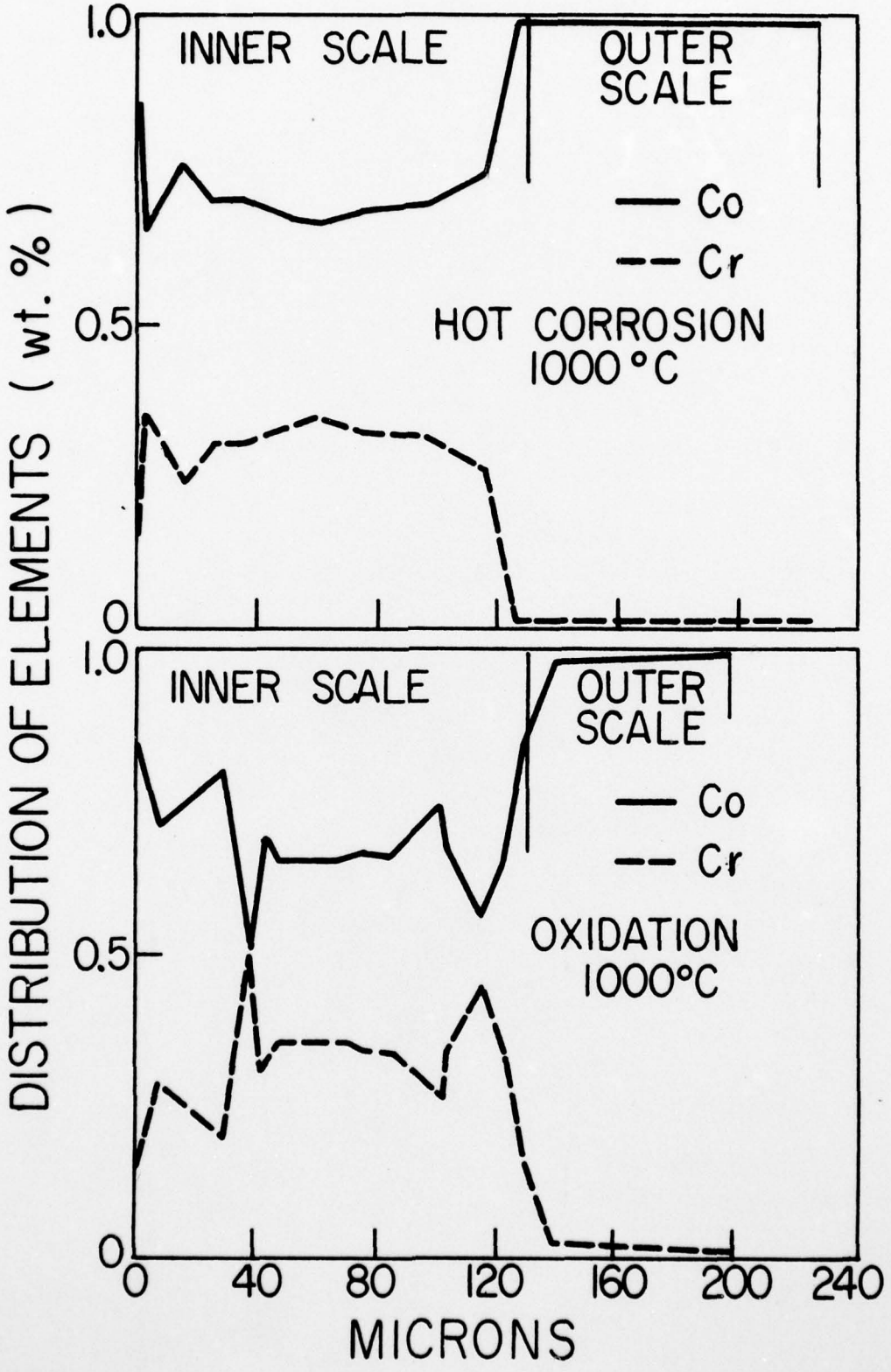
1.0
INNER SCALE
OUTER SCALE
Co
Cr
0.5
HOT CORROSION
1000 °C
0
1.0
INNER SCALE
OUTER SCALE
Co
Cr
0.5
OXIDATION
1000°C
0
DISTRIBUTION OF ELEMENTS (wt. %)
0
40
80
120
160
200
240
MICRONS

oxidation process can only be obtained by decomposition of CoO. The cobalt ions formed from the decomposition of CoO diffuse outward and a cavity is formed replacing CoO molecules. The particles of Cr_2O_3 can also serve as vacancy condensation sites and porosity can accumulate at the surface of the Cr_2O_3 particle.

The porosity correspondingly reduces the available area for solid state diffusion but the transport of gaseous oxygen is enhanced across the pores. The Cr_2O_3 particles eventually become surrounded by pores and partially by CoO. The Cr_2O_3 and CoO gradually react to form $CoCr_2O_4$, which could explain the absence of a continuous film of Cr_2O_3 anywhere within the scale.

The oxidation results for the Co-Cr alloys show that the overall reaction is parabolic in nature and that the porosity formed in the scales aids in the transport of oxygen across the cavities. Furthermore, the formation of the spinel, $CoCr_2O_4$, blocks the solid state diffusion of cobalt ions by reducing the solid state diffusion area.

2. Hot Corrosion

Based on the results obtained for the oxidation of Co-15 Cr, it was decided to study this alloy under hot corrosion conditions. The parabolic rate constant observed under hot corrosion conditions was 48×10^{-10} $gm^2 \cdot cm^{-4} \cdot sec^{-1}$ as compared to 40 $gm^2 \cdot cm^{-4} \cdot sec^{-1}$ for the oxidized specimen as shown in Table 3. The kinetic data indicate no marked differences between the oxidation and hot corrosion of Co-15 Cr.

Metallographic examination of the scales formed after hot corrosion revealed a double-layered structure with an inner porous layer and an outer more compact layer. The hot corrosion specimen also exhibited

much less porosity in the outer layer than the oxidized specimen as shown in Figure 7. Microprobe analysis showed a more uniform distribution of chromium in the inner layer as compared to the profile for the oxidized specimen, as shown in Figure 8. The outer layer is composed of 99 wt. % CoO for both oxidation and hot corrosion. No trace of sodium or sulfur was detected by the probe.

The hot corrosion of cobalt-chromium alloys has been studied by various investigators (23,67,68,72). It was found that the degree of acceleration of the oxidation rate usually decreased as the chromium content was increased. At chromium contents greater than 20%, a protective layer of Cr_2O_3 usually formed which was unaffected by the salt (68,72). Since the oxidation rate of Co-15 Cr did not increase under conditions of a continuous supply of Na_2SO_4 to the sample surface, it can be concluded that the formation of the spinel $CoCr_2O_4$ and possibly Cr_2O_3 as dispersed particles, which are not fluxed by the Na_2SO_4, block the outward diffusion of cobalt ions. This also reduces the amount of porosity within the scale.

C. Cobalt-Silicon Binary Alloys

1. Oxidation

The oxidation rates for a series of cobalt-silicon alloys varying in composition from 0.01 to 10 wt. % silicon were determined at an oxygen pressure of 0.1 atm. and 1000°C. The oxidation kinetics for some of these alloys are shown in Figure 9. The corresponding parabolic rate constants listed in Table 4 were then plotted as a function of weight percent silicon in the alloy as shown in Figure 10.

Figure 9. Weight Gain ($\Delta m/A$) as a Function of Time for the Oxidation and Hot Corrosion of Selected Cobalt-Silicon Alloys at 1000°C and P_{O_2} = 0.1 atm.

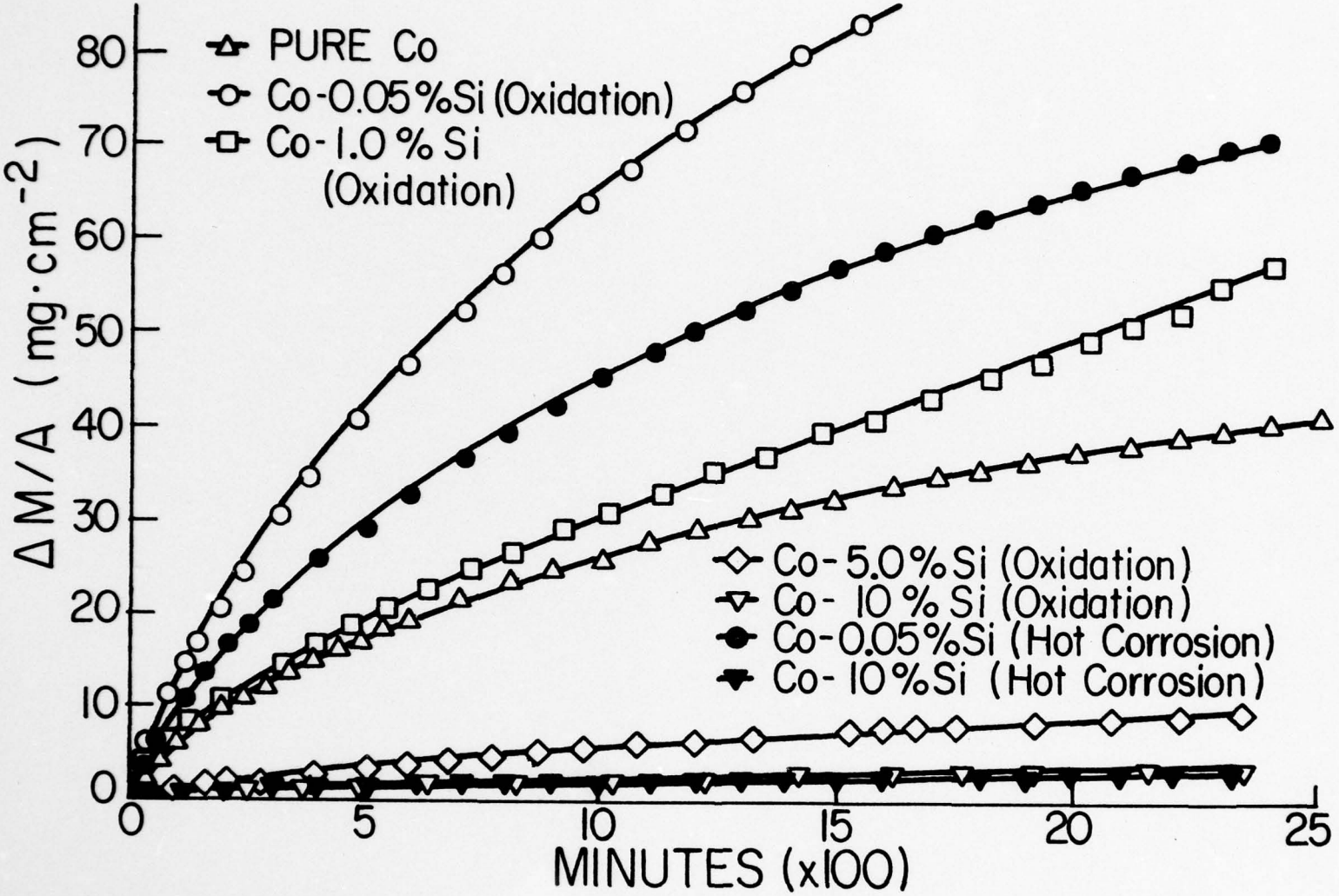
PURE Co
Co-0.05%Si (Oxidation)
Co-1.0 % Si
(Oxidation)
Co-5.0%Si (Oxidation)
Co- 10 % Si (Oxidation)
Co-0.05%Si (Hot Corrosion)
Co- 10%Si (Hot Corrosion)
ΔM/A (mg·cm⁻²)
MINUTES (x100)
0
10
20
30
40
50
60
70
80
0
5
10
15
20
25

Figure 10. Parabolic Rate Constants (K_p) of Cobalt-Silicon Alloys as a Function of Weight Percent Silicon in an Oxidizing Environment at 1000°C and P_{O_2} = 0.1 atm.

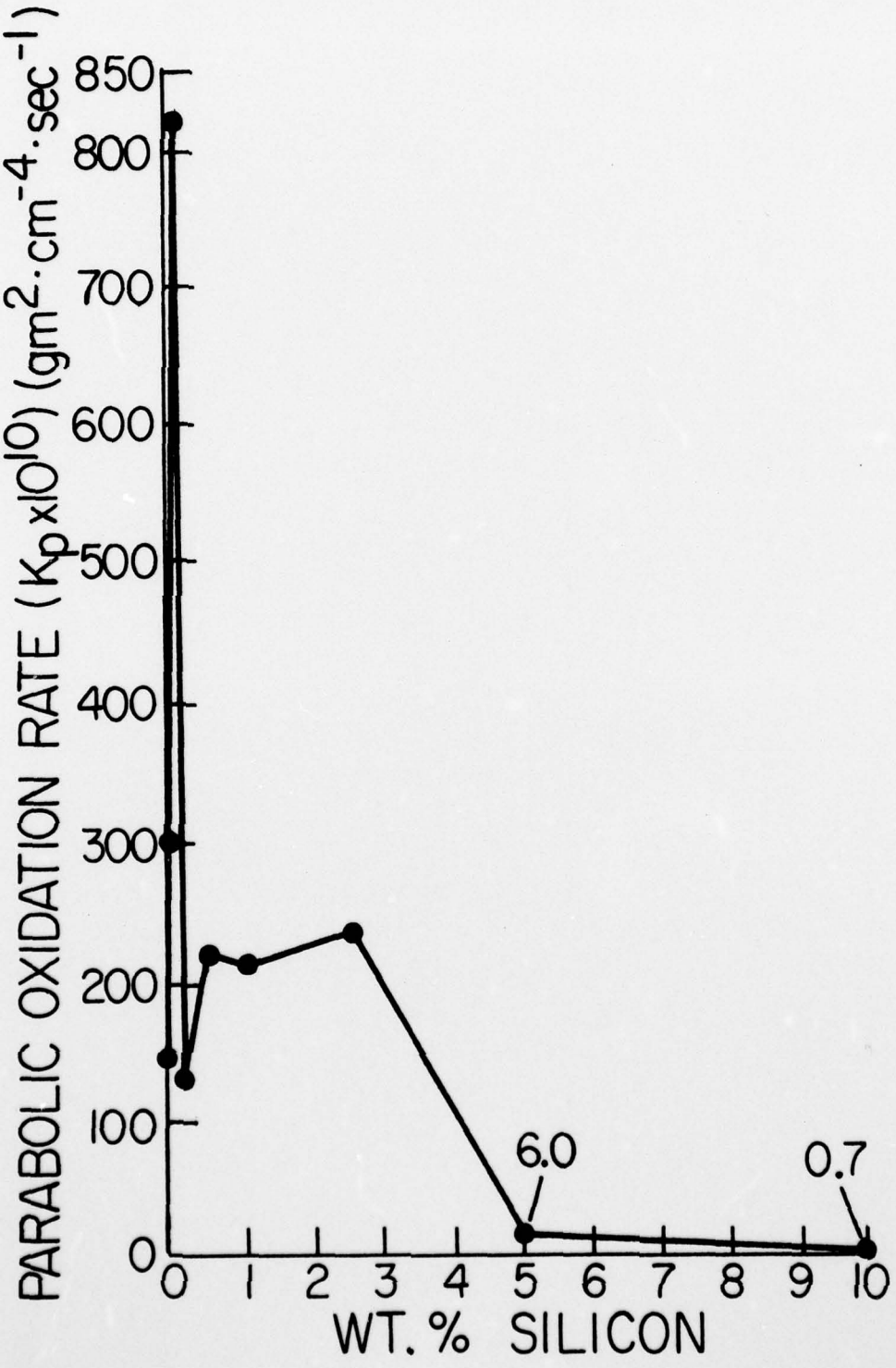
PARABOLIC OXIDATION RATE ($K_p \times 10^{10}$) ($gm^2 \cdot cm^{-4} \cdot sec^{-1}$)
850
800
700
600
500
400
300
200
100
0
6.0
0.7
0 1 2 3 4 5 6 7 8 9 10
WT. % SILICON

The increase in oxidation rates for Co-0.01 Si (K_p = $301x10^{-10}$ $gm^2 \cdot cm^{-4} \cdot sec^{-1}$) and CoO-0.05 Si ($K_p$ = $833x10^{-10}$ $gm^2 \cdot cm^{-4} \cdot sec^{-1}$) alloys as compared to the oxidation rate for pure cobalt (K_p = $138x10^{-10}$ $gm^2 \cdot cm^{-4} \cdot sec^{-1}$) can be interpreted in terms of the Wagner point defect theory. This theory states that small additions of higher valent cations such as Si^{4+} ions to a p-type semiconductor such as CoO will cause an increase in the number of cobalt ion vacancies and hence an increase in the oxidation rate. Metallographic examination of the scale formed on the Co-0.05 Si alloy showed a double-layered structure with a very porous outer layer and a more compact inner layer. The large amount of porosity observed may be responsible in part for the increased oxidation rate, since the cavities partially short-circuit the diffusion of oxygen through the scale. The total scale thickness was 800 microns. Analysis by microprobe techniques showed the average composition of each layer to be 99 wt. % CoO. Initial examination of the scale by x-ray diffraction did reveal the presence of some Co_3O_4, which probably may form when CoO is cooled. The excess oxygen in the CoO may precipitate in the form of Co_3O_4 (20,8).

Alloys with greater than 2.5 wt. % silicon additions exhibited a decrease in the oxidation rate as shown in Figure 10. The x-ray diffraction studies of the scales formed on these alloys show the composition to be predominantly CoO. The scale formed on Co-2.5 Si (K_p = $233x10^{-10}$ $gm^2 \cdot cm^{-4} \cdot sec^{-1}$) did contain a small percentage of the spinel Co_2SiO_4. The presence of Co_2SiO_4 could account for the reduction in the doping effect of Si^{4+} along with a corresponding decrease in the oxidation rate for these alloys, since the diffusion

of Co through Co_2SiO_4 would be slower than through CoO. The dispersed particles of Co_2SiO_4 serve to effectively reduce the solid-state diffusion area in the inner oxide layer. Another possibility is the formation of a thin (<10 microns) layer of SiO_2 adjacent to the metal/oxide interface. Microprobe analysis of the metal/oxide interface is quite difficult, since the irradiated surface area (10 to 20 microns) is greater than the width of the thin film of SiO_2; consequently, interference from the metal substrate usually occurs when probing in this region.

The results obtained for the oxidation of Co-5 Si and Co-10 Si show a sharp decrease in the oxidation rate as compared to pure cobalt. The parabolic rate constants for Co-5 Si and Co-10 Si alloys are 6 and 0.7x 10^{-10} $gm^2 \cdot cm^{-4} \cdot sec^{-1}$, respectively, as listed in Table 4. The microstructure of the Co-5 Si alloy shown in Figure 11 consists of a double-layered scale approximately 20 microns thick as compared to an average scale thickness of 300 microns for pure cobalt. The inner layer is compact, while the outer layer is extremely porous with a highly irregular outer surface. The presence of CoO, Co_2SiO_4 and some Co_3O_4 was confirmed by x-ray diffraction. Microprobe analysis indicated a homogenous distribution of 90 wt. % CoO and 10 wt. % Co_2SiO_4 throughout the scale.

The oxidation of the Co-10 Si specimen resulted in an irregular thin film (10 microns), containing small pores accompanied by internal oxidation along the metal/oxide interface, as shown in Figure 12. The scale was composed of CoO, Co_2SiO_4 and some Co_3O_4 as identified by x-ray diffraction.

The parabolic oxidation rates obtained for the cobalt-silicon binary alloys indicate the reaction is controlled by solid-state

TABLE 4

PARABOLIC OXIDATION RATES AND WEIGHT CHANGE INFORMATION

FOR COBALT-SILICON ALLOYS

Wt. %-Cr (Nominal)	Oxidation		Hot Corrosion	
	K_p	Total ΔM/A (1800 Min)	K_p	Total ΔM/A (1800 Min)
0.00	138	38.12	150	38.8
0.01	301	56.00	---	---
0.05	833	90.00	393	62.91
0.10	129	37.70	---	---
0.50	220	48.00	---	---
1.00	210	44.50	---	---
2.50	233	48.30	---	---
5.00	6	7.47	---	---
10.00	0.7	2.40	0.367	1.80

K_p units ($gm^2 \cdot cm^{-4} \cdot sec^{-1} \times 10^{-10}$)

ΔM/A units ($mg \cdot cm^{-2}$)

Figure 11. Micrograph of the Scale Formed on Co-5 Si After Oxidation at 1000°C and P_{O_2} = 0.1 atm. for 2800 minutes.

AD-A053 745 PENNSYLVANIA STATE UNIV UNIVERSITY PARK APPLIED RESE--ETC F/G 11/6
HOT CORROSION AND OXIDATION STUDIES ON COBALT-BASED ALLOYS.(U)
JUL 77 V F HOCK N00017-73-C-1418
UNCLASSIFIED ARL/PSU/TM-77-274 NL

2 OF 2
AD A053745

END
DATE FILMED
6 -78
DDC

Co—5 Si
(OXIDATION)
500 X

Figure 12. Micrographs of Scales Formed on Co-10 Si After Oxidation and Hot Corrosion at 1000°C and P_{O_2} = 0.1 atm. for 2800 minutes.

Co—10 Si
(OXIDATION)
500 X

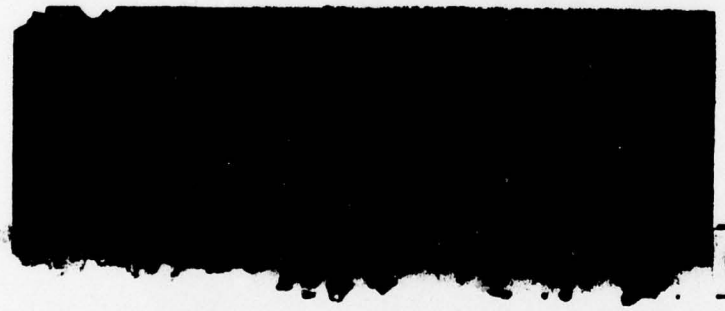

Co—10 Si
(HOT CORROSION)
500 X

diffusion of the cobalt ions. However, since the scales formed are generally double-layered containing more than one oxide phase, the transport through the scale becomes complex. A transport mechanism is postulated based on the assumption that the diffusion of Co in CoO is faster than in Co_2SiO_4 and much faster than in SiO_2. Since self-diffusion data are not available for Co in Co_2SiO_4, the assumption is based on the previously discussed cobalt-chromium system, where it has been shown that Co diffuses slow in Cr_2O_3 and $CoCr_2O_4$ than in CoO.

The initial oxidation, especially of the alloys containing the higher silicon contents, probably involves the simultaneous formation of CoO and SiO_2. After a continuous film is formed, the oxidation becomes controlled by the outward diffusion of the cobalt ions through the CoO phase. The CoO phase continues to grow on top of the alloy surface. The considerable porosity present may be associated with the decomposition of CoO at the metal/oxide interface, which produces oxygen ions for the internal oxidation of silicon to SiO_2 particles. The correspondingly formed cobalt ion will then diffuse outward through the CoO layer. The removal of one CoO molecule may then result in cavity formation. The cobalt ions also continue to diffuse from the metal/oxide interface but their diffusion path is blocked by the SiO_2 particles, which can serve as sites for cobalt vacancy condensation. This will also create porosity or cavities. The available area for the solid-state diffusion of cobalt is continually reduced by the formation of SiO_2 particles and cavities. The SiO_2 particles surrounded by CoO eventually react to form the Co_2SiO_4 spinel. In all the oxides examined in this study, no evidence of an SiO_2 phase was found.

In postulating any transport mechanism for cobalt ions within the scale, the blocking effect by the spinel and the rapid short-circuiting transport of oxygen across the cavities must be taken into account.

2. Hot Corrosion

The two alloys chosen for exposure to the hot corrosion environment previously described were Co-0.05 Si and Co-10.0 Si. Figure 9 shows the effect of condensation of Na_2SO_4 on the specimen surface at 1000°C. The total weight gain after 1800 minutes was 62.91 mg/cm^2 for Co-0.05 Si and 1.80 mg/cm^2 for Co-10 Si, which is about 2/3 of the total weight gain for the oxidized specimens. The corresponding parabolic rate constants are 393 and 0.367 $gm^2 \cdot cm^{-4} \cdot sec^{-1}$. for Co-0.05 Si and Co-10.0 Si, respectively.

The scale formed on the Co-0.05 Si specimen after hot corrosion retained the double-layered structure but differed in appearance from the oxidized specimen. The inner layer which comprised over 60% of the total scale thickness of 580 microns was compact and contained small irregular pores. The outer layer was quite porous with a separation of the oxide bands occurring near the oxide/gas interface. Examination of the scale by x-ray diffraction and microprobe analysis showed the composition of both layers to be 99 wt. % CoO.

Metallographic examination of the scale formed on Co-10 Si after hot corrosion revealed a microstructure similar to that of the

oxidized sample, as shown in Figure 12, but with less internal oxidation on the hot corroded sample. The total scale thickness was approximately 10 microns. Microprobe analysis showed the composition to be either 90% CoO + 10% Co_2SiO_4 or 80% CoO + 20% Co_2SiO_4. The variable probe results were due to interference from the metal substrate, since the scale width is approximately the size of the irradiated sample area. No trace of sodium or sulfur was found within the scale.

The most probable explanation for the decrease in oxidation rates of the hot corroded samples is the formation of an initial thin film of SiO_2 at the metal/oxide interface, which restricts the outward diffusion of cobalt ions and therefore reduces porosity. Fluxing of an SiO_2 scale by Na_2SO_4 may occur, but since SiO_2 is an ionic conducting scale, no increase in rate is anticipated.

In summary, the experimental results obtained for the oxidation and hot corrosion of cobalt-silicon binary alloys provide a reasonable pattern of decreasing oxidation rates with increasing silicon content.

D. Cobalt-5 Chromium-Silicon Ternary Alloys

The basis of this research program was the development of a protective external layer of SiO_2 on the alloy surface. Since SiO_2 is an ionic conducting compound, its rate of growth, which is controlled by movement of electrons, should not be increased significantly by the formation of a liquid layer of Na_2SO_4 on the sample surface.

In order to achieve the formation of an outer layer of SiO_2, a third alloy element such as chromium must be added to the binary

cobalt-silicon system. The chromium acts as a regulator by reducing the partial pressure of oxygen at the scale-alloy interface, thereby promoting the formation of an external SiO_2 layer, rather than its precipitation as an internal oxide (76). This occurs because Cr_2O_3 and SiO_2 predominate over cobalt oxide in the transient scale and Cr_2O_3 provides oxygen to the alloy at a much slower rate (lower, P_{O_2}) than the cobalt oxide. This facilitates diffusion of silicon up to the metal surface, where a protective layer of SiO_2 is formed immediately beneath the thin transient scale (76,77).

There is, however, very little experimental evidence available in the literature to support this theory. One of the major reasons for this is that SiO_2 grows so slowly that the initial nuclei are overgrown rapidly by Cr_2O_3, which continues to thicken until the SiO_2 succeeds in piling up at the alloy/oxide interface, and coalesces to provide a protective layer, which eventually slows the oxidation rate below that of the Co-Cr alloy. The SiO_2 layer is often too thin to be detected by metallographic or microprobe techniques.

Combining the ternary theory with the results obtained from the oxidation and hot corrosion of the Co-Cr and Co-Si binary systems, a series of Co-Cr-Si ternary alloys were designed for testing under identical environmental conditions as those experienced by the binary alloys. Discussion of the oxidation and hot corrosion behavior of the Co-Cr-Si ternary alloys will follow presentation of the experimental results.

1. Oxidation

The oxidation behavior of Co-5 Cr with 1, 2.5, 5 and 10% silicon additions is shown in Figure 13. The parabolic rate constants

Figure 13. Weight Gain ($\Delta m/A$) as a Function of Time for the Oxidation and Hot Corrosion of Co-5 Cr-Si Alloys at 1000°C and P_{O_2} = 0.1 atm.

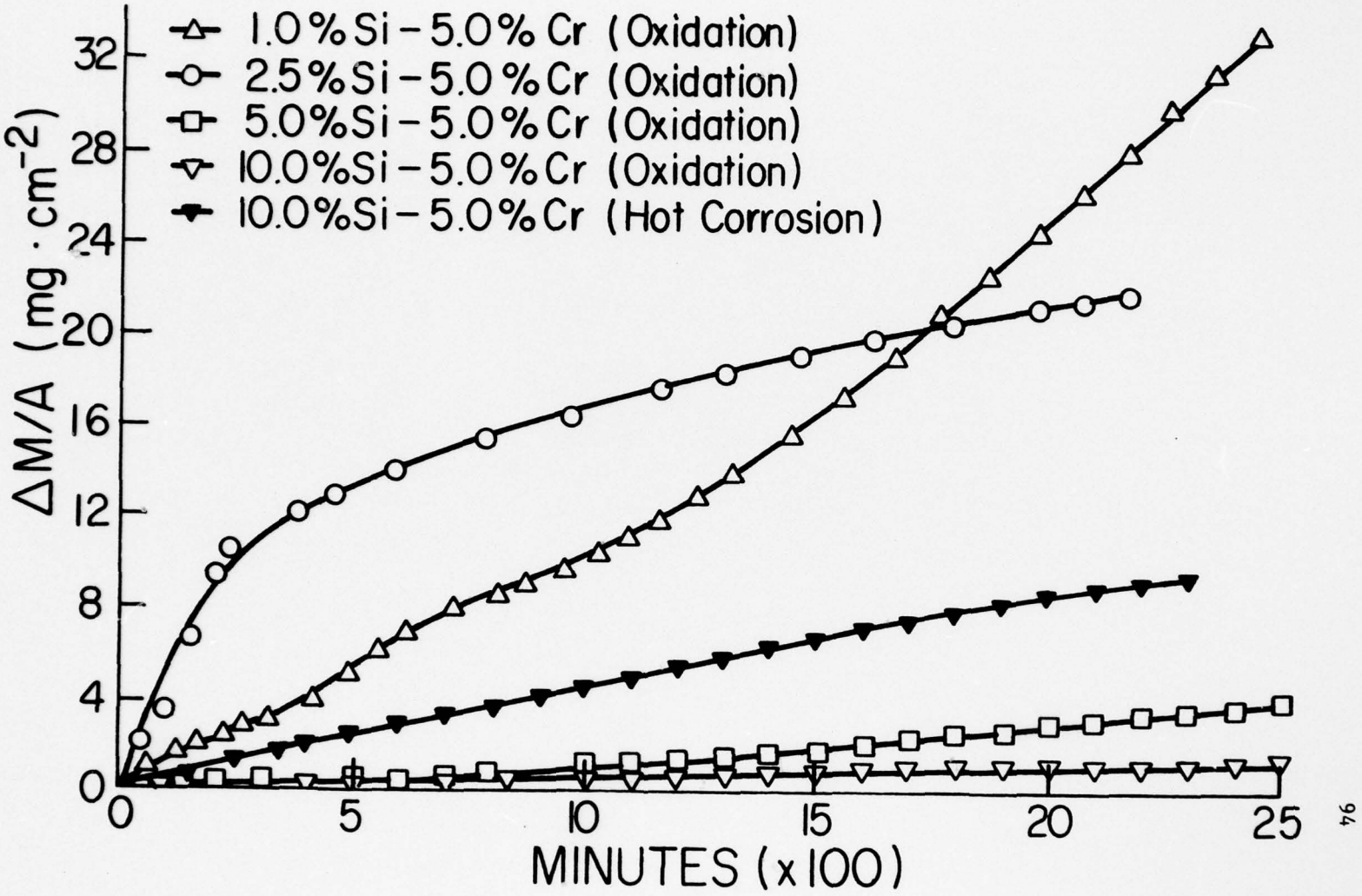
1.0%Si-5.0%Cr (Oxidation)
2.5%Si-5.0%Cr (Oxidation)
5.0%Si-5.0%Cr (Oxidation)
10.0%Si-5.0%Cr (Oxidation)
10.0%Si-5.0%Cr (Hot Corrosion)
ΔM/A (mg·cm⁻²)
0
4
8
12
16
20
24
28
32
0
5
10
15
20
25
MINUTES (x100)

94

listed in Table 5 are shown in Figure 14 as a function of increasing silicon content. The kinetic data show a sharp decrease in the oxidation rate for corresponding increases in silicon content. The K_p of 0.097×10^{-10} $gm^2 \cdot cm^{-4} \cdot sec^{-1}$ for Co-5 Cr-10 Si represents a decrease of four orders of magnitude in oxidation rate as compared to 290×10^{-10} $gm^2 \cdot cm^{-4} \cdot sec^{-1}$ for Co-5 Cr-1 Si. Metallographic examination of the scales formed on these alloys revealed a double-layered structure for Co-5 Cr-1 Si and Co-5 Cr-2.5 Si alloys with a compact outer layer containing some large pores and an inner porous layer. Cracking was also evident within the inner layer as shown in Figure 15. The average scale thickness decreased from 600 microns for the 1% Si addition to 170 microns for the 2.5% Si addition.

The scale formed on Co-5 Cr-5 Si was double-layered,but the outer layer exhibited a honeycomb structure with extremely large pores. The inner layer was compact with virtually no porosity as can be seen in Figure 16. The scale thickness was 50 microns. The oxidation of Co-5 Cr-10 Si resulted in the formation of a thin film oxide layer which was only four microns thick.

Microprobe analysis and x-ray diffraction of the scales formed on Co-5 Cr samples with 1% and 2.5% silicon additions confirmed the outer layer to be 98% CoO for the 1% silicon sample and 99% CoO for the 2.5% Si sample. The inner layer was composed of CoO with some $CoCr_2O_4$ and Co_2SiO_4 present. A typical profile for Co-5 Cr-2.5 Si is shown in Figure 17. Analysis of the 5% silicon sample by x-ray diffraction showed the presence of CoO, $CoCr_2O_4$ and Co_2SiO_4. It was not possible to analyze the thin film formed on the Co-5 Cr-10 Si alloy.

TABLE 5

PARABOLIC OXIDATION RATES AND WEIGHT CHANGE INFORMATION

FOR COBALT-CHROMIUM-SILICON ALLOYS

Wt. %-Si (Nominal)	Wt. %-Cr (Nominal)	Oxidation		Hot Corrosion	
		K_p	Total ΔM/A (1800 Min)	K_p	Total ΔM/A (1800 Min)
0.0	0.0	138	38.12	150	38.8
1.0	5.0	290*	20.73 (60.8*)	255	52.7
2.5	"	28	20.15	14	12.7
5.0	"	2	2.46	0.708	2.09
10.0	"	0.097	0.94	9.00	7.72
1.0	10.0	15	13.8	19	20.77
2.5	"	0.213**	0.17 (2.48**)	3.0	5.58
5.0	"	0.04	0.61	1.0	3.05
10.0	"	0.00197**	0.10 (0.34**)	0.0167	0.53
1.0	15.0	0.0016***	0.019 (0.16***)	2.0	4.7
2.5	"	0.0020***	0.145 (0.26**)	5.0	4.85
5.0	"	0.35***	1.90 (3.46***)	2.0	4.79
10.0	"	0.093***	1.12 (1.82***)	9.0	7.62

K_p units ($gm^2 \cdot cm^{-4} \cdot sec^{-1} \times 10^{-10}$)

ΔM/A units ($mg \cdot cm^{-2}$)

*Run duration 4,000 min.
**Run duration 10,000 min.
***Run duration 6,000 min.

Figure 14. Parabolic Rate Constants (K_p) of Co-5 Cr-Si Alloys as a Function of Weight Percent Silicon in an Oxidizing Environment at 1000°C and P_{O_2} = 0.1 atm.

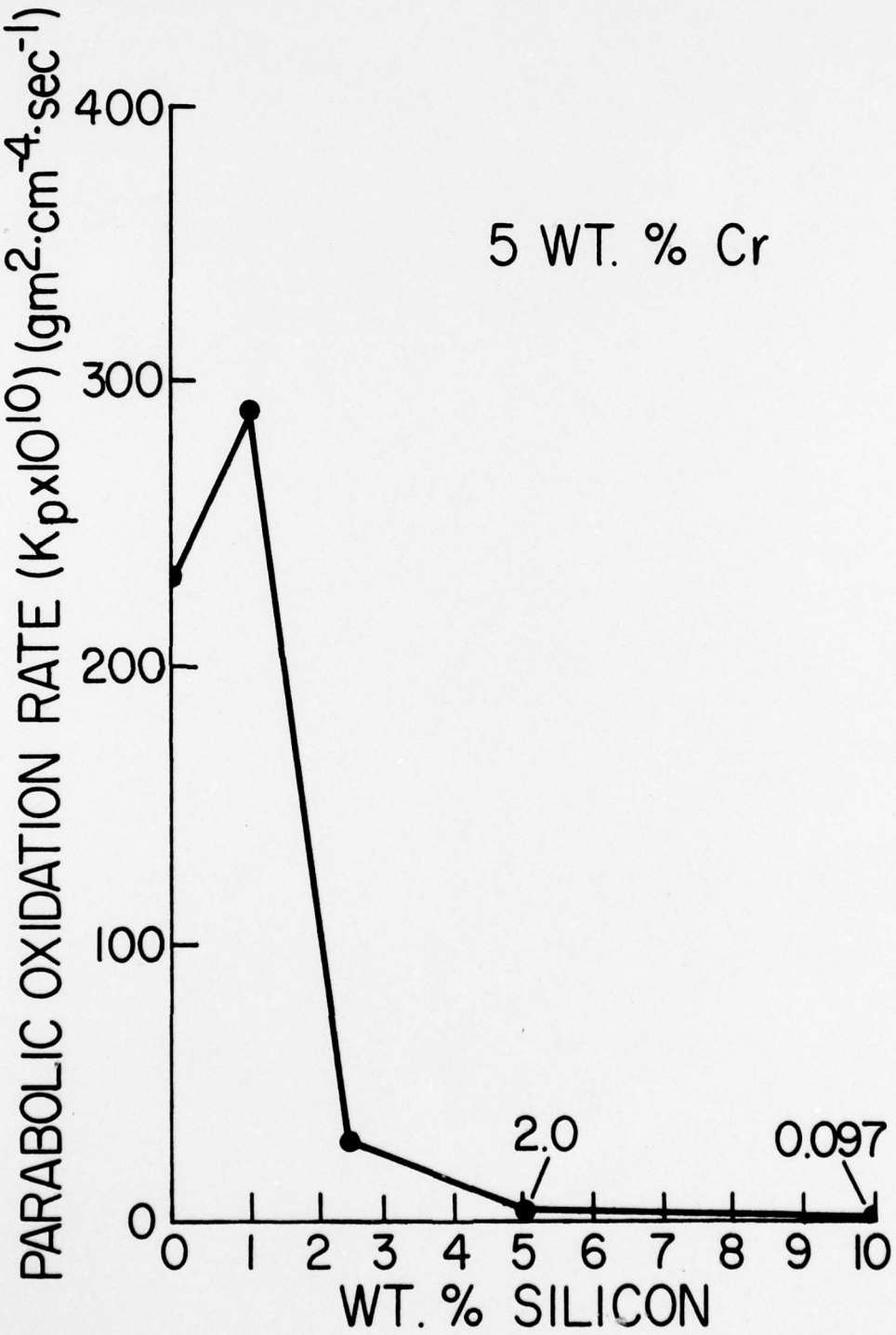
PARABOLIC OXIDATION RATE ($K_p \times 10^{10}$) ($gm^2 \cdot cm^{-4} \cdot sec^{-1}$)
400
300
200
100
0
5 WT. % Cr
2.0
0.097
0 1 2 3 4 5 6 7 8 9 10
WT. % SILICON

Figure 15. Micrographs of the Scales Formed on Co-5 Cr-2.5 Si After Oxidation and Hot Corrosion at 1000°C and P_{O_2} = 0.1 atm.

Co—5 Cr—2.5 Si
(OXIDATION)
350 X

Co—5 Cr—2.5 Si
(HOT CORROSION)
350 X

Figure 16. Micrograph of the Scale Formed on Co-5 Cr-5 Si After Oxidation at 1000°C and P_{O_2} = 0.1 atm.

Co—5 Cr—5 Si
(OXIDATION)
500 X

Figure 17. Microprobe Profile of the Scale Formed on Co-5 Cr-2.5 Si After Hot Corrosion and Oxidation at 1000°C and P_{O_2} = 0.1 atm.

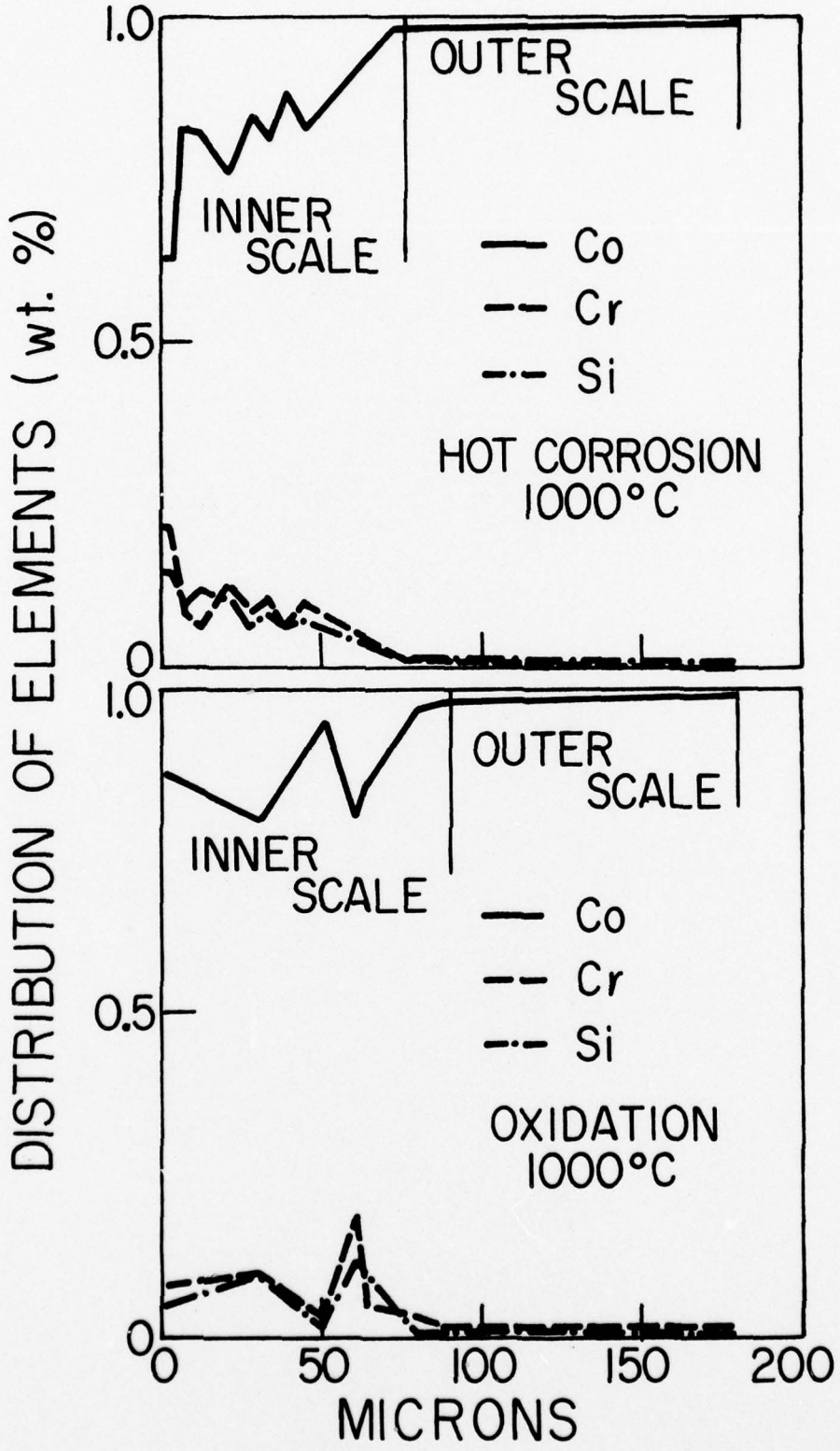
1.0
0.5
0
OUTER SCALE
INNER SCALE
Co
Cr
Si
HOT CORROSION 1000°C
OXIDATION 1000°C
DISTRIBUTION OF ELEMENTS (wt. %)
0
50
100
150
200
MICRONS

2. Hot Corrosion

The kinetic data presented in Table 5 show that the hot corrosion rate decreased as the silicon content is increased up to 10 wt. %. The increase in the hot corrosion rate for Co-5 Cr-10 Si as compared to the oxidized sample is shown in Figure 13. The microstructure of the oxides formed after hot corrosion of Co-5 Cr with 1 and 2.5% silicon additions are shown in Figures 18 and 15, respectively. They reveal a double-layered structure similar in nature to the oxidized samples. No attempt was made to examine the oxides formed on the alloys with 5 and 10 wt. % silicon additions.

Microprobe analysis of the scales formed on Co-5 Cr-1 Si and Co-5 Cr-2.5 Si show the outer layer to be 98 wt. % CoO and an inner layer of CoO with some $CoCr_2O_4$ and Co_2SiO_4. The spinel concentration decreases in the inner oxide layer as it moves toward the double-layer interface as can be seen in Figure 17. Attempts to probe the scales formed on Co-5 Cr with 5 and 10% silicon additions were unsuccessful due to the thin oxide layers formed on these alloys.

E. Cobalt-10 Chromium-Silicon Ternary Alloys

1. Oxidation

The kinetic curves in Figure 19 show a sharp drop in weight gain at any given time as the silicon content is increased to 10 wt. %. The parabolic rate constant of 0.00197×10^{-10} $gm^2 \cdot cm^{-4} \cdot sec^{-1}$ for Co-10 Cr-10 Si indicates a decrease of four orders of magnitude in the oxidation rate as compared to 15×10^{-10} $gm^2 \cdot cm^{-4} \cdot sec^{-1}$ for the Co-10 Cr-1 Si specimen. In all cases, the oxidation rate was much

Figure 18. Micrograph of the Scale Formed on Co-5 Cr-1 Si After Hot Corrosion at 1000°C and P_{O_2} = 0.1 atm.

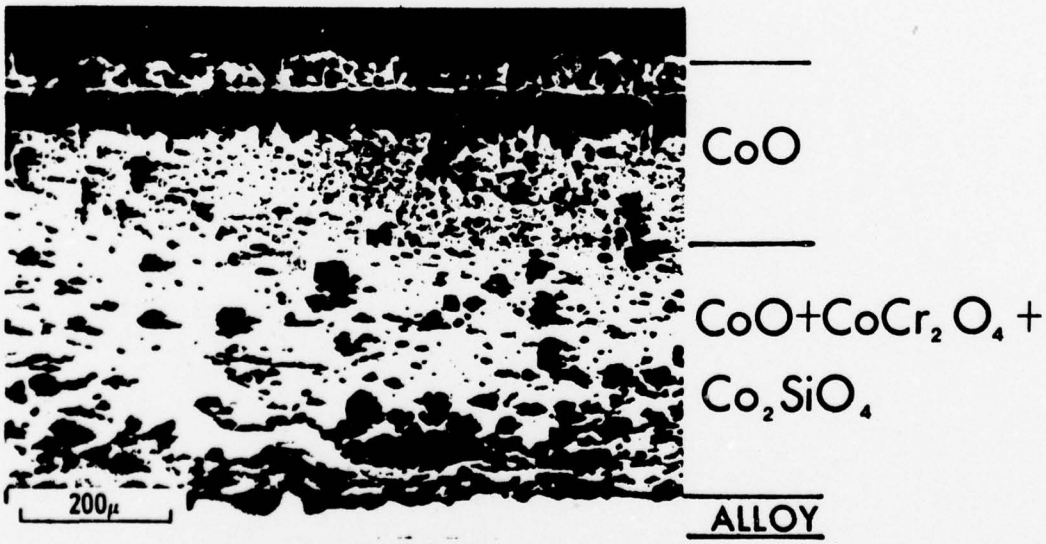

Co—5 Cr—1 Si
(HOT CORROSION)
110 X

Figure 19. Weight Gain ($\Delta m/A$) as a Function of Time for the Oxidation and Hot Corrosion of Co-10 Cr-Si Alloys at 1000°C and P_{O_2} = 0.1 atm.

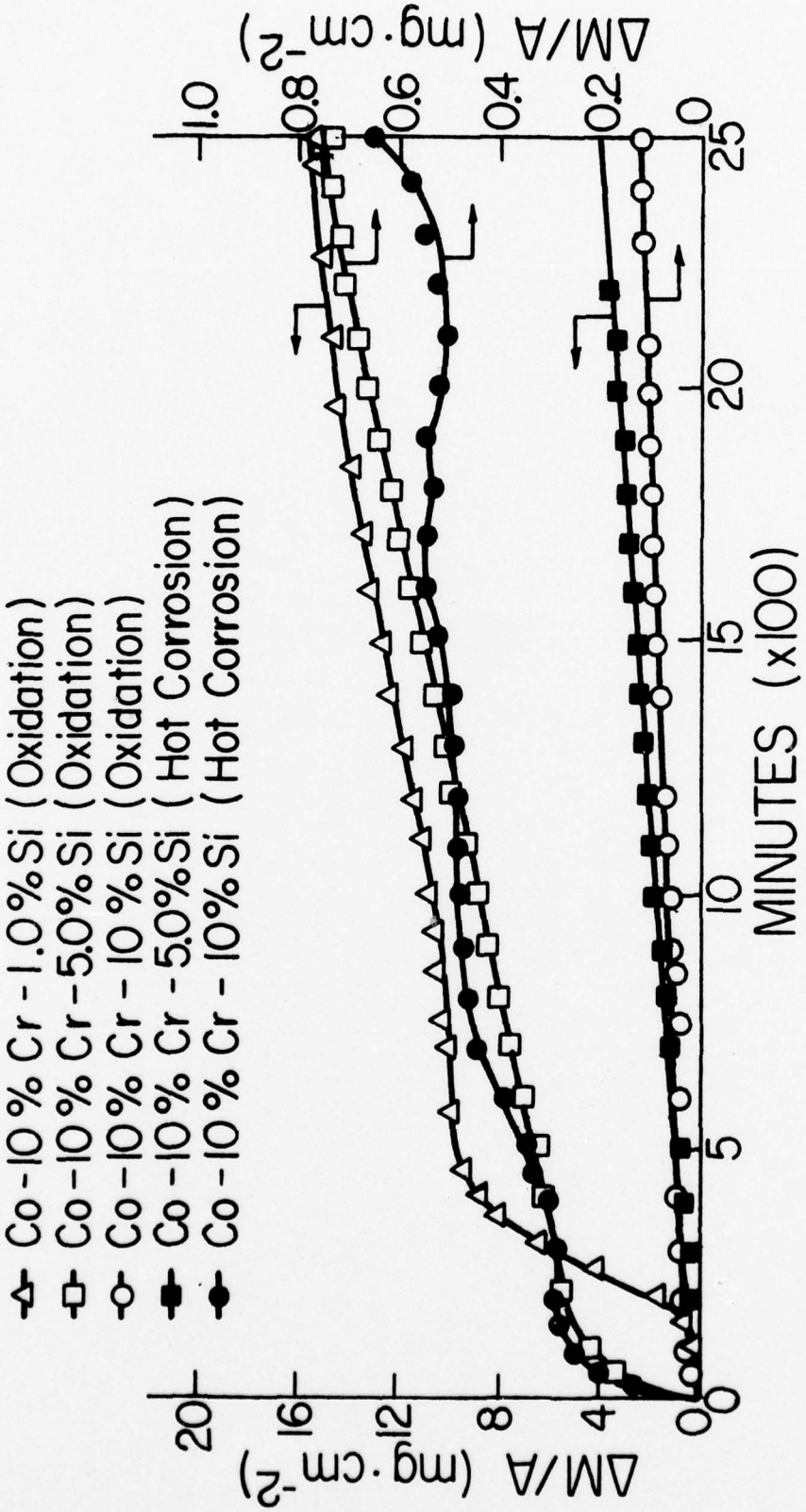
Co-10% Cr-1.0% Si (Oxidation)
Co-10% Cr-5.0% Si (Oxidation)
Co-10% Cr-10% Si (Oxidation)
Co-10% Cr-5.0% Si (Hot Corrosion)
Co-10% Cr-10% Si (Hot Corrosion)
ΔM/A (mg.cm⁻²)
MINUTES (x100)
0
4
8
12
16
20
0.2
0.4
0.6
0.8
1.0
5
10
15
20
25

lower than that of pure cobalt ($K_p = 138 \times 10^{-10}$ $gm^2 \cdot cm^{-4} \cdot sec^{-1}$). The parabolic rate constants listed in Table 5 and shown in Figure 20 for Co-10 Cr-2.5 and 10 wt. % silicon additions were calculated from $(\Delta m/A)^2$ values taken over long time periods (run duration 10,000 minutes). The Co-10 Cr-10 Si specimen exhibited one of the best oxidation rates observed for the binary and ternary systems. No evidence of spalling was observed for the Co-10 Cr-Si group as can be seen from Figure 19.

Metallographic examination of the scale formed on the Co-10 Cr-1 Si sample after oxidation revealed a double-layered structure with an outer porous layer and a more compact inner layer. There was extensive cracking evident within both layers as shown in Figure 21. The scale thickness was approximately 200 microns. Surface roughening and some internal oxidation were observed at the metal/oxide interface for the Co-10 Cr-10 Si specimen. The total scale thickness was less than 4 microns.

Microprobe analysis of oxide layer formed on Co-10 Cr-1 Si shows an outer layer of 99% CoO and an inner layer of CoO with dispersed particles of $CoCr_2O_4$ and Co_2SiO_4. A typical profile of this oxide is presented in Figure 22. The oxide layer formed on Co-10 Cr-10 Si was too thin to probe successfully.

2. Hot Corrosion

The rate of oxidation under hot corrosion conditions shows a sharp decrease as the silicon content is increased. This is identical to the results obtained for the oxidation experiments as can be seen in Figure 19. The parabolic rate constants listed in Table 5 were

Figure 20. Parabolic Rate Constants (K_p) of Co-10 Cr-Si Alloys as a Function of Weight Percent Silicon in an Oxidizing Environment at 1000°C and P_{O_2} = 0.1 atm.

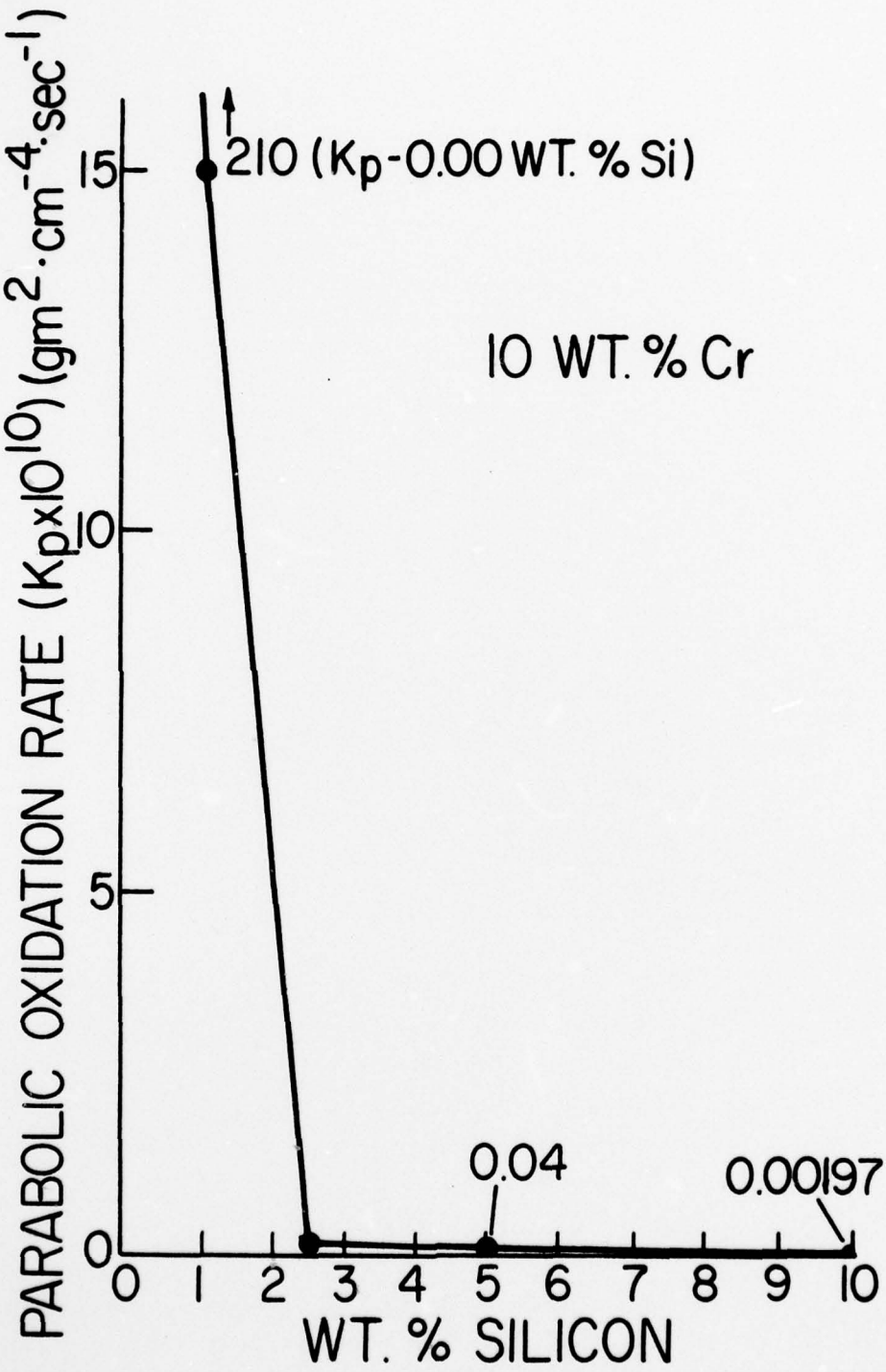
PARABOLIC OXIDATION RATE ($K_p \times 10^{10}$) ($gm^2 \cdot cm^{-4} \cdot sec^{-1}$)
15
10
5
0
210 (K_p-0.00 WT. % Si)
10 WT. % Cr
0.04
0.00197
0 1 2 3 4 5 6 7 8 9 10
WT. % SILICON

Figure 21. Micrographs of the Scales Formed on Co-10 Cr-1 Si After Hot Corrosion and Oxidation at 1000°C and P_{O_2} = 0.1 atm.

Co—10 Cr—1 SI
(OXIDATION)
200 X

Co—10 Cr—1 SI
(HOT CORROSION)
180 X

Figure 22. Microprobe Profiles of the Scales Formed on Co-10 Cr-1 Si After Oxidation and Hot Corrosion at 1000°C and P_{O_2} = 0.1 atm.

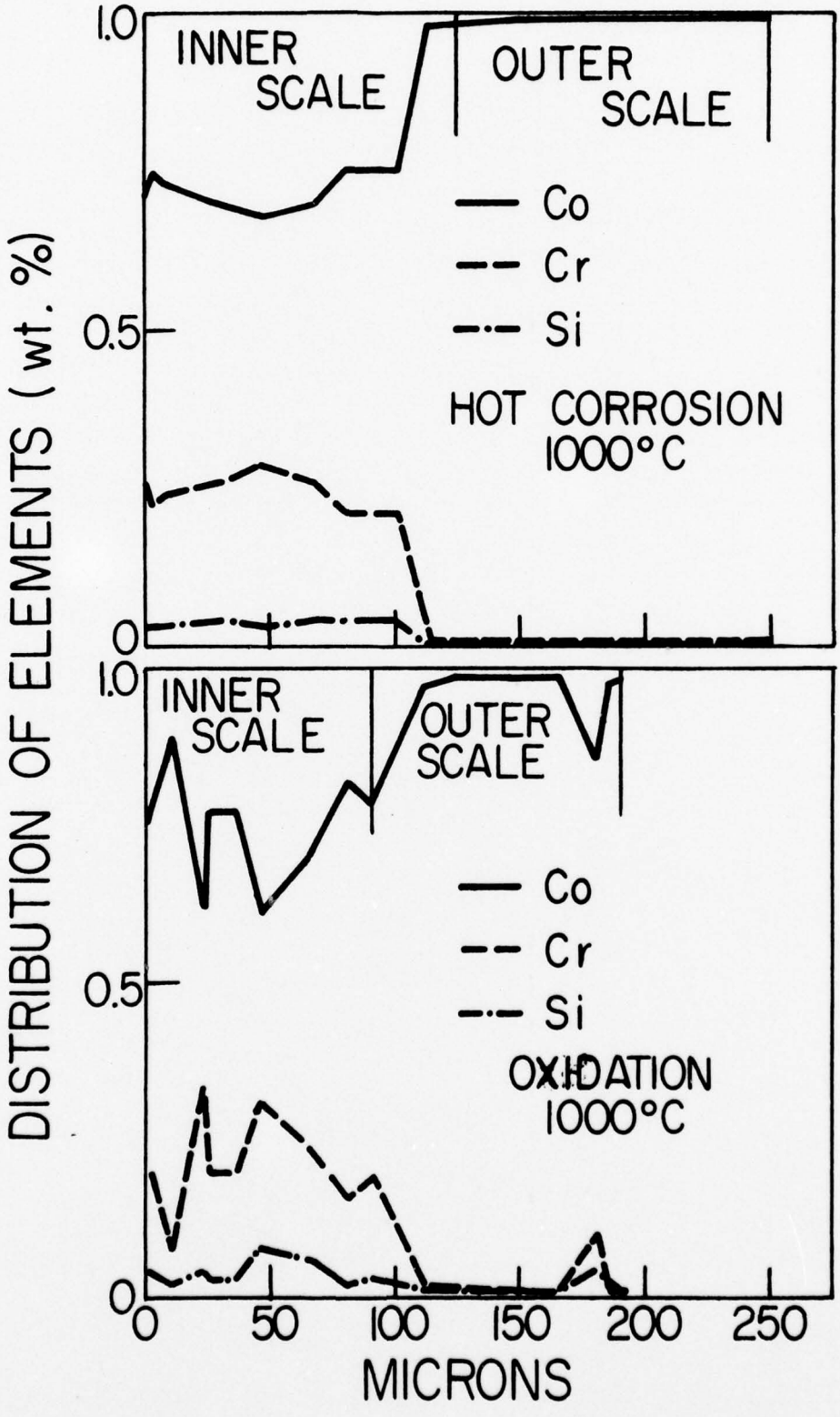
1.0
INNER SCALE
OUTER SCALE
Co
Cr
Si
HOT CORROSION 1000°C
0.5
0
1.0
INNER SCALE
OUTER SCALE
Co
Cr
Si
OXIDATION 1000°C
0.5
0
0
50
100
150
200
250
MICRONS
DISTRIBUTION OF ELEMENTS (wt. %)

slightly higher under hot corrosion conditions compared to the oxidation kinetics. The Co-10 Cr-10 Si exhibited one of the lowest rates of oxidation for both the hot corrosion and oxidizing environments. A comparison of the weight gains as a function of time for hot corrosion and oxidation of this alloy is depicted in Figure 23. There is some indication of spalling under the hot corrosion conditions.

The microstructure of Co-10 Cr-1 Si is represented in Figure 21. A typical double-layered structure is observed with a more compact outer layer than the oxidized specimen. The scale thickness (330 microns) is somewhat greater than that of the oxidized specimen (200 microns).

A typical microprobe profile of the oxide layer is shown in Figure 22. The outer layer is 99 wt. % CoO with an inner layer composed of CoO and the spinel $CoCr_2O_4$ and Co_2SiO_4. A more uniform distribution of these oxide compounds is indicated for the hot corrosion sample.

F. Cobalt-15 Chromium-Silicon Ternary Alloys

1. Oxidation

The results of the thermogravimetric studies are presented in Figures 24 and 25. In all cases,the oxidation is described by the parabolic rate law. The parabolic rate constants listed in Table 5 are shown in Figure 25 as a function of weight percent silicon. The slight increase in oxidation rate as the silicon content is increased is opposite to that observed for the Co-5 Cr-Si and Co-10 Cr-Si groups. However, this group performed far better under oxidizing

Figure 23. Comparison of the Weight Gain ($\Delta m/A$) as a Function of Time for the Hot Corrosion and Oxidation of Co-10 Cr-10 Si at 1000°C and P_{O_2} = 0.1 atm.

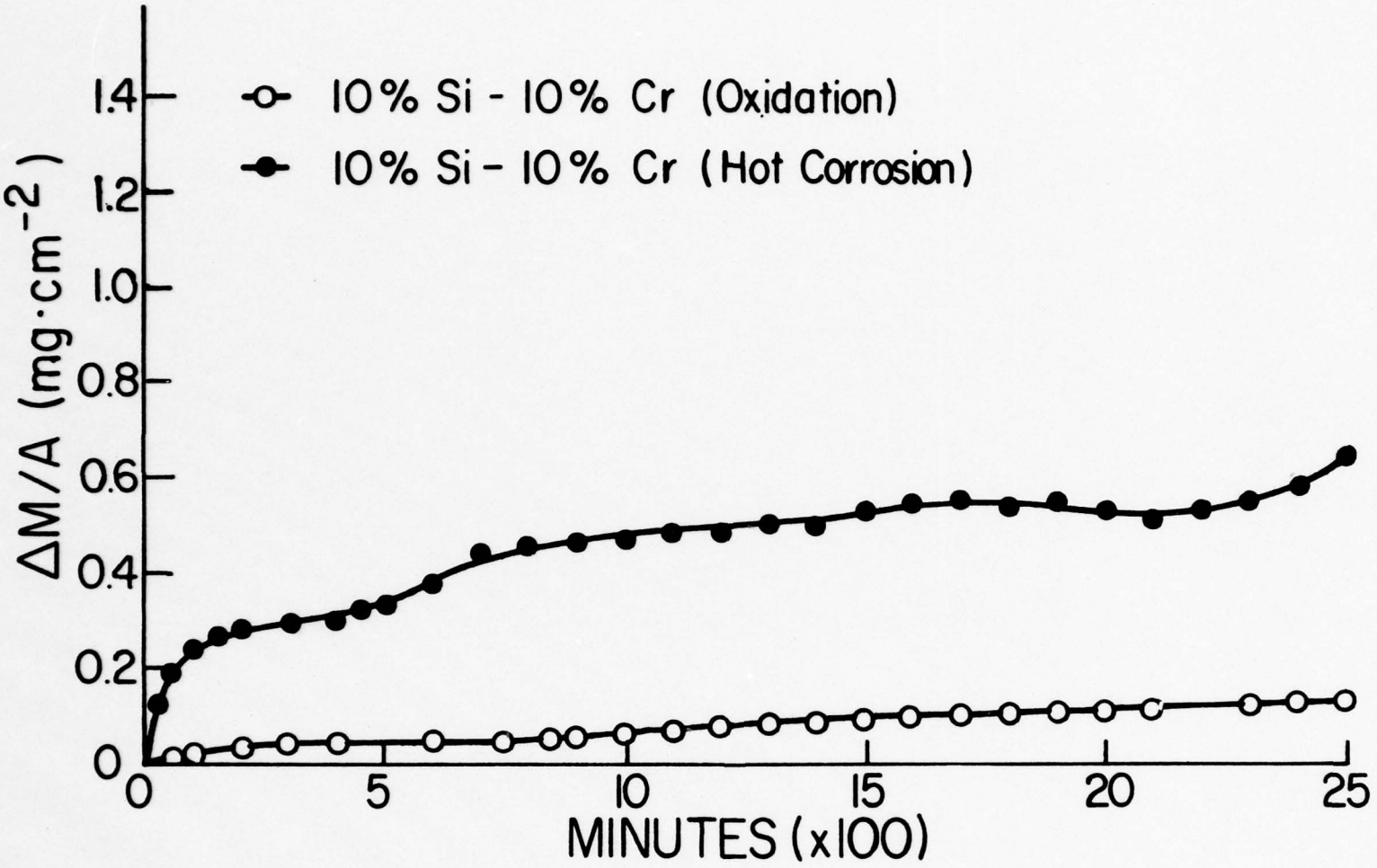
10% Si - 10% Cr (Oxidation)
10% Si - 10% Cr (Hot Corrosion)
ΔM/A (mg·cm⁻²)
1.4
1.2
1.0
0.8
0.6
0.4
0.2
0
0
5
10
15
20
25
MINUTES (x100)

Figure 24. Weight Gain ($\Delta m/A$) as a Function of Time for the Oxidation of Co-15 Cr-Si Alloys at 1000°C and P_{O_2} = 0.1 atm.

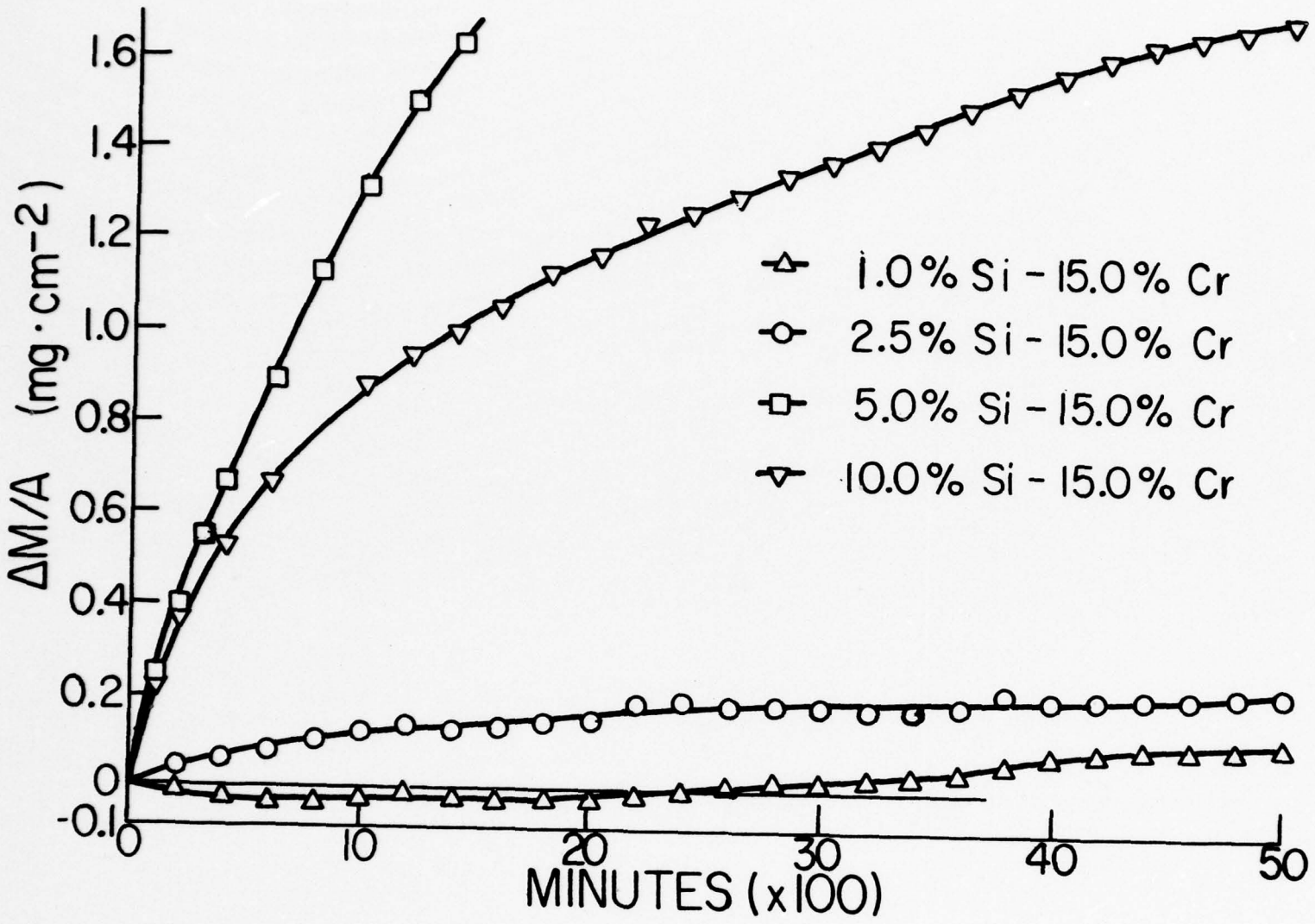
1.6
1.4
1.2
1.0
0.8
0.6
0.4
0.2
0
-0.1
ΔM/A (mg·cm⁻²)
0
10
20
30
40
50
MINUTES (x100)
1.0% Si - 15.0% Cr
2.5% Si - 15.0% Cr
5.0% Si - 15.0% Cr
10.0% Si - 15.0% Cr

Figure 25. Parabolic Rate Constants (K_p) of Co-15 Cr-Si Alloys as a Function of Weight Percent Silicon in an Oxidizing Environment at 1000°C and P_{O_2} = 0.1 atm.

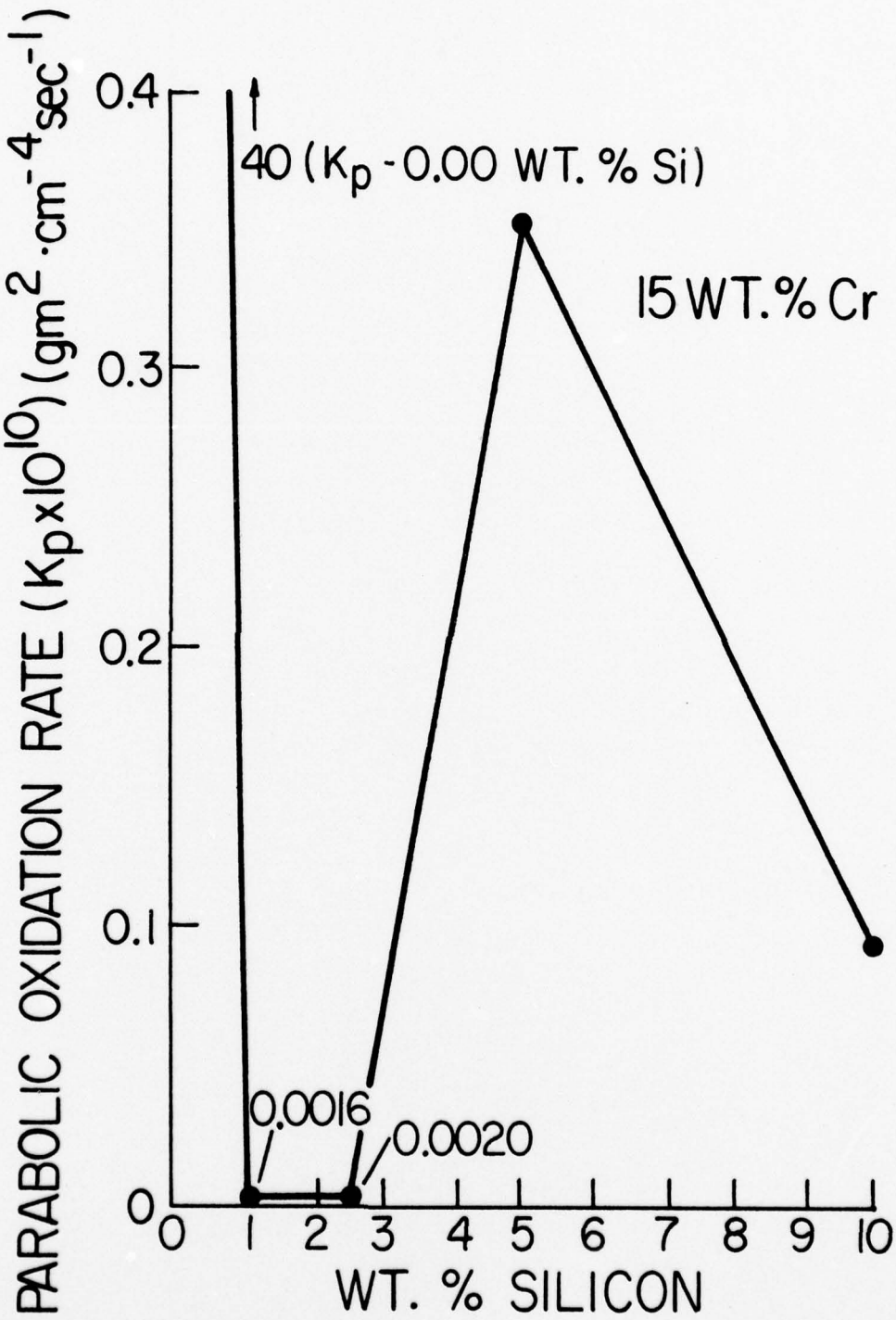
PARABOLIC OXIDATION RATE ($K_p \times 10^{10}$) ($gm^2 \cdot cm^{-4} sec^{-1}$)
0.4
0.3
0.2
0.1
0
40 (K_p - 0.00 WT. % Si)
15 WT. % Cr
0.0016
0.0020
0 1 2 3 4 5 6 7 8 9 10
WT. % SILICON

conditions than any of the other groups previously studied. The Co-15 Cr-1 Si specimen exhibited the lowest oxidation rate observed, 0.0016×10^{-10} $gm^2 \cdot cm^{-4} \cdot sec^{-1}$, which is many orders of magnitude lower than the oxidation rate of pure cobalt.

The oxidation of this group of alloys resulted in the formation of thin film oxide layers, which were difficult to analyze. The microstructure of a patch of oxide formed on Co-15 Cr-1 Si is shown in Figure 26. A double-layered structure is evident, with a slightly porous outer layer and a very compact inner layer, apparently of a different structure than the outer layer. It should be emphasized that the microstructure observed in Figure 26 may not be typical of the oxide layer formed on this alloy since most of the thin oxide film (< 4 microns) had been removed during sample preparation and x-ray diffraction studies.

Microprobe analysis of the oxide layer formed on Co-15 Cr-1 Si is shown in Figure 27. The outer layer is composed of CoO except near the double-layer interface and oxide/gas interface, where the chromium concentration is increased. The inner layer shows the highest chromium concentration of any sample studied. This could indicate the formation of a Cr_2O_3 layer during the initial stages of oxidation. No evidence of Cr_2O_3 was found by x-ray diffraction, however.

2. Hot Corrosion

Since the Co-15 Cr-Si group of alloys exhibited some of the lowest rates of oxidation, it was decided to study this group under isothermal and cyclic hot corrosion conditions. The cyclic environment

Figure 26. Micrograph of the Scale Formed on Co-15 Cr-1 Si After Oxidation at 1000°C and P_{O_2} = 0.1 atm.

$CoO + CoCr_2O_4 + Co_2SiO_4$

ALLOY

20μ

Co—15 Cr—1 Si
(OXIDATION)
700 X

Figure 27. Microprobe Profile of the Scale Formed on Co-15 Cr-1 Si After Oxidation at 1000°C and P_{O_2} = 0.1 atm.

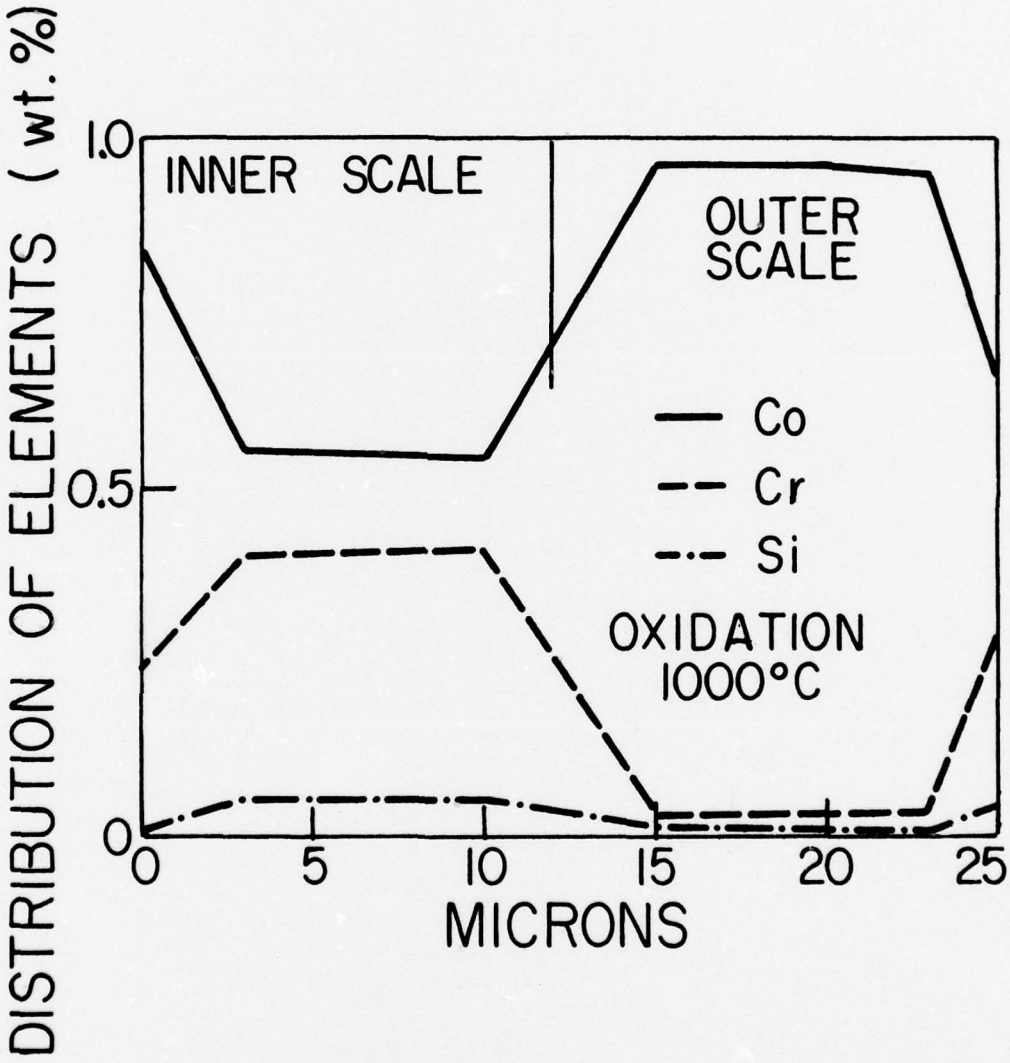
DISTRIBUTION OF ELEMENTS (wt. %)
1.0
0.5
0
INNER SCALE
OUTER SCALE
Co
Cr
Si
OXIDATION
1000°C
0
5
10
15
20
25
MICRONS

provides a more severe test of scale adherence and also more closely duplicates conditions existing within a gas turbine.

a. Isothermal. Exposing samples of Co-15 Cr-Si alloys to a continuous supply of Na_2SO_4 throughout the oxidation period resulted in a substantial increase in the oxidation rate for all specimens, as shown in Table 5. Figure 28 shows the weight gain ($\Delta m/A$) as a function of time for the isothermal hot corrosion of Co-15 Cr-Si alloys. The kinetics indicate the possibility of some transition from protective parabolic oxidation to non-protective linear oxidation as can be seen in Figure 28. This group as a whole exhibited good hot corrosion resistance.

b. Cyclic. The hot corrosion resistance of Co-15 Cr with 1, 2.5, and 5 wt.% additions of silicon was determined under cyclic conditions. Specimens were automatically cycled between the test temperature of 1000°C and room temperature once every 250 minutes. The furnace was lowered every 250 minutes for 10 minutes to allow the sample to cool to ambient temperature. The results of the cyclic tests are shown in Figures 29, 30 and 31. The cyclic environment in all cases accelerated the hot corrosion rate probably by spalling the protective oxide layer. The Co-15 Cr-2.5 Si specimen exhibited the highest degree of spalling of the alloys tested.

In considering the oxidation behavior of the Co-Cr-Si system, it is apparent that additions of silicon up to 10 wt.% decrease the oxidation rate as much as several orders of magnitude when compared to the oxidation of pure cobalt at 1000°C and an oxygen pressure of

Figure 28. Weight Gain ($\Delta m/A$) as a Function of Time for the Isothermal Hot Corrosion of Co-15 Cr-Si alloys at 1000°C and P_{O_2} = 0.1 atm.

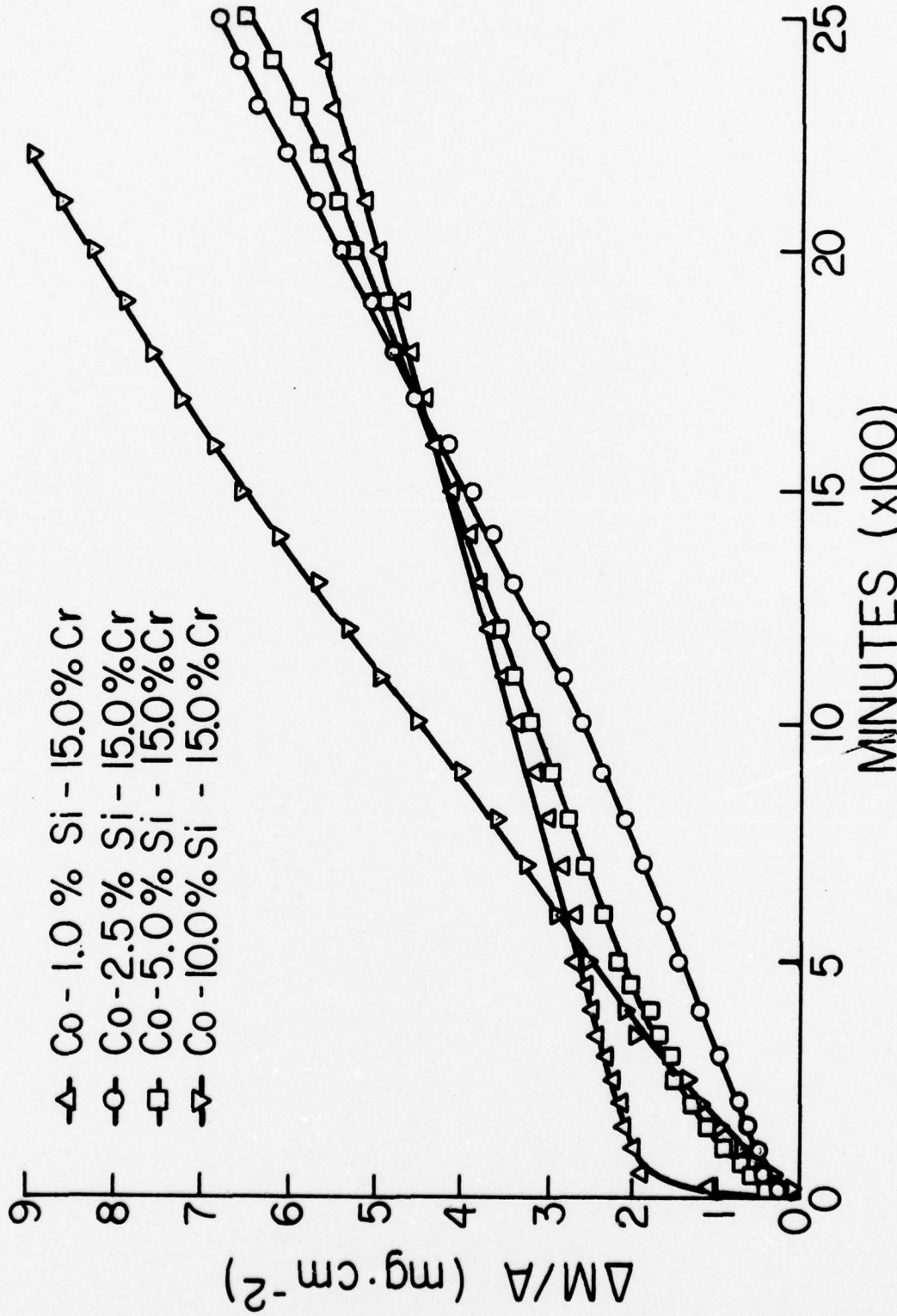
Co - 1.0 % Si - 15.0% Cr
Co - 2.5 % Si - 15.0% Cr
Co - 5.0 % Si - 15.0% Cr
Co - 10.0 % Si - 15.0% Cr
ΔM/A (mg.cm⁻²)
MINUTES (x100)
0
1
2
3
4
5
6
7
8
9
0
5
10
15
20
25

Figure 29. Comparison of the Cyclic and Isothermal Hot Corrosion Behavior of Co-15 Cr-1 Si at 1000°C and P_{O_2} = 0.1 atm.

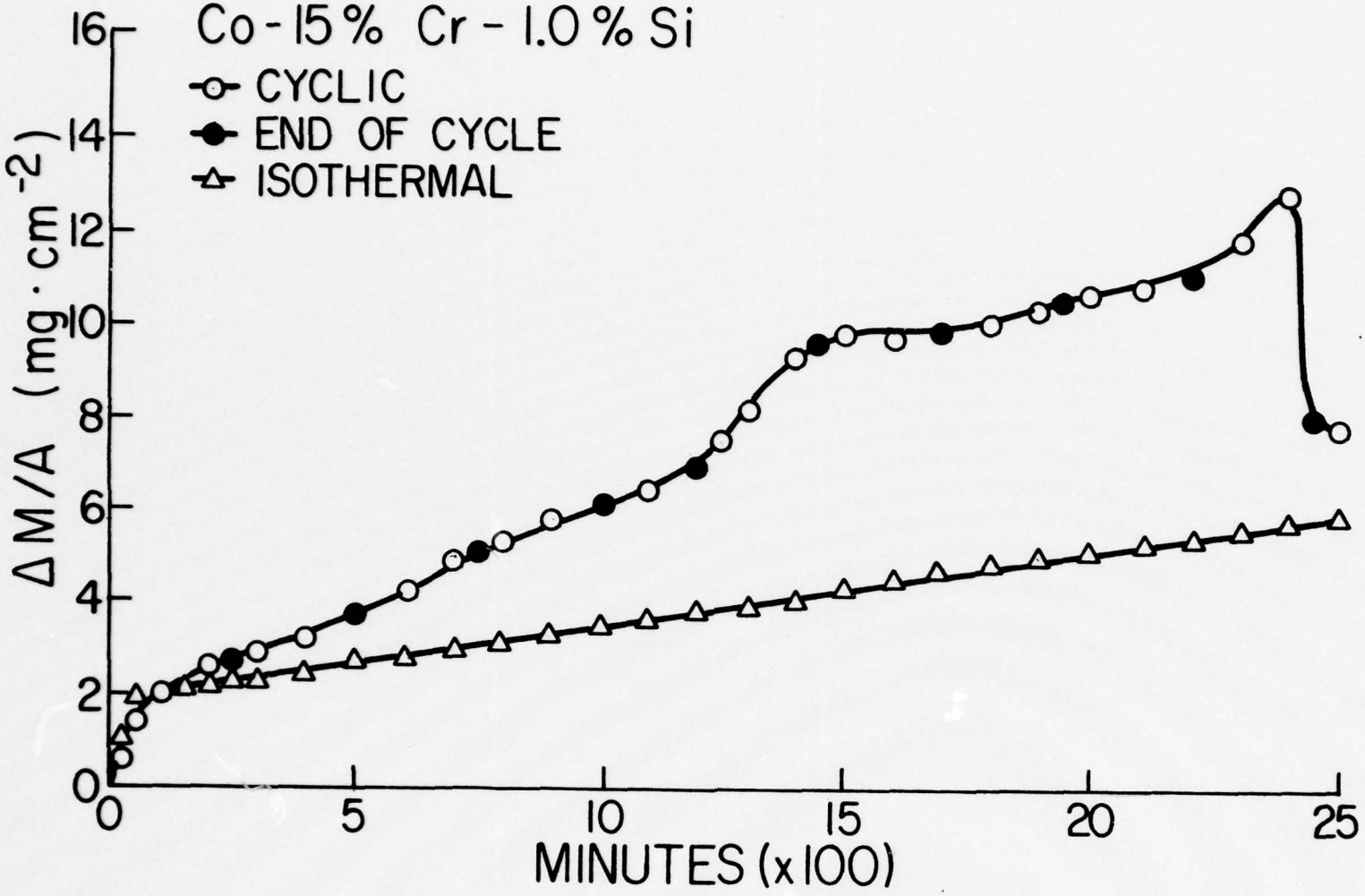
Co - 15 % Cr - 1.0 % Si
CYCLIC
END OF CYCLE
ISOTHERMAL
ΔM/A (mg · cm⁻²)
0
2
4
6
8
10
12
14
16
0
5
10
15
20
25
MINUTES (x 100)

Figure 30. Comparison of the Cyclic and Isothermal Hot Corrosion Behavior of Co-15 Cr-2.5 Si at 1000°C and P_{O_2} = 0.1 atm.

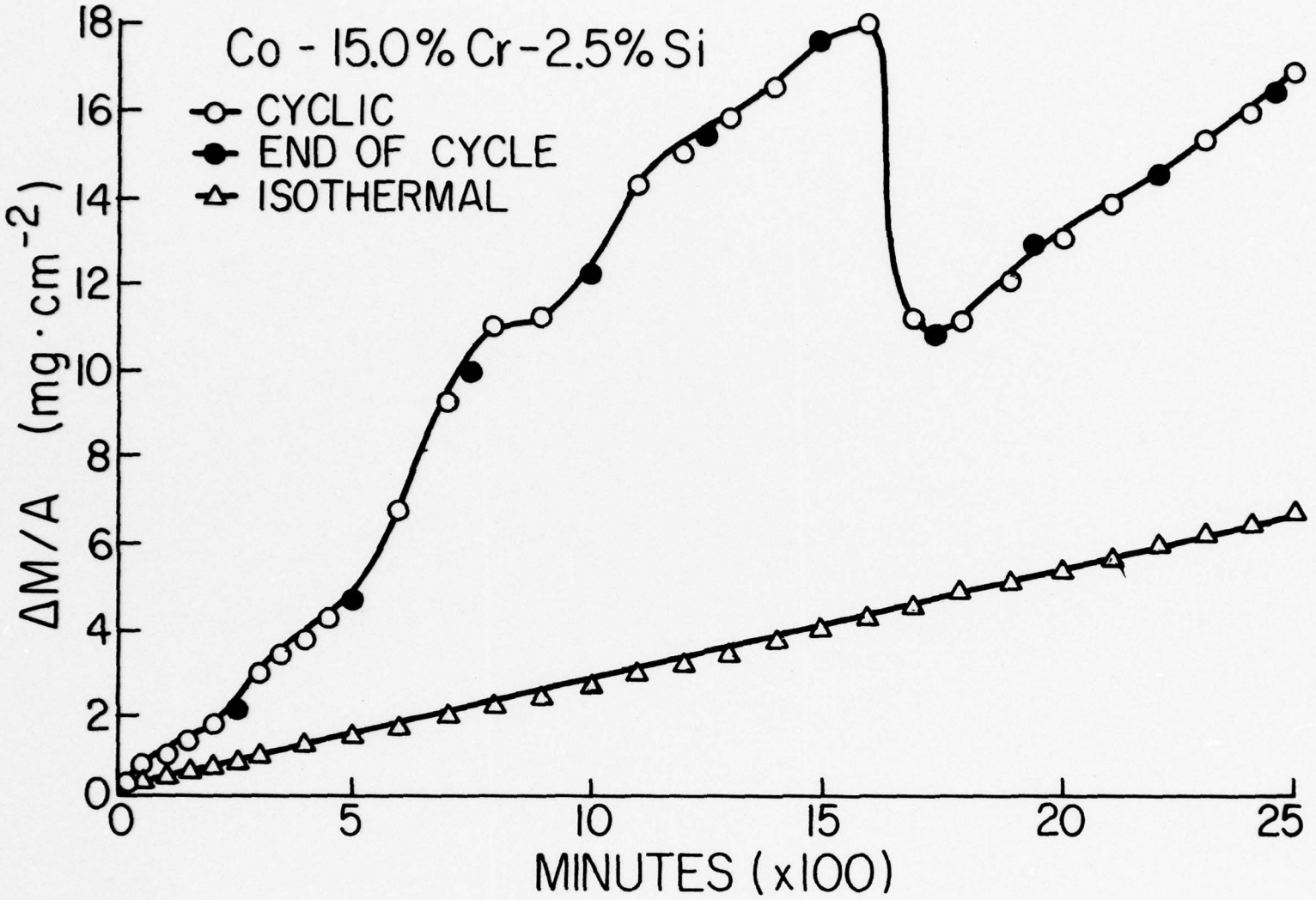
Co - 15.0% Cr - 2.5% Si
CYCLIC
END OF CYCLE
ISOTHERMAL
ΔM/A (mg·cm⁻²)
MINUTES (x100)
0
2
4
6
8
10
12
14
16
18
0
5
10
15
20
25

Figure 31. Comparison of the Cyclic and Isothermal Hot Corrosion Behavior of Co-15 Cr-5 Si at 1000°C and P_{O_2} = 0.1 atm.

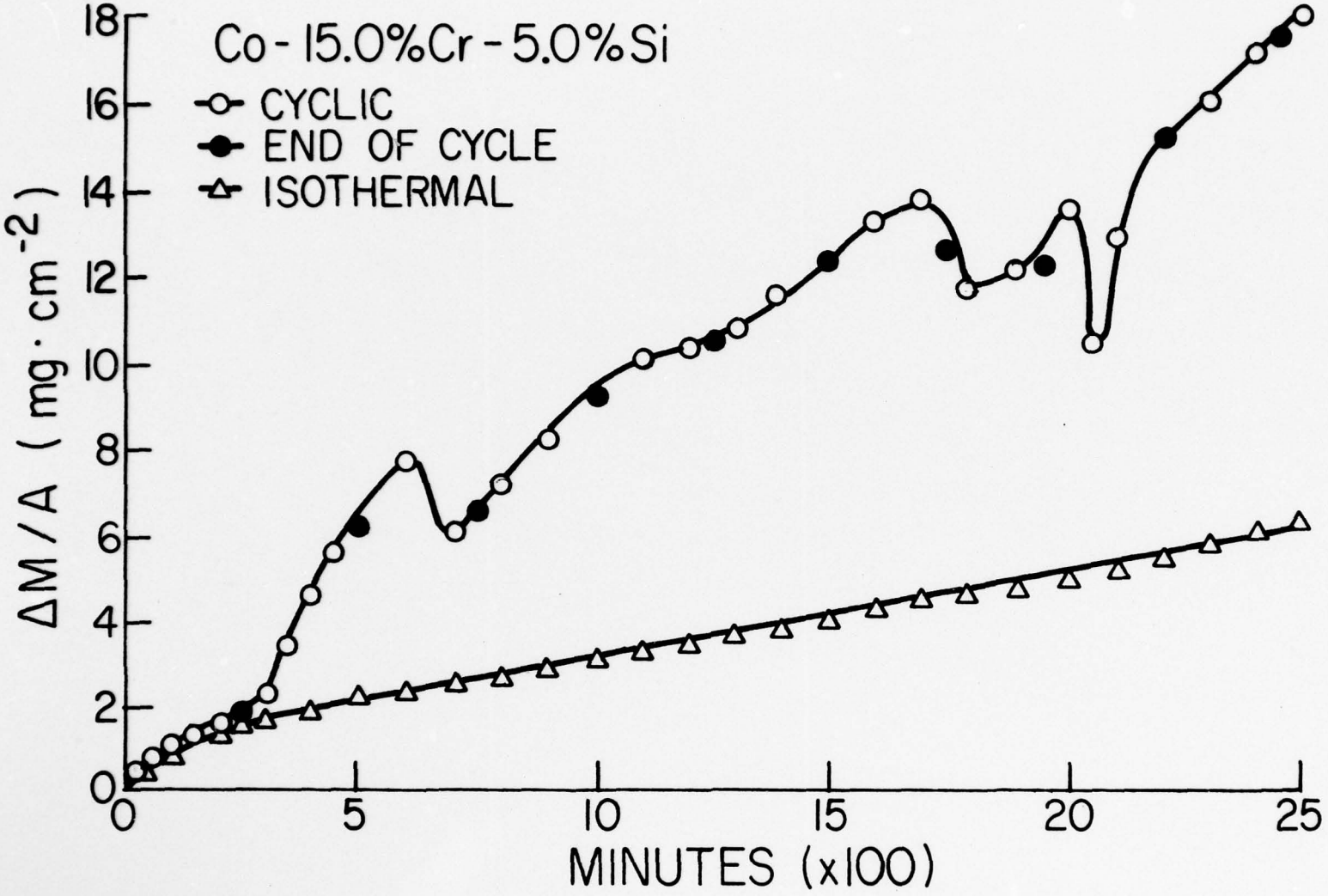
Co - 15.0%Cr - 5.0%Si
CYCLIC
END OF CYCLE
ISOTHERMAL
ΔM/A (mg · cm⁻²)
MINUTES (x100)
0
2
4
6
8
10
12
14
16
18
0
5
10
15
20
25

0.1 atmosphere. An example of this is Co-10 Cr-10 Si; the parabolic oxidation rate constant (K_p) for this alloy is 0.00197×10^{-10} $gm^2 \cdot cm^{-4} \cdot cm^{-1}$ as compared to 138×10^{-10} $gm^2 \cdot cm^{-4} \cdot cm^{-1}$ for pure cobalt. Although the oxidation kinetics are generally parabolic for the Co-Cr-Si alloys, they differ drastically in scale formation and structure. The scales formed on the Co-Cr alloys with low silicon additions, except for Co-15 Cr-1 and 2.5 Si alloys, generally are double-layered with an outer layer of CoO and an inner layer of CoO with some dispersed particles of $CoCr_2O_4$ and Co_2SiO_4. The alloys with higher silicon additions of up to 10 wt. % generally form thin films averaging from 4 to 20 microns in thickness. They are composed of CoO with higher percentages of $CoCr_2O_4$ (possibly some Cr_2O_3) and slightly higher percentages of Co_2SiO_4.

The experimental results indicate that the theory of adding chromium to cobalt-silicon alloys in order to promote the formation of an outer layer of SiO_2, which offers excellent oxidation resistance, is practical. The formation of the spinel Co_2SiO_4 may be a good indication of the initial existence of an outer layer of SiO_2. The SiO_2 particles which grow under an outer layer of CoO and Cr_2O_3 may react with the CoO to form Co_2SiO_4 as previously discussed for the oxidation of the cobalt-silicon alloys. If a layer of SiO_2 is present, it would be extremely thin, of the order of a few microns. Increasing the amount of chromium and silicon also results in increased spinel formation and therefore a decrease in the oxidation rate. The presence of the spinels Co_2SiO_4 and $CoCr_2O_4$ within the oxide layer serves to reduce the oxidation rate of the

alloy by blocking the solid state diffusion of cobalt ions via reduction of the solid state diffusion area.

The accelerated oxidation rates associated with hot corrosion of nickel-based alloys (43) were not as noticeable for the Co-Cr-Si alloys. The Co-Cr-Si alloys exhibited slightly higher oxidation rates in a hot corrosion environment as compared to an oxidizing environment. The low rates of oxidation observed under hot corrosion conditions are in agreement with results obtained by other investigators (68, 72, 70), which show that cobalt-based alloys are superior, in hot corrosion resistance, to nickel-based alloys.

The decrease in oxidation rates for the hot corrosion samples is a function of the increasing silicon content. The Co-10 Cr-10 Si alloy exhibited the best hot corrosion resistance with a parabolic rate constant (K_p) of 0.0167×10^{-10} $gm^2 \cdot cm^{-4} \cdot sec^{-1}$. The formation of an initial thin film (<10 microns) of SiO_2 on the alloy surface may be the reason for the low hot corrosion rates exhibited by the Co-Cr alloys with the higher silicon contents. The formation of the spinels $CoCr_2O_4$ and Co_2SiO_4 also aid in retarding the hot corrosion rate. The experimental results also indicate thermal cycling is detrimental to the hot corrosion resistance of Co-15 Cr-Si alloys by causing spalling of the normally protective oxide layer and exposing the alloy surface to attack by the corroding environment.

VI. SUMMARY AND CONCLUSIONS

The rates of oxidation and hot corrosion of pure cobalt, cobalt-chromium, cobalt-silicon, and cobalt-chromium-silicon alloys were determined at 1000°C in oxygen at a pressure of 0.1 atmosphere. The hot corrosion studies were conducted under conditions of a continuous supply of Na_2SO_4 to the sample surface. In addition, the effect of thermal cycling on the hot corrosion resistance of the Co-15 Cr-Si alloy group was also investigated.

For the cobalt-chromium alloys, it was found that a considerable decrease in the oxidation and hot corrosion rates occurred at chromium concentrations around 15 wt. %. The cobalt-silicon binary alloys showed a dramatic increase in the rate of oxidation up to 0.05 wt. % silicon according to normal doping theory. At silicon concentrations greater than 5 wt. %, a marked decrease in oxidation and hot corrosion was observed.

Generally, the series of cobalt-chromium-silicon alloys exhibited much better oxidation and hot corrosion resistance than the binary alloys. The lowest rates were obtained for alloys with high silicon contents. One alloy in particular, Co-10 Cr-10 Si, exhibited the lowest total weight gain per unit area for both oxidation and hot corrosion. The hot corrosion resistance of the Co-15 Cr-Si alloys were decreased by thermal cycling.

The conclusions drawn from the present study are:

a. The mechanism governing the oxidation of cobalt-based alloys at 1000°C and a partial pressure of oxygen at 0.1 atmosphere is the

solid state diffusion of Co cations in a CoO network via a vacancy mechanism.

b. This diffusion is influenced by the porosity of the inner layer, which reduces the solid state diffusion area but enhances the transport of oxygen across the pore.

c. The formation of the spinels $CoCr_2O_4$ and Co_2SiO_4 inhibits the solid state diffusion of cobalt ions by a blocking effect.

The present study also indicates that the theory of adding chromium to cobalt-silicon alloys in order to promote the formation of an outer layer of SiO_2, whose growth rate is controlled by movement of the electrons, may be applicable to the cobalt-chromium-silicon system.

VII. SUGGESTIONS FOR FUTURE RESEARCH

Although the present study has elucidated a number of aspects concerning the mechanisms of oxidation and hot corrosion of cobalt-chrome-silicon alloys, there are some aspects which require further investigation.

The scale formation as a function of time should be studied to determine if and when a layer of SiO_2 develops on the alloy surface after oxidation and hot corrosion. The oxidation and hot corrosion rates as a function of oxygen pressure should also be investigated.

Further studies utilizing the scanning electron microscope at high magnification to study the thin film oxides formed on alloys with high chromium and silicon concentration should be undertaken. The effect of thermal cycling on the hot corrosion resistance of cobalt-based alloys requires additional investigation. In conjunction with the thermal cycling studies, the effect of elements, such as yttrium, on improving scale adherence should be determined.

A comparison should be made between the oxidation and hot corrosion rates obtained for wrought Co-Cr-Si alloys as opposed to those obtained for the cast alloys utilized in this investigation.

If possible, the self-diffusion rates of Co, Cr and Si in SiO_2 and Co_2SiO_4 should be determined, since they are of primary importance in any study concerning the solid state diffusion processes in the scale.

REFERENCES

(1) Mahorter, R. G., In: "Proceedings of the 1974 Gas Turbine Materials in the Marine Environment Conference", Metals and Ceramics Information Center, Battelle, Columbus Laboratories, MCIC-75-27, pp. 1-10 (1974).

(2) Hauffe, K., Oxidation of Metals, Plenum Press (1965).

(3) Wagner, C., and Schottky, W., Z. Physik. Chem., (B)11: 163 (1930).

(4) Wagner, C., and Koch, E., Z. Physik. Chem., (B)32: 439 (1936).

(5) Carter, R. E., and Richardson, F. D., J. Metals, 6: 1244 (1954).

(6) Carter, R. E., and Richardson, F. D., Trans. A.I.M.E., 200: 1244 (1954).

(7) Carter, R. E., and Richardson, F. D., Trans. A.I.M.E., 203: 336 (1955).

(8) Bridges, D. W., Baur, J. P., and Fassell, Jr., W. M., J. Electrochem. Soc., 103: 614 (1956).

(9) Douglass, D. L., "Oxidation of Metals and Alloys", American Society for Metals, Metals Park, Ohio (1971).

(10) Kofstad, P. K., High Temperature Oxidation of Metals, Wiley, New York (1966).

(11) Wagner, C., J. Electrochem. Soc., 99: 369 (1952).

(12) Tammann, G., Z. Anorg. U. Allgem. Chem., 111: 78 (1920).

(13) Pilling, N. B., and Bedworth, R. E., J. Inst. Metals, 29: 529 (1923).

(14) Wagner, C., Z. Physik. Chem., (B)21: 25 (1933).

(15) Wagner, C., "Atom Movements", American Society of Metals, Cleveland, Ohio (1950).

(16) Wagner, C., J. Electrochem. Soc., 103: 627 (1956).

(17) Wagner, C., Z. Electrochem. Soc., 63: 773 (1959).

(18) Preece, A., and Lucas, G., J. Inst. Metals, 81: 219 (1952).

REFERENCES (Cont.)

(19) Phalnikar, C. A., Evans, E. B., and Baldwin, Jr., W. M., J. Electrochem. Soc., 103: 429-438 (1956).

(20) Kofstad, P. K., and Hed, A. Z., J. Electrochem. Soc., 116: 224-229, 229-234 (1969).

(21) Kofstad, P. K., and Hed, A. Z., J. Electrochem. Soc., 116: 1542-1550 (1969).

(22) Wood, G. C., Wright, I. G., Hodgkiess, T., and Whittle, D. P., Werkst. Korros., 21: 900 (1970).

(23) Davin, A., Coutsouradis, D., and Habraken, L., Cobalt, 35: 69-77 (1967).

(24) Douglass, D. L., and Armijo, J. S., Oxidation of Metals, 3: 185-202 (1971).

(25) Wood, G. C., and Boustead, J., Corrosion Sci., 8: 719 (1968).

(26) Giggons, C. S., Kear, B. H., Pettit, F. S., and Tein, J. K., Met. Trans., 5: 1685 (1974).

(27) Beltram, A. M., "The Role of Yttrium in the High Temperature Oxidation Mechanism of Co-30 Cr Alloys", M. Sc. Thesis, Rensselaer Polytechnic Institute (1968).

(28) Wlodek, S. T., "The Oxidation of L-605 and X-40", Report FPD-12, General Electric, Cincinnati, Ohio (1964).

(29) Lowell, C. E., and Drell, I. L., "High Temperature X-ray Diffraction Study of the Oxidation of WI-52", paper presented at N.A.C.E. Corrosion Research Conference, Cleveland, pp. 18-21 (1968).

(30) Felton, E. J., and Gregg, R. A., Am. Soc. Metals Trans. Quart., 57: 804-822 (1964).

(31) Kosack, R., and Lombard, C. A., SAMPE J., pp. 47-51 (1967).

(32) Bollenrath, R., Wirth, G., and Rhode, W., Cobalt, 20: 117-135 (1963).

(33) Wheaton, H. L., Cobalt, 29: 163-170 (1965).

(34) Reid, W. T., Corey, R. C., and Cross, B. J., Trans. A.S.M.E., 67: 279 (1945).

(35) Bornstein, N. S., DeCrescente, M. A., and Roth, H. A., In: "Proceedings of the 1974 Gas Turbine Materials in the Marine Environment Conference", Metals and Ceramics Information Center, Battelle, Columbus Laboratories, MCIC-75-27, pp. 115-160 (1974).

REFERENCES (Cont.)

(36) Goebel, J. A., Felton, E. J., and Pettit, F. S., In: "Proceedings of the 1974 Gas Turbine Materials in the Marine Environment Conference", Metals and Ceramics Information Center, Battelle, Columbus Laboratories, MCIC-75-27, pp. 93-114 (1974).

(37) DeCrescente, M. A., and Bornstein, N. S., Corrosion, 24: 127 (1968).

(38) Pontony, D. A., and Vasu, K. I., J. Inorg. Nucl. Chem., 30: 755-779 (1968).

(39) Vialatte, M., and Apert, C., Corrosion et Anticorrosion, 14: 57-68 (1966).

(40) Rausch, J. J., McAndrew, J. B., and Simcoe, C. R., In: "Metallurgy Society Conference on High Temperature Materials II", Cleveland, Ohio, 1961, pp. 259-279 (1963).

(41) Douglass, D. L., and Armijo, J. S., Oxidation of Metals, 2: 207 (1970).

(42) Betteridge, W., "The Nimonic Alloys", Arnold, London (1959).

(43) Kerr, T. W., M. Sc. Thesis, The Pennsylvania State University (1975).

(44) Jones, D. E., and Stringer, J., Oxidation of Metals, 9: 409-413 (1975).

(45) Stringer, J., Wilcox, B. A., and Jaffee, R. I., Oxidation of Metals, 5: 11 (1972).

(46) Simons, E. L., Browning, G. V., and Liebhafsky, H. A., Corrosion, 11: 505 (1955).

(47) Danek, Jr., G. J., J. Nav. Eng., p. 859 (Dec., 1965).

(48) Seybolt, A. U., Trans. Metall. Soc., A.I.M.E., 242: 1955-1961 (1968).

(49) Quets, J. M., and Dresher, W. H., J. Mater., 4: 583-599 (1969).

(50) Bornstein, N. S., and DeCrescente, M. A., Trans. Metall. Soc., A.I.M.E., 245: 1947 (1969).

(51) Bornstein, N. S., and DeCrescente, M. A., Met. Trans., 2: 1971-1983 (1971).

(52) Goebel, J. A., and Pettit, F. S., Met. Trans., 1: 1943-1954 (1970).

(53) Goebel, J. A., Pettit, F. S., and Goward, G. W., Met. Trans., 4: 261 (1973).

REFERENCES (Cont.)

(54) Goward, G. W., J. Metals, 22: 31 (1970).

(55) Goward, G. W., and Boone, D. H., Oxidation of Metals, 3: 475 (1971).

(56) Goward, G. W., In: "Gas Turbine Materials Conference Proceedings", NAV SEC/NASC, Washington, D.C., p. 85 (1972).

(57) Goward, G. W., In: "Proceedings of the 1974 Gas Turbine Materials in the Marine Environment Conference", Metals and Ceramics Information Center, Battelle, Columbus Laboratories, MCIC-75-27, pp. 277-298 (1974).

(58) Kaufman, M., In: "Proceedings of the 1974 Gas Turbine Materials in the Marine Environment Conference", Metals and Ceramics Information Center, Battelle, Columbus Laboratories, MCIC-75-27, pp. 15-20 (1974).

(59) Decker, R. F., In: "High Temperature Materials in Gas Turbines" eds. P. R. Sahm and M. O. Speidel, Elsevier Scientific Publishing Co., Amsterdam, pp. 49-64 (1974).

(60) Wright, I. G., In: "Proceedings of the 1974 Gas Turbine Materials in the Marine Environment Conference", Metals and Ceramics Information Center, Battelle, Columbus Laboratories, MCIC-75-27, pp. 357-378 (1974).

(61) Wheatfall, W. L., "Are Cobalt-Base Alloys Intrinsically More Resistant to Hot Corrosion than Alloys Based on Nickel", AGARD Conference Proceedings, No. 120 (1973).

(62) Stringer, J., and Whittle, D. P., In: "High Temperature Materials in Gas Turbines", eds. P. R. Sahm and M. O. Speidel, Elsevier Scientific Publishing Co., Amsterdam, pp. 283-311 (1974).

(63) Dibs, R. R., "Dynamic Gas Temperature Measurements in a Gas Turbine Transition Duct Exit", Am. Soc. Mech. Eng., paper no. 73-GT-7 (1972).

(64) Tschinkel, J. G., Corrosion, 28: 161 (1972).

(65) Stringer, J., In: "Corrosion Problems in Energy Conversion and Generation", ed. C. S. Tedmon, Jr., The Electrochemical Society, Princeton, N.J. (1974).

(66) Dean, A. V., "Investigation into the Resistance of Various Nickel and Cobalt-Base Alloys to Sea Salt Corrosion at Elevated Temperatures", N.G.T.E. Report (1964).

REFERENCES (Cont.)

(67) Kuintzle, C., In: "Proceedings of the 1974 Gas Turbine Materials in the Marine Environment Conference", Metals and Ceramics Information Center, Battelle, Columbus Laboratories, MCIC-75-27, pp. 381-395 (1974).

(68) Johnson, D. M., Whittle, D. P., and Stringer, J., Corrosion Sci., 15: 649-661 (1975).

(69) Johnson, D. M., Whittle, D. P., and Stringer, J., Werkst. Korros., 26: 611 (1975).

(70) Kaufman, M., Trans. A.S.M., 62: 590 (1969).

(71) Wagenheim, N. T., Cobalt, 48: 129 (1970).

(72) Johnson, D. M., Whittle, D. P., and Stringer, J., Corrosion Sci., 15: 649-661 (1975).

(73) El-Dahshan, M. E., Stringer, J., and Whittle, D. P., Cobalt, 57: 182 (1972).

(74) Sims, C. T., Bergman, P. A., and Beltram, A. M., "Progress in the Development of Hot Corrosion-Resistant Alloys for Marine Applications", A.S.M.E. paper no. 69-GT-16 (1969).

(75) Kubaschewski, O., and Hopkins, B. E., Oxidation of Metals and Alloys, 2nd edn., Butterworths, London (1967).

(76) Wagner, C., Corrosion Sci., 5: 751 (1965).

(77) Wood, G. C., Oxidation of Metals, 2: 11 (1970).

(78) Hoke, J., Private communication.

APPENDIX

Addition to the Hot Corrosion Experimental Method.

The rate of deposition of Na_2SO_4 on the sample surface was determined prior to the start of the hot corrosion series of experiments. This was accomplished by suspending an alumina blank in the reaction chamber with a platinum chain. Both the chain and alumina coupon were weighed prior to suspension in the chamber.

The weight gain (Δm) of the alumina blank and platinum chain was then recorded as a function of time for 2800 minutes, since this was the run duration for all hot corrosion experiments. The increase in weight of the alumina blank and chain was due to the condensation of Na_2SO_4 on the surface, since no reaction of Na_2SO_4 with either the alumina or platinum is expected.

The weight gain due to the condensation of Na_2SO_4 on the blank sample surface was then subtracted from the total weight gain of the hot corrosion sample as a function of time.

After completion of the hot corrosion blank run, the surfaces of the platinum chain and alumina blank were washed with distilled water and the sodium and sulfate content of the wash solution was determined in the Mineral Constitution Laboratory of The Pennsylvania State University. The results are listed below:

	ppm
Na_2O	0.85
SO_3	11

Total Na_2O content - 0.09 mg.

Total SO_3 content - 1.17 mg.

The above results show Na_2SO_4 was definitely deposited on the sample surface throughout the hot corrosion runs.

DISTRIBUTION

Commander (NSEA 09G32)
Naval Sea Systems Command
Department of the Navy
Washington, D. C. 20362 — Copies 1 and 2

Commander (NSEA 0342)
Naval Sea Systems Command
Department of the Navy
Washington, D. C. 20362 — Copies 3 and 4

Defense Documentation Center
5010 Duke Street
Cameron Station
Alexandria, VA 22314 — Copies 5 through 16